National Library of Canada
Bibliothèque nationale du Canada

Canadian Theses Service
Services des thèses canadiennes

Ottawa, Canada
K1A 0N4

CANADIAN THESES

THÈSES CANADIENNES

NOTICE

The quality of this microfiche is heavily dependent upon the quality of the original thesis submitted for microfilming. Every effort has been made to ensure the highest quality of reproduction possible.

If pages are missing, contact the university which granted the degree.

Some pages may have indistinct print especially if the original pages were typed with a poor typewriter ribbon or if the university sent us an inferior photocopy.

Previously copyrighted materials (journal articles, published tests, etc.) are not filmed.

Reproduction in full or in part of this film is governed by the Canadian Copyright Act, R.S.C. 1970, c. C-30.

AVIS

La qualité de cette microfiche dépend grandement de la qualité de la thèse soumise au microfilmage. Nous avons tout fait pour assurer une qualité supérieure de reproduction.

S'il manque des pages, veuillez communiquer avec l'université qui a conféré le grade.

La qualité d'impression de certaines pages peut laisser à désirer, surtout si les pages originales ont été dactylographiées à l'aide d'un ruban usé ou si l'université nous a fait parvenir une photocopie de qualité inférieure.

Les documents qui font déjà l'objet d'un droit d'auteur (articles de revue, examens publiés, etc.) ne sont pas microfilmés.

La reproduction, même partielle, de ce microfilm est soumise à la Loi canadienne sur le droit d'auteur, SRC 1970, c. C-30.

THIS DISSERTATION
HAS BEEN MICROFILMED
EXACTLY AS RECEIVED

LA THÈSE A ÉTÉ
MICROFILMÉE TELLE QUE
NOUS L'AVONS REÇUE

Canada

NL-339 (r.86/06)

THE UNIVERSITY OF ALBERTA

# ADAPTIVE FILTERING APPLIED TO GASTRIC ELECTRICAL ACTIVITY

BY

RANDALL GORDON RUDE

A THESIS

SUBMITTED TO THE FACULTY OF GRADUATE STUDIES AND RESEARCH

IN PARTIAL FULFILMENT OF THE REQUIREMENTS FOR THE DEGREE

OF MASTER OF SCIENCE

DEPARTMENT OF ELECTRICAL ENGINEERING

EDMONTON, ALBERTA

SPRING 1987

Permission has been granted to the National Library of Canada to microfilm this thesis and to lend or sell copies of the film.

The author (copyright owner) has reserved other publication rights, and neither the thesis nor extensive extracts from it may be printed or otherwise reproduced without his/her written permission.

L'autorisation a été accordée à la Bibliothèque nationale du Canada de microfilmer cette thèse et de prêter ou de vendre des exemplaires du film.

L'auteur (titulaire du droit d'auteur) se réserve les autres droits de publication; ni la thèse ni de longs extraits de celle-ci ne doivent être imprimés ou autrement reproduits sans son autorisation écrite.

ISBN 0-315-37787-9

THE UNIVERSITY OF ALBERTA

RELEASE FORM

NAME OF AUTHOR: Randall Gordon Rude

TITLE OF THESIS: Adaptive Filtering Applied to Gastric Electrical Activity

DEGREE: Master of Science in Electrical Engineering

YEAR THIS DEGREE GRANTED: 1987

Permission is hereby granted to THE UNIVERSITY OF ALBERTA LIBRARY to reproduce single copies of this thesis and to lend or sell such copies for private, scholarly or scientific research purposes only.

The author reserves other publication rights, and neither the thesis nor extensive extracts from it may be printed or otherwise reproduced without the author's written permission.

Randall G. Rude

#506 5204 Dalton Dr., N.W.
Calgary, Alberta
T3A 3H1

Date: Dec. 15, 1986

THE UNIVERSITY OF ALBERTA

FACULTY OF GRADUATE STUDIES AND RESEARCH

The undersigned certify that they have read, and recommend to the Faculty of Graduate Studies and Research for acceptance, a thesis entitled "Adaptive Filtering Applied To Gastric Electrical Activity"
submitted by Randall Gordon Rude
in partial fulfilment of the requirements for the degree of Master of Science
in Electrical Engineering.

Supervisor

Date: Oct 10-'86

For my parents, with love.

## Abstract

Monitoring the human electrogastrogram using transcutaneous electrodes is preferable to in situ techniques for a variety of reasons, not the least of which is patient comfort. Unfortunately, the signal detected at the surface of the abdomen suffers from distortion from several sources. This distortion can change the shape of the waveform or bury it in noise, thus obscuring the medical information known to be contained in the relative slopes of the rising and falling edges. Through the proper application of a digital adaptive filter, the electrogastrogram can be reconstructed in sufficient detail to obtain the necessary information.

The filter chosen for this task is a least mean-squared error (LMS) adaptive filter similar to the type first published by Bernard Widrow in 1960. This filter is based on an iterative algorithm that learns the characteristics of the input signal and suppresses the noise while passing the signal components. Since the filter acts to remove additive noise, signal components will not be affected by the suppression of noise components at the same frequencies. Random noise as well as signals generated by the heart, lungs, duodenum, and other organs are removed from the electrogastrogram.

A software package written in the C programming language for IBM-AT and IBM-XT Personal Computers provides the capability of filtering patient records that have been stored in computer data files. The waveform obtained using this software can be displayed graphically, and stored in another file for archival purposes.

Several improvements in the application of the adaptive filter to off-line signal processing are developed.

Thank you, Dr. Kingma, for giving me the opportunity to earn this degree, and for being the best possible supervisor.

Thanks (in alphabetical order) to Jide, Jim, Mak., Mark, and Randy for keeping me sane.

## Table of Contents


1. Introduction.....1

2. Adaptive Filtering Theory.....9
   2.1. The Adaptive Filter.....9
   2.2. The Adaptive Noise Canceller.....16
   2.3. The Adaptive EGG Filter.....21
   2.4. The LMS Algorithm.....23
   2.5. Adaptive Filter Implementation.....27

3. Waveshape Analysis.....31
   3.1. Effect of Signal Parameters on Waveshape.....31
   3.2. FFT Analysis of Signal Parameters.....34
   3.3. Limitations of FFT Analysis.....35
   3.4. Spectral Comparison.....46
   3.5. Apparent Phase Shift.....47
   3.6. Slope Identification.....53
   3.7. Relevant Signal Components.....55

4. Experimental Results.....57
   4.1. An Ideal Example of Convergence.....57
   4.2. A Non-ideal Example of Convergence.....65
   4.3. Adaptive Filter Versus Fixed Filter.....68
   4.4. Signal Tracking.....74
   4.5. Application of the Adaptive EGG Filter.....87
   4.6. Recovering a Simulated EGG.....94

5. Results Obtained From Patient Records.....103
   5.1. Patient Record #1.....103
   5.2. Patient Record #2.....113
   5.3. Patient Record #3.....123

6. Conclusions.....134

References.....136

## List of Tables

3-1: Signal Parameters for Fig. 3-1.....31
3-2: Signal Parameters for Fig. 3-3.....40
3-3: Signal Parameters for Fig. 3-6.....40
3-4: Signal Parameters for Table 3-5.....49
3-5: Results of Apparent Phase Shift Test.....50
3-6: More Apparent Phase Shift Results.....52

4-1: Signal Parameters for Fig. 4-2.....57
4-2: Signal Parameters for Fig. 4-3.....57
4-3: Signal Parameters for Fig. 4-7.....65
4-4: Fixed Filter Parameters For Stationary Test.....68
4-5: Signal Parameters for Figs. 4-13 and 4-17.....74
4-6: Fixed Filter Parameters For Sweep Test.....79
4-7: Filter Parameters for H(z).....87
4-8: Signal Parameters for Fig. 4-26.....94
4-9: Signal Parameters for Simulated Respiration.....94
4-10: Filter Parameters for H(z).....99

5-1: H(z) Parameters For EGG Recovery.....108

## List of Figures


1-1: A Transcutaneous Electrogastrogram.....3

2-1: The Adaptive Filter.....10
2-2: The Transversal Filter.....11
2-3: The Adaptive Linear Combiner.....15
2-4: The Adaptive Noise Canceller.....17
2-5: The Adaptive EGG Filter.....20

3-1: An Example of a Waveshape.....32
3-2: An Example of Changing a Waveshape.....33
3-3: A 3.75 cpm Sine Wave.....37
3-4: Magnitude Spectrum of Fig. 3-3.....38
3-5: Phase Spectrum of Fig. 3-3.....39
3-6: A 3.0 cpm Sine Wave.....41
3-7: Magnitude Spectrum of Fig. 3-6.....42
3-8: Phase Spectrum of Fig. 3-6.....43
3-9: Phase Spectrum in the Next Window.....48

4-1: Example of ANC Application.....58
4-2: Input Signal d.....59
4-3: Input Signal x.....60
4-4: Output Signal z After Convergence.....62
4-5: Magnitude Spectrum of Fig. 4-4.....63
4-6: Phase Spectrum of Fig. 4-4.....64
4-7: The d Input Average Magnitude Spectrum.....66
4-8: The Input Signal d.....67
4-9: Output Signal After Convergence.....69
4-10: Magnitude Spectrum of Fig. 4-9.....70
4-11: Phase Spectrum of Fig. 4-9.....71
4-12: Output of the Fixed Digital Filter.....72
4-13: Input Signal Before Linear Sweep.....75
4-14: Output Signal Before Linear Sweep.....76
4-15: Magnitude Spectrum of Fig. 4-14.....77
4-16: Phase Spectrum of Fig. 4-14.....78
4-17: Input Signal After Linear Sweep.....80
4-18: Output Signal After Linear Sweep.....81
4-19: Magnitude Spectrum of Fig. 4-18.....82
4-20: Phase Spectrum of Fig. 4-18.....83
4-21: Fixed Filter Output Before Linear Sweep.....85
4-22: Fixed Filter Output After Linear Sweep.....86
4-23: The Output Signal After Convergence.....88
4-24: Magnitude Spectrum of Fig. 4-23.....89
4-25: Phase Spectrum of Fig. 4-23.....90
4-26: A Simulated Electrogastrogram.....91
4-27: Magnitude Spectrum of Fig. 4-26.....92
4-28: Phase Spectrum of Fig. 4-26.....93
4-29: Magnitude Spectrum of the Simulated Signal.....95

4-30: The Output Signal After Convergence.....96
4-31: Magnitude Spectrum of Fig. 4-30.....97
4-32: Phase Spectrum of Fig. 4-30.....98
4-33: The Simulated Transcutaneous EGG.....100

5-1: Average Spectrum of Patient Record #1.....104
5-2: A Window From Patient Record #1.....105
5-3: Magnitude Spectrum of Fig. 5-2.....106
5-4: Phase Spectrum of Fig. 5-2.....107
5-5: Average Spectrum of Filtered Record #1.....109
5-6: The Output Signal After Convergence.....110
5-7: Magnitude Spectrum of Fig. 5-6.....111
5-8: Phase Spectrum of Fig. 5-6.....112
5-9: Average Spectrum of Patient Record #2.....114
5-10: A Window From Patient Record #2.....115
5-11: Magnitude Spectrum of Fig. 5-10.....116
5-12: Phase Spectrum of Fig. 5-10.....117
5-13: Average Spectrum of Filtered Record #2.....119
5-14: The Output Signal After Convergence.....120
5-15: Magnitude Spectrum of Fig. 5-14.....121
5-16: Phase Spectrum of Fig. 5-14.....122
5-17: Average Spectrum of Patient Record #3.....124
5-18: A Window From Patient Record #3.....125
5-19: Magnitude Spectrum of Fig. 5-18.....126
5-20: Phase Spectrum of Fig. 5-18.....127
5-21: Average Spectrum of Filtered Record #3.....129
5-22: The Output Signal After Convergence.....130
5-23: Magnitude Spectrum of Fig. 5-22.....131
5-24: Phase Spectrum of Fig. 5-22.....132

## List Of Abbreviations

| | |
|---|---|
| ALC | Adaptive Linear Converter |
| ANC | Adaptive Noise Canceller |
| cpm | cycles per minute |
| dB | deciBels |
| ECG | Electrocardiogram |
| EGG | Electrogastrogram |
| Hz | Hertz (cycles per second) |
| IBM | International Business Machines |
| LMS | Least Mean Squared error |
| mV | milliVolts |
| mVpp | milliVolts measured peak to peak |
| PLL | Phase Locked Loop |
| SNR | signal to noise ratio |
| RAM | random access memory |

## List Of Matrices

| | |
|---|---|
| $\underline{P}$ | cross correlation vector of d and x |
| $\underline{R}$ | autocorrelation matrix of x |
| $\underline{R}^{-1}$ | inverse of $\underline{R}$ |
| $\underline{X}_k$ | input vector to the adaptive linear combiner |
| $\underline{X}_k^T$ | transpose of $\underline{X}_k$ |
| $\underline{W}$ | vector of constant filter coefficients |
| $\underline{W}^T$ | transpose of $\underline{W}$ |
| $\underline{W}_0$ | initial weight vector |
| $\underline{W}_k$ | weight vector at sample time k |
| $\underline{W}_k^T$ | transpose of $\underline{W}_k$ |
| $\underline{W}^*$ | optimal (Wiener) weight vector |

## List Of Symbols

| | |
|---|---|
| $d$ | desired response (training) input signal |
| $h$ | subscript identifying a filter in a cascade |
| $H(z)$ | z transform of the transfer function of a fixed digital filter |
| $H_h(z)$ | z transform of the transfer function a one fixed digital filter in a cascade |
| $k$ | subscript identifying the sample index |
| $L$ | number of adaptive filter weights |
| $M$ | misadjustment of the LMS adaptive algorithm |
| $min$ | subscript identifying a minimum value |
| $n_d$ | noise present at the d input |
| $n_x$ | noise present at the x input |
| $n_y$ | noise present at the y output |
| $Q$ | quality factor of a digital filter |
| $s$ | an arbitrary signal |
| $T_{MSE}$ | time constant of the adaptive learning curve |
| $w_1$ | a constant filter coefficient |
| $w_{1k}$ | an adaptive filter weight value at sample time k |
| $W(z)$ | z transform of the transfer function of the adaptive linear combiner |
| $x$ | input to the adaptive linear combiner |
| $y$ | output of the adaptive linear combiner |
| $z$ | error signal of the adaptive filter |
| $\mu$ | the adaptive convergence parameter |

## List Of Operators

| | |
|---|---|
| $z^{-1}$ | unit sample delay |
| $E[\ ]$ | statistical expectation |
| $tr[\ ]$ | trace of a matrix |
| $\nabla$ | gradient |
| $\Sigma$ | summation |
| $\partial$ | partial derivative |

## 1. Introduction

The electrogastrogram (EGG) has been shown to convey useful medical information about the health of the human stomach [1]. Of particular interest are the frequencies of the signal components, as well as the relative slopes of the rising and falling edges of the waveform, which indicate whether the contractions of the stomach are travelling in the oral or aboral directions. It is possible to monitor this signal by placing electrodes in the vicinity of the source (ie. in the stomach), but this procedure suffers from two disadvantages : first, it is uncomfortable for the patient; and second, in some cases the insertion of electrodes may not be possible for medical reasons.

Monitoring the EGG using electrodes placed on the skin over the abdomen has two advantages over in situ procedures. First, this transcutaneous procedure is non-invasive, so there is no discomfort to the patient. Second, there is no blockage of the patient's throat. Since the comfort of the patient is of primary concern, the surface recovery technique is preferable to procedures using internal electrodes.

The signal obtained using transcutaneous electrodes consists of a sum of signals generated by a variety of sources. Included in this potpourri are signals generated by organs such as the heart (the electrocardiogram or

ECG), lungs, duodenum, and stomach, as well as noise generated by patient movement, electromagnetic interference, and the data acquisition process. Some of these signals, the electrocardiogram and 60 Hertz hum for example, are of sufficiently high frequency that they can be suppressed using simple low pass filters. The acquisition process used to obtain the patient records typically samples the signal at 2.0 Hertz (120 cycles per minute or cpm), and then passes the signal through a low-pass filter with a cutoff (3 dB) frequency of 30 cpm. As a result, only components in the range from dc (0 cpm) to 30 cpm are normally present with significant power in the records.

However, enough extraneous signals remain in this range of frequencies to complicate the task of isolating the EGG waveform. Fig. 1-1 shows an actual transcutaneous signal in the frequency domain. The graph is an "average" magnitude spectrum, which means that the fast Fourier transform (FFT) of each 256 samples is computed and the power at each discrete frequency is accumulated. The final total in each bin is averaged over the number of FFT's that are computed. This technique is useful for detecting the peaks in a signal since the averaging tends to reduce the magnitude of random fluctuations in the signal while emphasizing the periodic components.

The graph shows that the patient record contains a significant amount of random noise. The patient's ECG

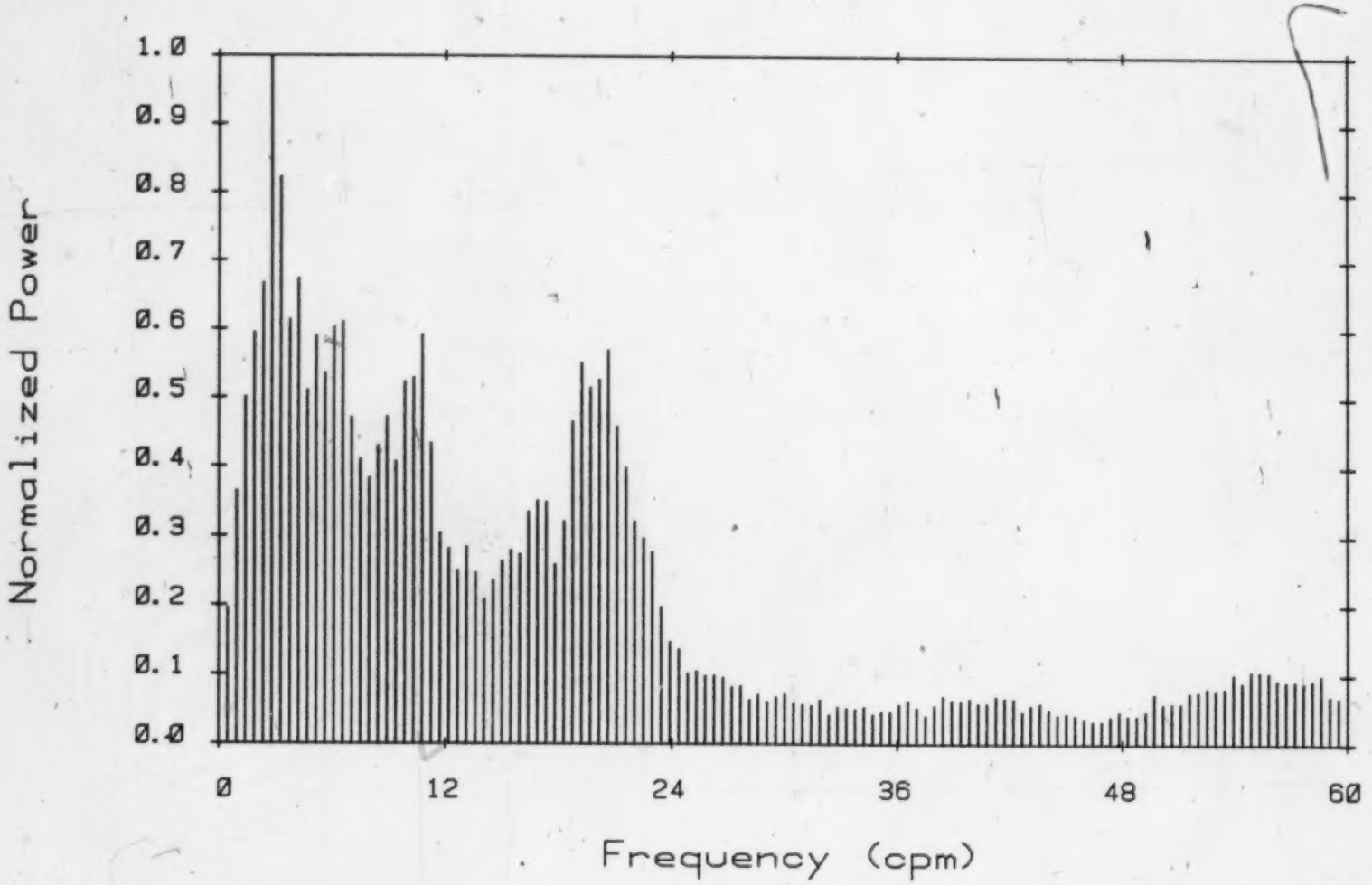


Fig. 1-1: A Transcutaneous Electrogastrogram

signal was probably quite strong during the acquisition process, because significant power lies in the vicinity of 55 cpm (even after low-pass filtering). A strong signal is also present at about 20 cpm, and is probably due to respiration. The largest peak in the spectrum is at 2.8125 cpm, and is caused by the fundamental frequency component of the EGG. The first and second harmonics of the EGG are just buried in the background noise, and lie at approximately 5.6 and 7.4 cpm, respectively.

This example illustrates the difficulties involved in filtering the EGG recovered using transcutaneous electrodes. The required filter must remove the following components :

a) the strong respiration and ECG signals, and the noise at frequencies greater than about 15 cpm;

b) the noise at those frequencies that lie between the harmonics of the EGG; and

c) the noise present at frequencies coinciding with the fundamental and harmonic frequencies of the EGG.

The first requirement could be met using an ordinary low-pass filter. Requirement b) would require a bank of high Q band-pass filters, which suffer from problems such as ringing and severe phase distortion. This would introduce different phase shifts into each harmonic of the EGG, and hence the waveshape would be changed. This would cause the medical information carried in the shape of the waveform would be altered in some unknown way, and the

filtered signal would be useless. The final requirement, however, can not be met by traditional filters, which perform the filtering operation by suppressing a part of the frequency spectrum and do not simply remove additive noise.

Another consideration is that the fundamental frequency of a biological signal is generally not constant. A bank of band-pass filters with sufficient bandwidth to pass the entire range of frequencies at which the components of the EGG might appear would also pass a significant amount of noise. Such a system would therefore be incapable of satisfying requirements b) and c).

In order for the non-invasive transcutaneous technique to be useful, it is necessary to implement a filter which will attenuate the previously mentioned interferences while not adding any significant distortion to the actual gastric waveform.

Some researchers have attempted to recover the transcutaneous electrogastrogram using a phase-locked-loop (PLL) [2,3]. The results obtained using this method are superior to those yielded by fixed digital filters, but the publications have dealt only with the recovery of the fundamental frequency component of the signal. There would seem to be a serious disadvantage in using PLL's to reconstruct an EGG waveform, because this task requires the recovery of the relative amplitudes and relative phase

shifts of the harmonic components of the signal. The PLL is capable of tracking a signal component with a time varying frequency, but the device does not allow for the direct recovery of the amplitude of the input signal [4]. Therefore, it does not seem likely that PLL's would be the best choice for reconstructing a transcutaneous EGG.

A better method of recovering the canine EGG has been published by Kentie et al [5,6]. This technique, which is the first published application of adaptive filtering to the EGG, provides significantly better noise suppression than the PLL method. However, the filter was not tested on the human EGG, and again the research was concerned only with recovery of the fundamental frequency component of the signal. In addition, the published results were obtained using extremely clean signals that did not require the special features of an adaptive filter.

These researchers also made two claims in their publication that were based upon incorrect assumptions. Both of these errors tend to reduce the effectiveness of the adaptive filter. First, they claim that a high (50th) order filter is necessary to satisfy the sampling theorem, but there seems to be no basis for making this statement. As will be shown in Chapter 2, the tracking error of the adaptive filter is directly proportional to the order of the filter. Therefore, it is imperative that the order of the filter be kept as low as possible while satisfying the

other constraints dictated by the theory of adaptive filtering.

The other erroneous assumption is that the output of the adaptive filter will become zero after convergence. In reality, the output of the filter as it is configured in this application will become a minimum, but will never become zero unless the EGG signal is identically zero. This fact is proven theoretically in Chapter 2. This assumption led Kentie et al to disable the adaptation of the filter after a finite number of iterations, which means that the automatic signal tracking capability of the adaptive filter was lost. If the fundamental frequency of the EGG was to drift after the adaptation was stopped, or if the characteristics of the interferences distorting the waveform were to change, the system would become useless.

A technique which represents a significant improvement over the Kentie method has been developed that will allow for the recovery of the fundamental frequency component of the human EGG as well as several harmonics. The adaptive filter described in this document will operate satisfactorily on very noisy signals, is of low order, and operates in a continuously adaptive mode which allows it to automatically track any drift in frequency and compensate for any changes in the nature of the distortion present in the transcutaneous signal. Since the EGG can be recovered non-invasively with

transcutaneous electrodes, all of the advantages of the surface-recovery procedure are retained.

# 2. Adaptive Filtering Theory

## 2.1. The Adaptive Filter

The theory behind adaptive filtering has been reasonably well developed in the literature. Much of the information has been published by Bernard Widrow [7-13], and the development in this chapter generally follows his publications.

The general form of the adaptive filter is shown in Fig. 2-1. There are two inputs : x is the actual input signal, and d is a training or reference input called the "desired response." Signal y is the output of the adaptive system W(z). The error signal z is formed as the difference between d and y

$$z_k = d_k - y_k \tag{2.1}$$

where the subscript k denotes the sample index. Thus, the error is zero when $d_k = y_k$, or when the output of the adaptive system is equal to the training signal. In practice, this is difficult to achieve because the desired response is usually not available. (If it was, the filter would probably not be necessary in the first place.) Therefore, the application of this type of filter depends upon the availability of a suitable training signal.

The block labelled W(z) is shown in more detail in Fig. 2-2. This configuration is nothing more than a simple transversal filter. The coefficients of W(z) are given the symbol w, and are assumed to be constant to

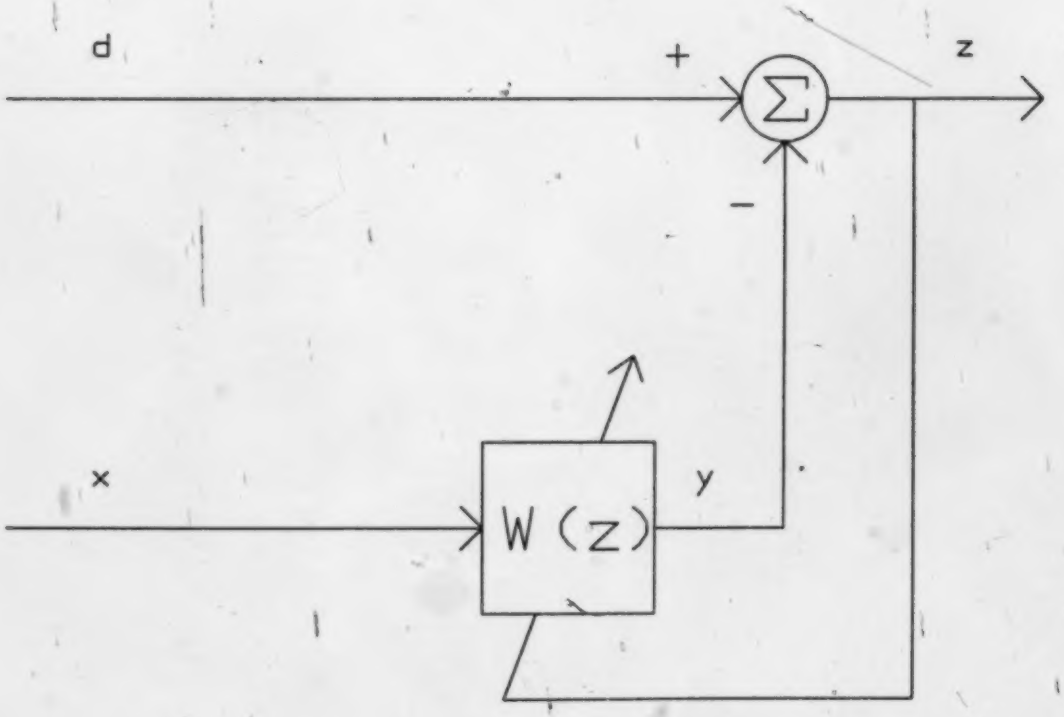


Fig. 2-1: The Adaptive Filter

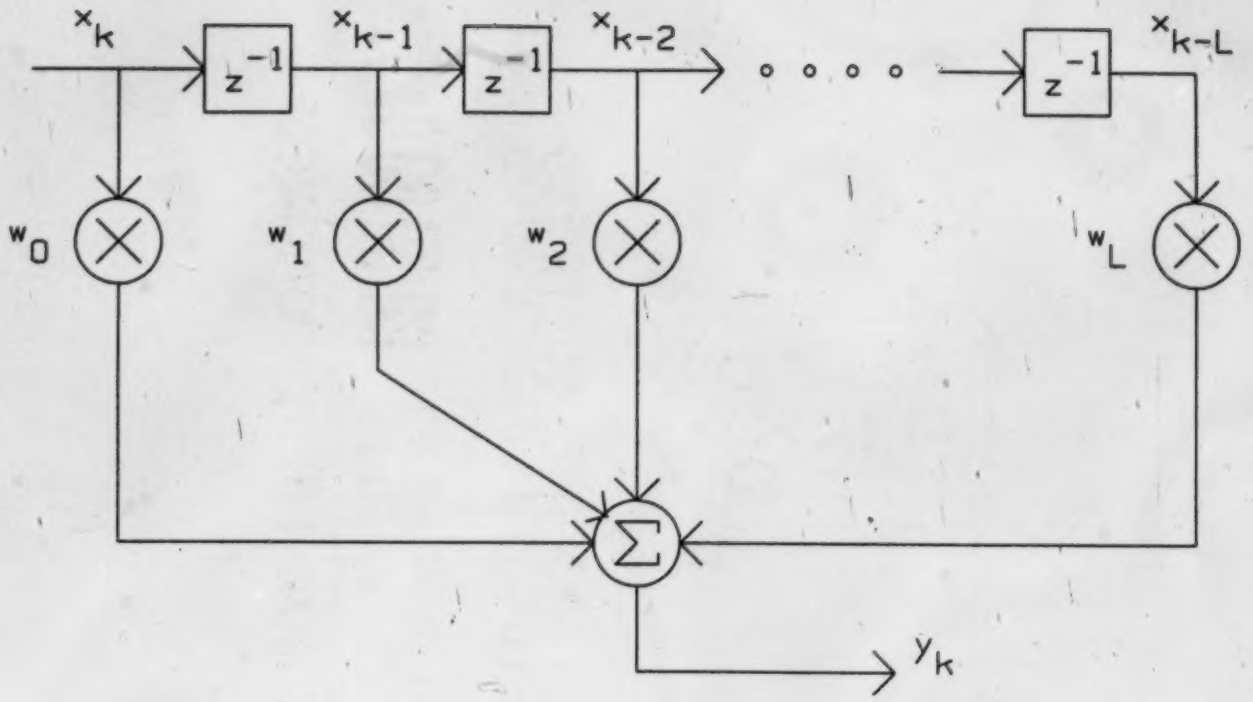


Fig. 2-2: The Transversal Filter

simplify the theoretical development (this has no effect on the generality of the results). From Fig. 2-2, the output $y_k$ of the transversal filter is given by

$$y_k = \sum_{l=0}^{L} w_l x_{k-l} \tag{2.2}$$

or in matrix-vector notation

$$y_k = \underline{W}^T \underline{X}_k = \underline{X}_k^T \underline{W} \tag{2.3}$$

where the input and coefficient vectors are given by

$$\underline{X}_k = [x_k \; x_{k-1} \; x_{k-2} \; \cdots \; x_{k-L}]^T \tag{2.4}$$

$$\underline{W} = [w_0 \; w_1 \; w_2 \; \cdots \; w_L]^T \tag{2.5}$$

and L is the number of unit delays in the transversal filter.

Substituting (2.3) into (2.1) yields

$$z_k = d_k - y_k = d_k - \underline{W}^T \underline{X}_k = d_k - \underline{X}_k^T \underline{W} \tag{2.6}$$

which is linear in $\underline{W}$. Squaring both sides of (2.6), we get

$$z_k^2 = d_k^2 + \underline{W}^T \underline{X}_k \underline{X}_k^T \underline{W} - 2 d_k \underline{X}_k^T \underline{W} \tag{2.7}$$

Equation (2.7) expresses the instantaneous squared error $z_k^2$ as a function of the input vector $\underline{X}_k$, the coefficient vector $\underline{W}$, and the training signal $d_k$.

Assuming that $z_k$, $d_k$ and $\underline{X}_k$ are statistically stationary, we can write the mean of (2.7) as

$$E[z_k^2] = E[d_k^2] + \underline{W}^T E[\underline{X}_k \underline{X}_k^T] \underline{W} - 2E[d_k \underline{X}_k^T] \underline{W} \tag{2.8}$$

where E[n] denotes the statistical mean of n. To simplify the notation, the following definitions are made :

$$\underline{R} = E[\underline{X}_k \underline{X}_k^T] \tag{2.9}$$

$$\underline{P} = E[d_k \underline{X}_k] \qquad (2.10)$$

The terms off the main diagonal in $\underline{R}$ are the cross-correlations of the components of the input vector $\underline{X}_k$, while the terms on the main diagonal are the mean squares of the input signal components at the sampling instants $k, k-1, \ldots, k-L$. The elements of $\underline{P}$ are the cross-correlations of the training signal $d_k$ and the elements of the input vector $\underline{X}_k$.

Substituting (2.9) and (2.10) into (2.8), we have

$$E[z_k^2] = E[d_k^2] + \underline{W}^T \underline{R} \underline{W} - 2\underline{P}^T \underline{W} \qquad (2.11)$$

which is an expression for the mean-squared error in the filter of Fig. 2-1. This expression is quadratic with respect to the coefficient vector $\underline{W}$. It can be shown [13] that the error surface described by (2.11) is a hyperparaboloid with a single, unique minimum. Therefore, with the choice of a suitable set of filter coefficients $\underline{W}$, it is theoretically possible to operate the filter at an optimal (Wiener) solution where the mean-squared error will be minimized.

When the minimum mean-squared error has been reached, the gradient of (2.11) will be zero :

$$\nabla = \frac{\partial E[z_k^2]}{\partial \underline{W}} = 2\underline{R}\underline{W} - 2\underline{P} = 0 \qquad (2.12)$$

which yields the coefficient weight vector

$$\underline{W}^* = \underline{R}^{-1} \underline{P} \qquad (2.13)$$

where $\underline{W}^*$ denotes the weight vector solution of (2.12) that minimizes the mean-squared error given by (2.11). Theoretically, (2.13) can be used to directly compute the optimal filter solution for any input signals d and x. However, this approach is impractical for three reasons. First, $\underline{R}$ and $\underline{P}$ may be large matrices, so the computations in (2.9) and (2.10) may be very time-consuming. Second, (2.13) requires the computation of $\underline{R}^{-1}$, which is also a lengthy task for a large matrix. Finally, in many filtering applications the input signals are not known a priori, in which case the computations of (2.9) and (2.10) and hence (2.13) are impossible. Therefore, to take advantage of the filter configuration of Fig. 2-1 it is necessary to employ some sort of algorithm to attempt to converge iteratively to the optimal (Wiener) solution $\underline{W}^*$ from some initial coefficient vector $\underline{W}_0$.

To accomplish this, the transversal filter of Fig. 2-2 can be replaced an "adaptive linear combiner" (ALC) of the type shown in Fig. 2-3 [10]. The ALC is in fact a type of transversal filter. However, in this case the filter coefficients are variables, and are updated iteratively at each sampling instant by an adaptive algorithm. The variable coefficients $\underline{W}_k$ are referred to as "adaptive filter weights" or simply "weights" to distinguish them from the more common constant coefficients $\underline{W}$.

Finally, it is interesting to examine the cross-

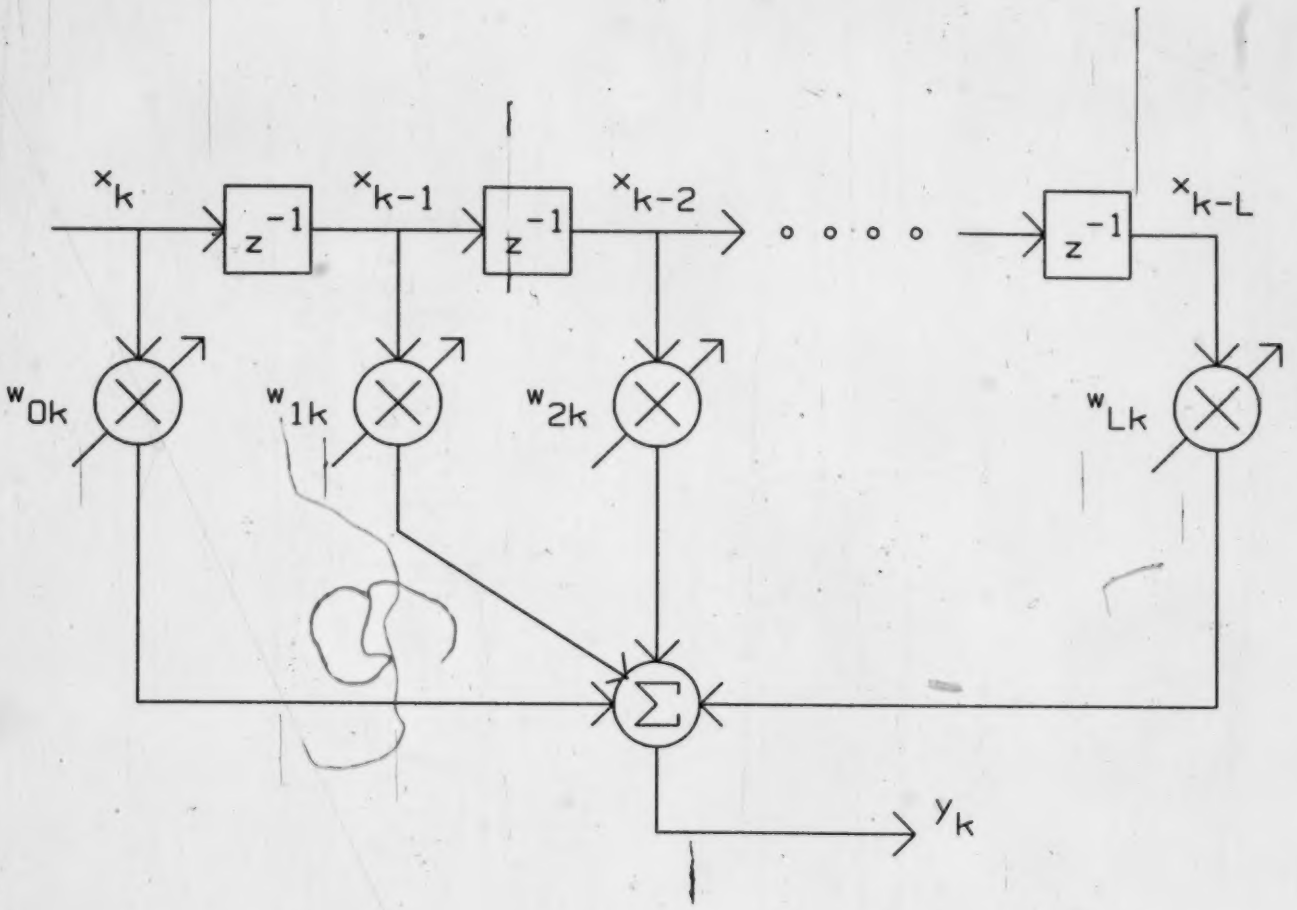


Fig. 2-3: The Adaptive Linear Combiner

correlation of the error signal $z_k$ and the input vector $\underline{X}_k$ after the adaptive filter has converged to the optimal solution $\underline{W}^*$. Multiplying both sides of the scalar equation (2.6) by $\underline{X}_k$ yields

$$z_k\underline{X}_k = d_k\underline{X}_k - \underline{X}_k\underline{X}_k^T\underline{W}_k \tag{2.14}$$

Taking the mean of (2.14), we get

$$\begin{aligned} E[z_k\underline{X}_k] &= E[d_k\underline{X}_k] - E[\underline{X}_k\underline{X}_k^T]\underline{W}_k \\ &= \underline{P} - \underline{R}\underline{W}_k \end{aligned} \tag{2.15}$$

where use has been made of the definitions (2.9) and (2.10). When $E[z_k\underline{X}_k]$ is minimized, $\underline{W}_k = \underline{W}^* = \underline{R}^{-1}\underline{P}$ and (2.15) becomes

$$\begin{aligned} E[z_k\underline{X}_k] &= \underline{P} - \underline{R}\underline{W}^* \\ &= \underline{P} - \underline{R}\underline{R}^{-1}\underline{P} \\ &= \underline{P} - \underline{P} \\ &= 0 \end{aligned} \tag{2.16}$$

Therefore, after convergence the error signal $z_k$ is (ideally) uncorrelated with the input vector $\underline{X}_k$.

In practice, the minimum of the error surface is usually not precisely reached for reasons that will be described in a later section. However, the weights do approach the minimum, and hence we can expect that the cross-correlation in (2.15) will be small.

## 2.2. The Adaptive Noise Canceller

A slight modification in the way the adaptive filter inputs are defined results in an extremely useful configuration called the Adaptive Noise Canceller (ANC)

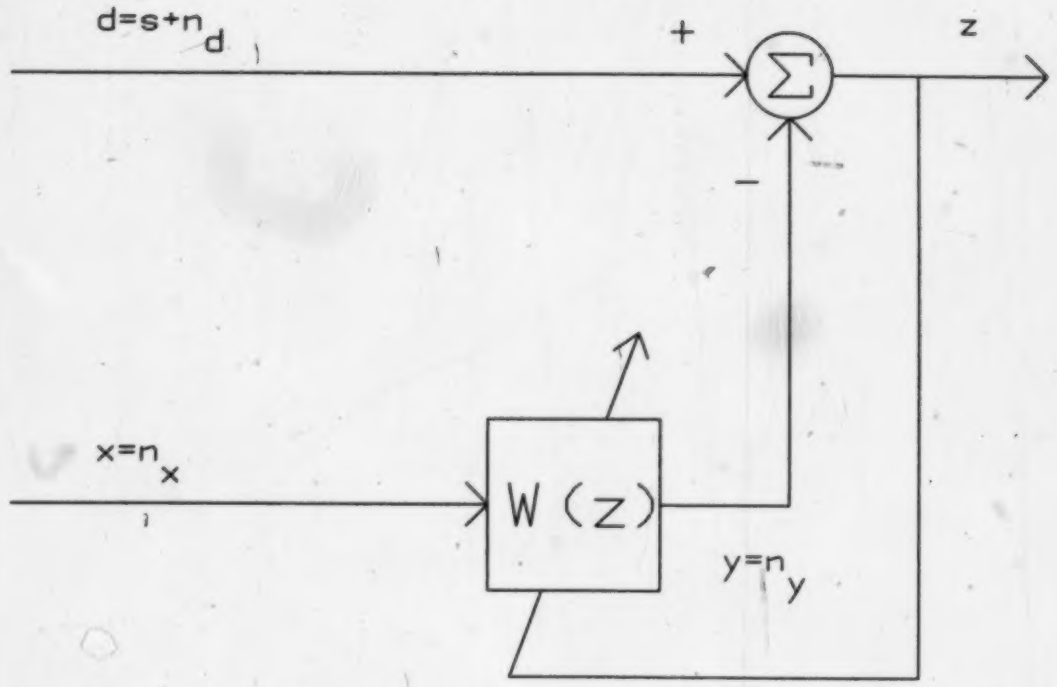


Fig. 2-4: The Adaptive Noise Canceller

[10]. This filter, which is shown in Fig. 2-4, uses a desired response d consisting of some signal s and additive noise $n_d$ which is uncorrelated with s

$$d = s + n_d \tag{2.17}$$

The input signal x consists of $n_x$, an estimate of $n_d$

$$x = n_x \tag{2.18}$$

We assume that s is uncorrelated with $n_x$, and that $n_d$ and $n_x$ are highly correlated. The ALC modifies $n_x$ to produce an output $n_y$

$$y = n_y \tag{2.19}$$

which is subtracted from d to produce the error signal z.

This configuration differs from the original Widrow adaptive filter in that there is noise present at the desired response input. In this case, the filter will attempt to minimize $E[z_k^2]$ by adjusting $n_y$ to cancel the signal d given by (2.17). The result of this will be that the noise $n_y$ will cancel $n_d$, and the signal appearing at z will be a least mean-squared error estimate of s.

To show this, we substitute (2.17) and (2.19) into (2.1) and get

$$\begin{aligned} z &= s + n_d - n_y \\ &= s + (n_d - n_y) \end{aligned} \tag{2.20}$$

The development of the previous section indicates that the mean-squared error is the parameter of interest. Therefore, we square both sides of (2.20) to obtain

$$z^2 = s^2 + (n_d - n_y)^2 + 2s(n_d - n_y) \tag{2.21}$$

Taking the mean of (2.21), we get

$$E[z^2] = E[s^2] + E[(n_d - n_y)^2] + 2E[s(n_d - n_y)] \quad (2.22)$$

Since we have assumed that s is uncorrelated with both $n_d$ and $n_y$, (2.22) reduces to

$$E[z^2] = E[s^2] + E[(n_d - n_y)^2] \quad (2.23)$$

which is another expression for the error surface of (2.11). The minimum of this surface is the point at which the mean-squared error is minimized. There are three signal components in the right-hand side of (2.23), but only one ($n_y$) is under the control of the filter. In attempting to minimize $E[z^2]$ the adaptive filter can not affect either s or $n_d$ since they are input signal components. The minimum of (2.23) is therefore

$$E[z^2]_{min} = E[s^2] + E[(n_d - n_y)^2]_{min} \quad (2.24)$$

This result means that, by minimizing the total output power, the ANC will minimize the output noise power. Therefore, the adaptive filter of Fig. 2-4 can recover the signal s by minimizing the mean-squared difference between the noise signals $n_d$ and $n_y$. The resulting output signal z will be a least mean-squared error estimate of s.

It is important to note that no mention has been made of bandwidth or cutoff frequencies on obtaining (2.24). The adaptive filter works to eliminate additive noise, and can remove noise components without affecting any signal component at the same frequency as the noise.

Equation (2.20) also reveals another interesting aspect of the behavior of the ANC. If the exact same signal is applied to both the d and x inputs, the output z

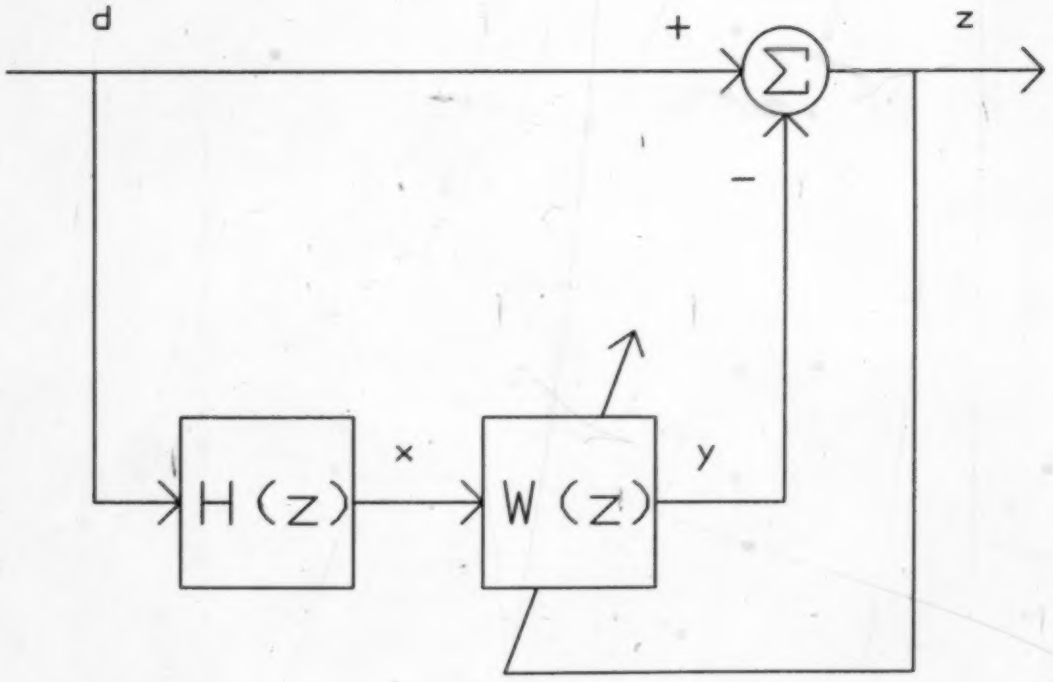


Fig. 2-5: The Adaptive EGG Filter

goes to zero. In other words, the ANC will "shut off" if it can not decrease the output power.

## 2.3. The Adaptive EGG Filter

The first application of an adaptive filter to the EGG was published by Kentie et al in 1981. The filter configuration is shown in Fig. 2-5, and is seen to be an ANC of the type shown in Fig. 2-4. The problem of obtaining a suitable input signal x has been solved by passing the EGG signal through a fixed band-reject filter H(z). The EGG is also applied directly to the desired response input d. After removing the fundamental frequency component of the EGG using H(z), the signal applied to the x input consists (ideally) of only the noise components present in the EGG. In reality, of course, there will be harmonics of the EGG as well as a (reduced) fundamental component at the output of H(z). In addition, a portion of the original noise will also be removed by H(z). The adaptive filter will still operate according to (2.23), however.

Employing the band-reject filter H(z) neatly eliminates the problem of deriving appropriate inputs for the adaptive filter. However, H(z) also limits two of the adaptive filter's valuable properties : application with no a priori information, and automatic signal tracking. The former is nullified because the approximate frequency of the fundamental component of the EGG must be known to

design H(z). The latter becomes a problem if the fundamental frequency of the EGG moves out of the rejection band of H(z). However, the nature of the EGG is well enough understood to allow the use of the filter of Fig. 2-5 with great success, as long as tachygastria does not occur.

Since the shape of the EGG waveform is of interest, the filter used by Kentie must be modified to allow for the recovery of several harmonics as well as the fundamental frequency component. This is accomplished quite simply by replacing H(z) by a cascade of band reject filters $H(z) = H_1(z)H_2(z)...H_h(z)$, where the filter with the subscript h removes to the harmonic at h times the fundamental frequency of the EGG. Each signal component removed by the filter bank will appear in the output signal z. The composite waveform thus obtained will be a least mean-squared error estimate of the significant part of the actual EGG.

In Chapter 1, it was stated that a bank of digital filters is unsuitable for recovery of the EGG, but the filter of Fig. 2-5 employs such a bank to derive the x input signal. However, the filters H(z) employed by the author are of low order and narrow bandwidth, so ringing and phase distortion are insignificant. The ALC will develop a transfer function that suppresses the signal components present at the x input, and will also partially correct for the magnitude and phase distortion caused by

the fixed digital filters as long as the distortion is small. Therefore, if the filters H(z) are designed such that the signal components of the EGG lie within the appropriate rejection bands, the signal appearing at the output will be unaffected by the distortion introduced by H(z).

## 2.4. The LMS Algorithm

There are several adaptive algorithms that have been used for updating the weight vector $\underline{W}_k$. Among these are algorithms based on the method of steepest descent and Newton's method.

For the case of the quadratic performance surface given by (2.11), the algorithm based on Newton's method

$$\underline{W}_{k+1} = \underline{W}_k - \frac{1}{2} \underline{R}^{-1} \nabla_k \qquad (2.25)$$

is particularly appealing because it always converges to the optimal solution in one iteration [13]! While this is an extremely appealing feature at first glance, the practical performance of a system operating under this algorithm is limited by two factors. First, the performance surface is usually non-stationary. A stationary performance surface would require that (2.25) be evaluated only once. In practical situations, the weights must be continuously updated. The second problem with this technique is that it is computationally complex. As (2.25) indicates, a matrix inversion and knowledge of the EXACT gradient of the performance surface are required

at each iteration. The inversion is a time-consuming operation, but more serious is the fact that the gradient is not usually known. Therefore, the gradient must be estimated, and the convergence time of the algorithm suffers.

The method of steepest descent does not attempt to converge in one step. Instead, it proceeds in the direction given by the negative of the gradient from some initial position $\underline{W}_0$ to the unique minimum given by $\underline{W}^*$

$$\underline{W}_{k+1} = \underline{W}_k + \mu(-\nabla_k) \tag{2.26}$$

For the quadratic performance surface, this equation can be solved using the gradient given by (2.12) to yield

$$\underline{W}_{k+1} = (\underline{I} - 2\mu\underline{R})\underline{W}_k + 2\mu\underline{R}\underline{W}^* \tag{2.27}$$

This equation involves a matrix inversion to compute $\underline{W}^*$, and contains a set of cross-coupled equations (in general, $\underline{R}$ is not a diagonal matrix.) Again, if the performance surface is stationary the matrix inversion is required only once. However, in practical situations this equation requires the computation of $\underline{R}$ and $\underline{W}^*$ at each iteration. The problems associated with these computations have already been discussed in Section 2.1.

In 1960, Widrow and Hoff proposed an extremely simple recursive algorithm to update the adaptive filter weights $\underline{W}_k$ that operates according to (2.24). The algorithm has become known as the Widrow-Hoff Least-Mean-Squares (LMS) algorithm, and the class of filters of the type shown in

Fig. 2-1 which operate according to this algorithm are known as LMS adaptive filters [8].

The LMS algorithm is based on the method of steepest descent, and obeys (2.26). It differs from that technique in that it estimates the gradient of the performance surface. From (2.11), the MSE at time k is given by

$$E[z_k^2] = E[d_k^2] + \underline{W}^T\underline{R}\underline{W} - 2\underline{P}^T\underline{W} \qquad (2.11)$$

For the LMS algorithm, this equation is approximated by

$$E[z_k^2] \simeq z_k^2 \qquad (2.28)$$

The validity of this assumption is demonstrated in [8] and [13]. The gradient estimate becomes [13]

$$\nabla_k = \frac{\partial z_k^2}{\partial \underline{W}_k} = 2z_k \frac{\partial z_k}{\partial \underline{W}_k} = -2z_k\underline{X}_k \qquad (2.29)$$

Using this estimate, (2.26) becomes

$$\underline{W}_{k+1} = \underline{W}_k + 2\mu z_k\underline{X}_k \qquad (2.30)$$

where $\mu$ is a constant that determines the stability and convergence rate of the algorithm, and is known as the "convergence factor" or the "convergence parameter".

Widrow has shown [8,13] that the LMS algorithm will converge if the following conditions are met :

$$0 < \mu < \frac{1}{tr[\underline{R}]} \qquad (2.31)$$

where $tr[\underline{R}]$ is the trace of the matrix $\underline{R}$ in (2.9), and is given by

$$tr[\underline{R}] = \sum_{l=0}^{L} x_{k-l}^2 \qquad (2.32)$$

The convergence time (in iterations or samples) of the LMS algorithm is approximately

$$T_{MSE} \simeq \frac{(L+1)}{4\mu tr[\underline{R}]} \qquad (2.33)$$

Another important parameter is what Widrow has named the "misadjustment" of the algorithm. The misadjustment M is defined as the "excess" mean-squared error divided by the minimum mean-squared error given by (2.24), and is approximated by

$$M \simeq \mu\, tr[\underline{R}] \qquad (2.34)$$

and is expressed as a dimensionless percentage [8,13].

To apply an LMS adaptive filter, (2.33) and (2.34) can be used to determine an approximate value of $\mu$ if $tr[\underline{R}]$ is known. In many cases, however, the adaptive filter is applied because its ability to learn the input signal eliminates the need for a priori information (which is required to compute $tr[\underline{R}]$). Thus, (2.33) and (2.34) are used only in off-line applications, and the selection of $\mu$ for real-time filtering is reduced to a trial and error procedure.

Finally, it is important to note that extensive comparisons of the three algorithms mentioned in this section have been made. For the quadratic performance

surface, the LMS algorithm has been shown in several publications to converge much faster than either Newton's method or the method of steepest descent. (These results are discussed in [13].) While the exact difference in performance depends on several factors, the LMS algorithm typically converges at a rate that can easily be hundreds or thousands of times faster than the other two algorithms when gradient estimation is employed. When this fact is coupled with the computational simplicity of (2.30), it is clear that the LMS algorithm is far superior to the other two techniques in applications that require an ANC of the type shown in Fig. 2-1.

## 2.5. Adaptive Filter Implementation

The LMS adaptive EGG filter described in Section 2.3 is one part of a multi-purpose signal processing package called ADF that has been developed by the author for use on IBM-XT and IBM-AT Personal Computers. The package also contains routines that perform fixed (non-adaptive) digital filtering, test signal generation, and disk file transfer operations for reading and writing data files. Graphs of time domain signals, frequency domain magnitude and phase spectra, correlation functions, filter transfer functions (including both the magnitude and phase response), and the adaptive filter training curve can be plotted either on the computer display or on a Hewlett

Packard HP7225B plotter. All of the results contained in this document have been obtained using this package.

The various functions are grouped into logical menus, and are in most cases accessed with a single keystroke. The entire ADF package is intended to be user-friendly while retaining maximum flexibility. As a result, the software is not limited to use in studying the application of the adaptive filter to processing the human electrogastrogram, but can be used with virtually any type of input data.

All of the patient records that have been used to demonstrate the adaptive filter were acquired by B. O. Familoni during preparation of his doctoral thesis [1], and are stored in computer data files. To analyze and process these records, the ADF software package reads a finite, user-selectable number of samples directly into the computer's Random Access Memory (RAM). All filtering operations are then performed "in memory", resulting in high-speed data processing.

Each of the four signals (d, x, y, and z) associated with the adaptive filter of Fig. 2-5 are stored in a unique double-precision array. This allows each signal to be examined graphically, and also provides the operator with the capability of performing various tests and then comparing the results. The computer can also save the value of any one of the adaptive filter's weights in another storage array during the filtering operation, and

the resulting "weight training curve" can be displayed graphically. This feature is invaluable in analyzing the performance of the adaptive filter.

All of the parameters (the number of weights, the convergence parameter $\mu$, and the definition of the input signals d and x) that determine the performance of the adaptive filter are under the control of the operator. Therefore, the filter can be operated in any mode, and can be used to process virtually any type of data.

The software can also calculate an estimate of the maximum value of $\mu$ that will guarantee convergence using (2.31). A default value of $\mu$, which is equal to ten percent of this maximum, is used by the adaptive filtering routine if no value is specified by the user. This default is usually a good starting point for filtering signals with no a priori information. Examination of a plot of the weight training curves will reveal whether this value of $\mu$ is too large or too small since the time constant $T_{MSE}$ given by (2.33) is inversely proportional to $\mu$ and the misadjustment M given by (2.34) is directly proportional to $\mu$.

One important aspect of an adaptive filtering procedure is the trade-off between fast convergence and small tracking error. Reducing the adaptive time constant by increasing $\mu$ will cause a proportional increase in the misadjustment, which produces a noisier output signal. On the other hand, minimizing the misadjustment will result

in a large time constant. Since the output of the filter is usually useful only after the filter has converged, a small time constant is desirable.

To allow for both a fast convergence rate and small tracking error, the input signal can be filtered using two (or more) passes. On the first pass, the weights are trained using a large value of $\mu$. The output signal is discarded. On the second (final) pass, $\mu$ is given a smaller value to reduce the misadjustment. However, since the weight vector is already close to the optimal solution $\underline{W}^*$, the time constant requirements are not of any concern. The output signal obtained on the second pass will be the best LMS approximation that the adaptive filter can produce. ADF saves the weight values after filtering is completed to support this method of filtering. The results presented in Chapter 5 of this document were all obtained using this technique.

Unfortunately, extension of the multiple-pass filtering method to an on-line system would be difficult because of the need for a priori information in determining the best values of u in each pass. However, for off-line filtering, this method provides the best means of recovering the EGG from the signal obtained using transcutaneous electrodes.

# 3. Waveshape Analysis

## 3.1. Effect of Signal Parameters on Waveshape

It is well known that all periodic functions can be represented mathematically as the sum of an infinite number of harmonically related sine and cosine waves [14]. Therefore, a periodic signal with any arbitrary waveshape can be formed by adding together an infinite number of sine and cosine waves. Such a sum is called a Fourier series. Of course, infinite sums are only useful in abstract mathematics. For engineering applications, an infinite sum can be approximated to a high degree of accuracy with a finite number of terms.

Any sine (or cosine) wave is completely defined by specifying three parameters: the amplitude, frequency, and phase. In a composite waveform, all three parameters must be known for each component in order for the waveform to be defined. If just one parameter of one component changes, the shape of the waveform can change significantly. To illustrate this fact, consider the composite waveform of Fig. 3-1. This signal consists of two sinusoids (fundamental plus one harmonic) with the

| Frequency (cpm) | Amplitude (mVpp) | Phase (degrees) |
|---|---|---|
| 3.75 | 100 | 0 |
| 7.50 | 50 | 90 |

Table 3-1: Signal Parameters for Fig. 3-1

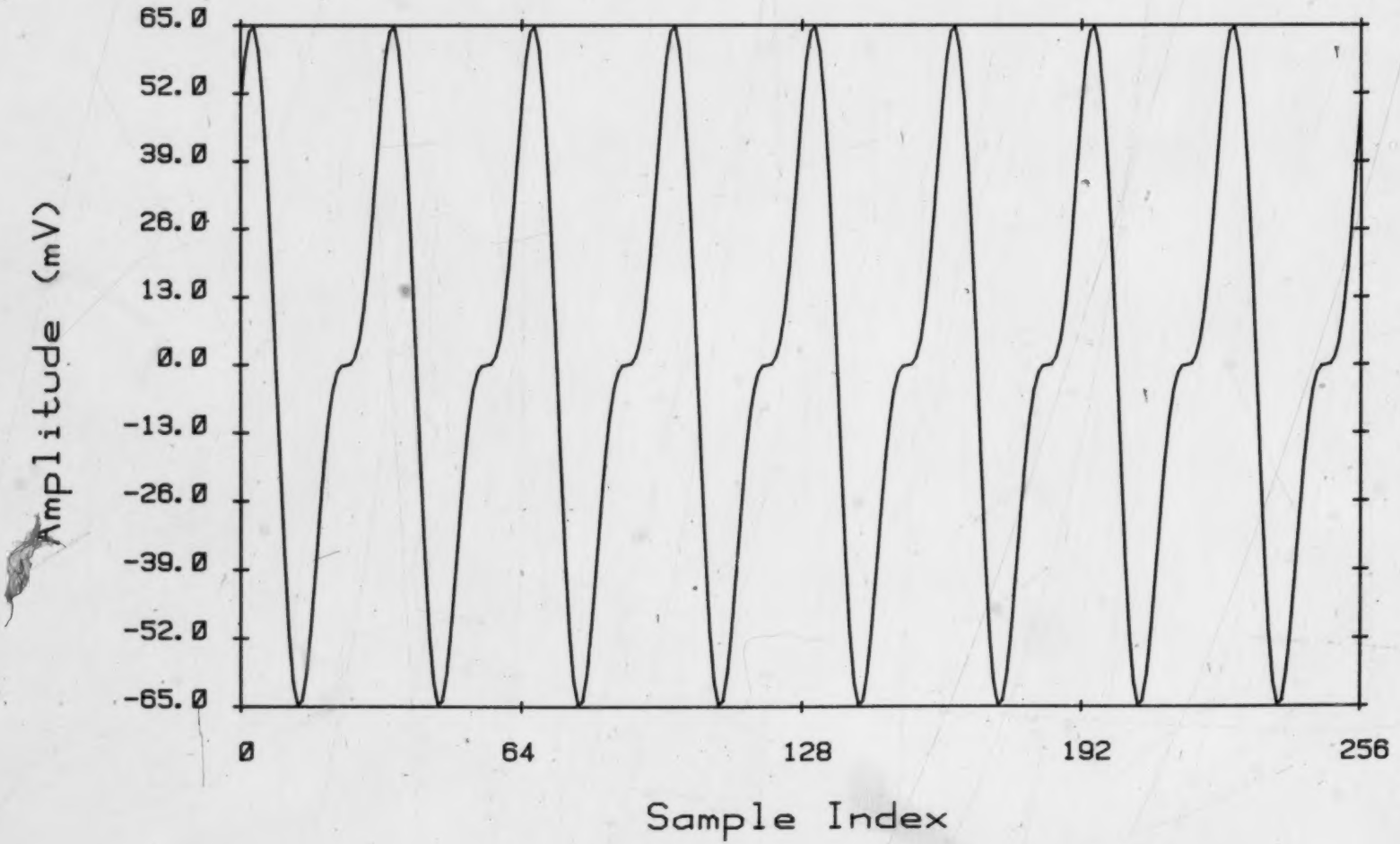


Fig. 3-1: An Example of a Waveshape

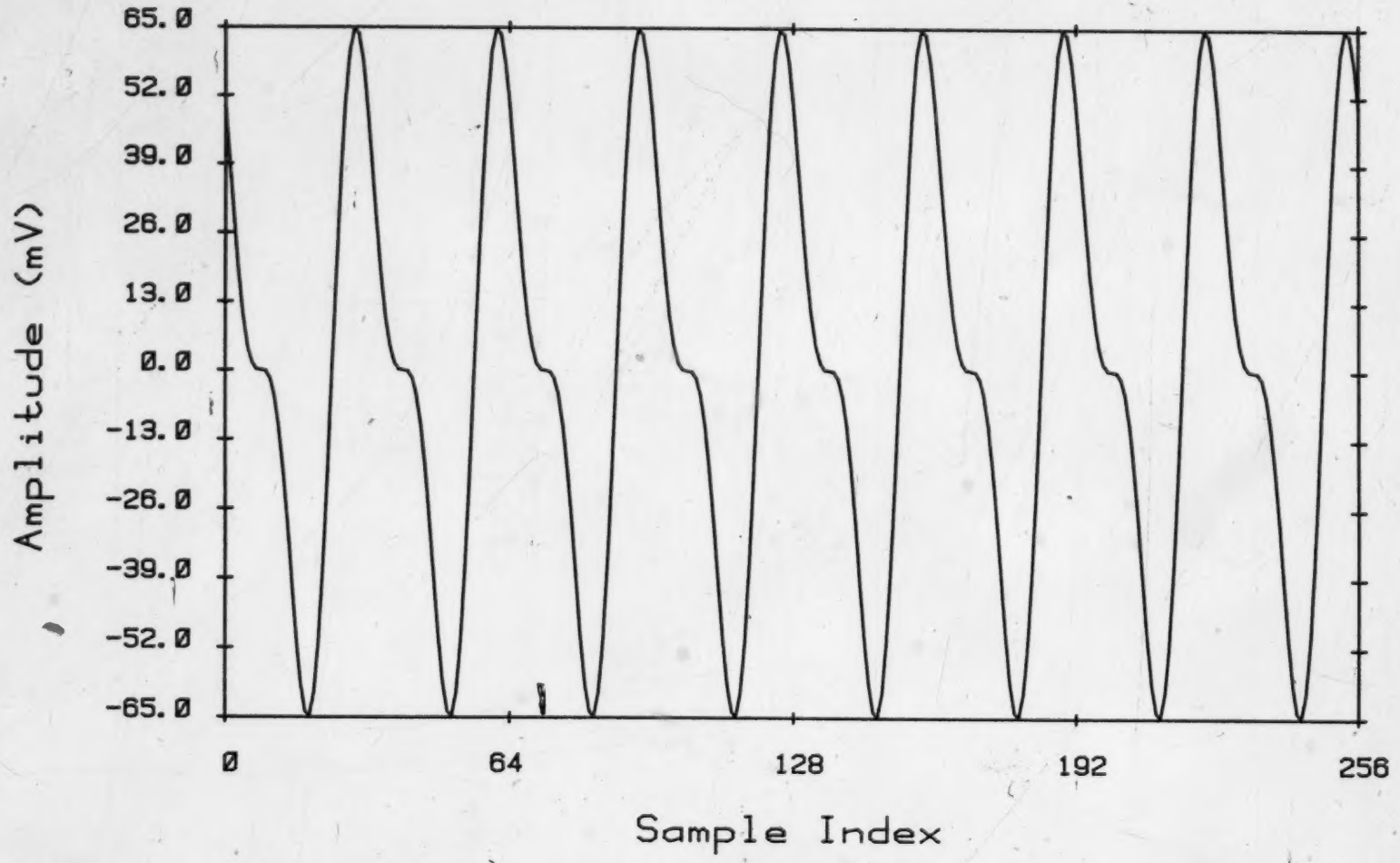


Fig. 3-2: An Example of Changing a Waveshape

parameters shown in Table 3-1. If we now change the phase of the harmonic by 180°, we obtain the signal of Fig. 3-2. Comparison of the two graphs clearly shows the drastic change in the shape of the waveform, a change caused by changing only one parameter of one component of the waveform.

In medical applications, there can be no degree of uncertainty in the interpretation of results obtained from patient records. Therefore, in order to properly recover the EGG using transcutaneous electrodes it is of the utmost importance that the parameters of the signal components are not altered by the filtering process because the shape of the waveform of interest.

### 3.2. FFT Analysis of Signal Parameters

The fast Fourier transform (FFT) is an extremely useful tool for analyzing the components of a periodic waveform [15]. The FFT provides both magnitude and phase information about a signal, and hence it is ideal for the study of signal parameters. However, practical FFT's must be computed using a finite number of samples. This means that the signal under consideration must be analyzed in sections or windows. All of the spectra in this document have been obtained using 256 point FFT's which have been pre-windowed using the half cycle sine function [15].

Since it is the EGG waveshape that is of interest, the FFT can be used to examine the signal after filtering

to determine how successful the filter was in recovering the signal without distorting the waveshape. The spectra computed using the FFT will report the magnitude and phase of each component of the waveform. These parameters can be compared with the corresponding parameters of the input signal. Any significant deviations in one or more of the parameters will indicate that the shape of the EGG waveform might have been changed by the filtering operation, and hence the results obtained from the signal will be of questionable value.

However, this type of comparitive analysis is not trivial. The results returned by the FFT are incomplete in the sense that they do not always precisely define the actual signal. Instead, they describe only that portion of the signal which lies within the 256 sample window of the transformation. The assumption here is that the signal within the window repeats itself with a periodicity of 256 samples both before and after the window under consideration. In practice, this is rarely the case, and hence the spectra generated using the FFT must be interpreted with care.

### 3.3. Limitations of FFT Analysis

There is a condition which must be satisfied if a signal is to be completely defined by the FFT. It concerns the frequencies of the components that make up the signal, and affects both the magnitude and phase

spectra reported by the FFT in a single window.

There is a set of discrete frequencies associated with any FFT, and the spectrum returned by the FFT defines the magnitude and phase at each frequency in the set. This set of frequencies is generated by the following equation :

$$f_i = \frac{f_s * i}{N} \quad ; \quad i = 0 , 1 , \ldots , \frac{N}{2} - 1 \qquad (3.1)$$

where $f_s$ is the sampling frequency and N is the number of points in the FFT. These frequencies are usually referred to as "bins" in the signal processing literature. For example, in an 256 point FFT with a sampling frequency of 120 cpm, the frequencies in cpm are given by

$$f_i = \frac{120 * i}{256} = 0.46875 * i \qquad (3.2)$$

Any sinusoid that exists at one of these discrete frequencies will fall exactly into one of the bins, and hence its magnitude and phase will be accurately reported by the FFT. However, any sinusoid at a frequency not included in this set will not be accurately defined by the FFT because it falls between two of the bins. This means that the magnitude and phase of the main lobe of the sinusoid are not reported by the FFT due to the discrete nature of the spectral information generated by the transformation. Instead, the FFT will report magnitudes and phase angles in the two adjacent bins that are some

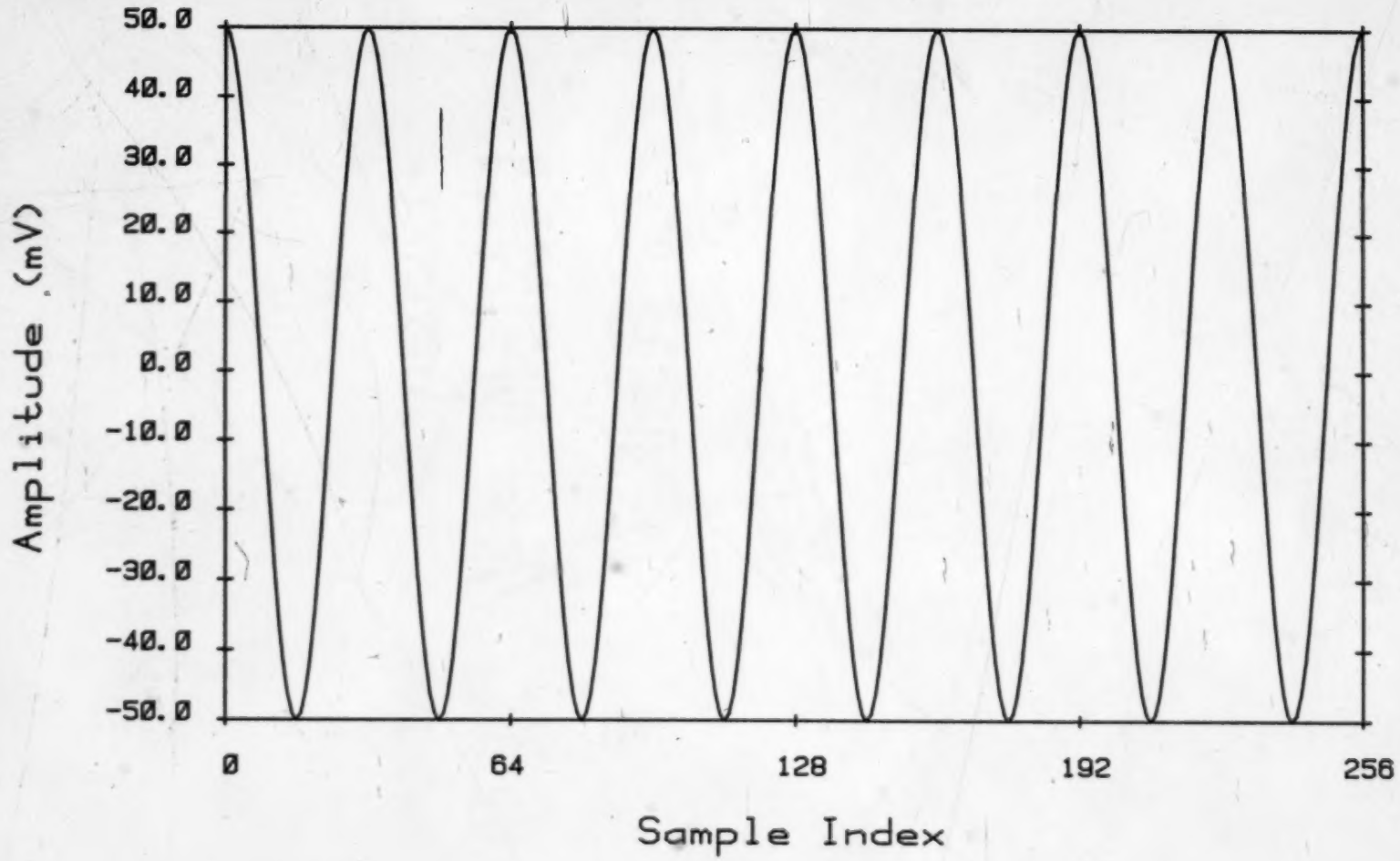


Fig. 3-3: A 3.75 cpm Sine Wave

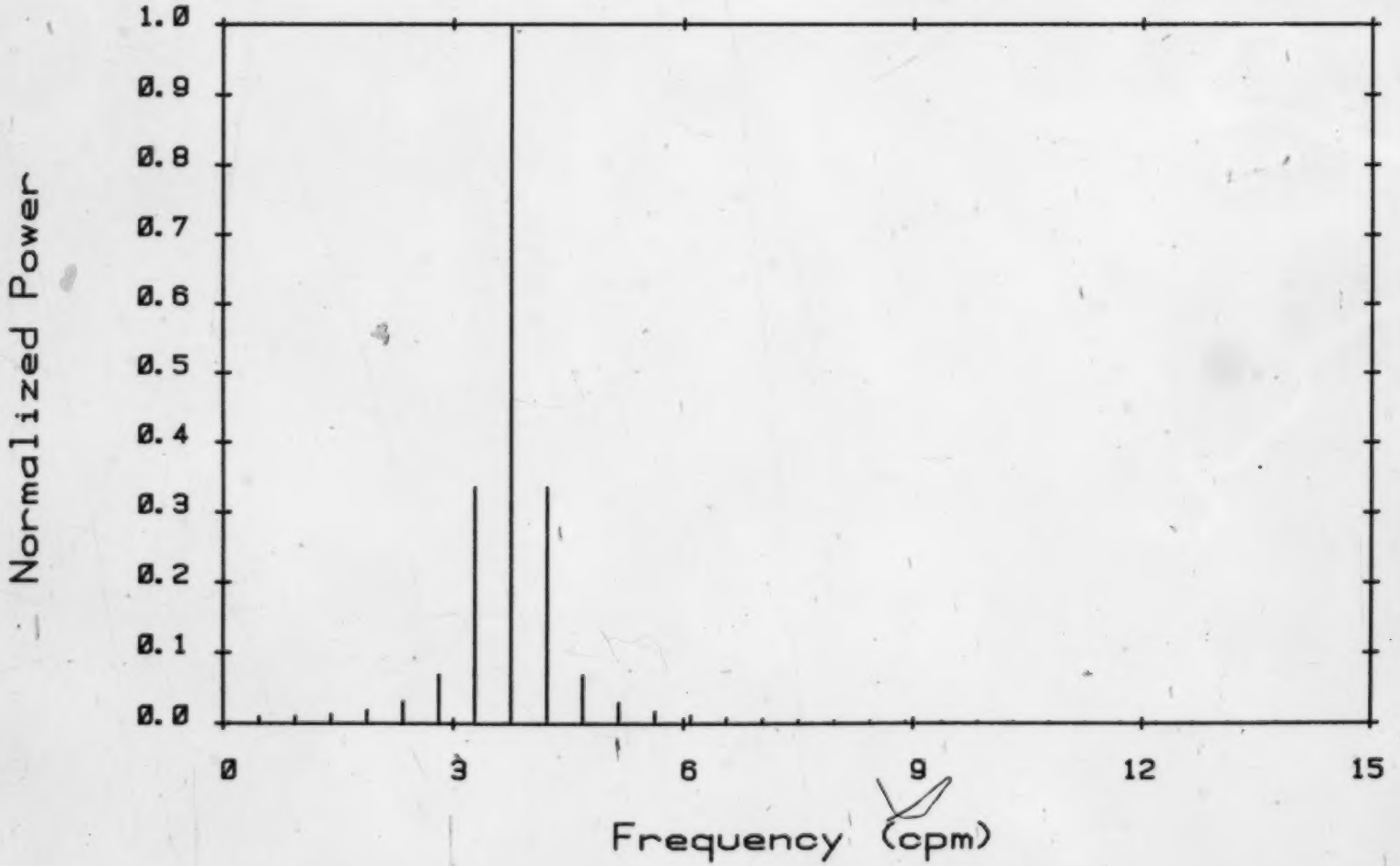


Fig. 3-4: Magnitude Spectrum of Fig. 3-3

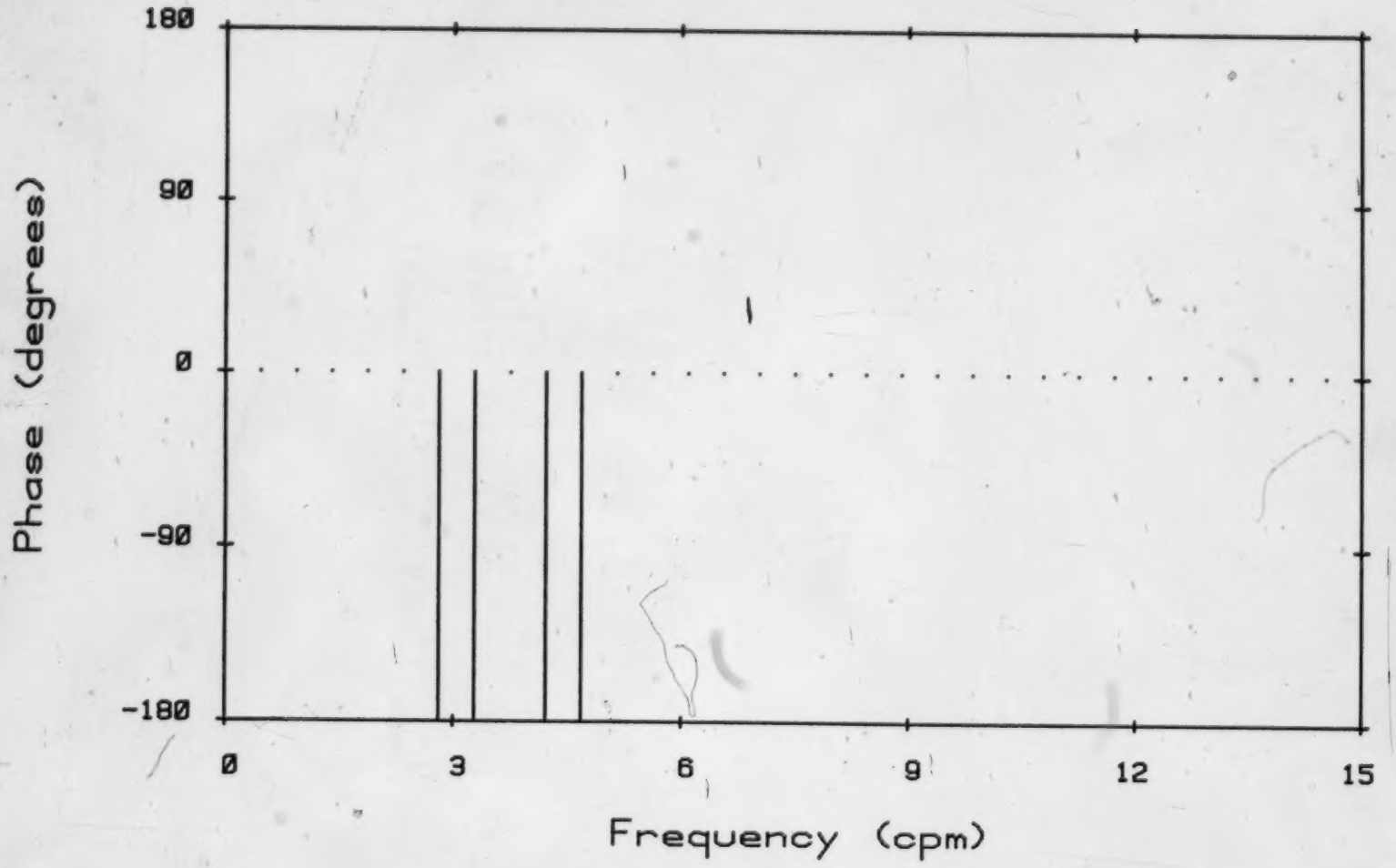


Fig. 3-5: Phase Spectrum of Fig. 3-3

fraction of the actual main-lobe values.

To illustrate this point, consider the FFT of a simple sine wave. The signal is shown in the time domain in Fig. 3-3, and the magnitude and phase spectra returned by the FFT are plotted in Figs. 3-4 and 3-5. (For each FFT presented in this document, only a portion of the phase spectrum is shown. Any spectral component with a magnitude less than some arbitrary level has its phase angle set to zero. This level is usually set to 5% of the magnitude of the largest spectral component. This technique cleans up the phase spectrum by ignoring the phase angles of insignificant signal components, and is necessary because the FFT returns a phase angle even for bins in which the magnitude is zero.) The parameters of the sine wave are given in Table 3-2. This sine wave falls exactly into the eighth bin of the 256 point FFT when the sampling frequency is 120 cpm, because from (3.2) we have $f_8 = 0.46875 * 8 = 3.75$ cpm. Therefore, the FFT

| Frequency (cpm) | Amplitude (mVpp) | Phase (degrees) |
|---|---|---|
| 3.75 | 100 | 0 |

Table 3-2: Signal Parameters for Fig. 3-3

| Frequency (cpm) | Amplitude (mVpp) | Phase (degrees) |
|---|---|---|
| 3.0 | 100 | 0 |

Table 3-3: Signal Parameters for Fig. 3-6

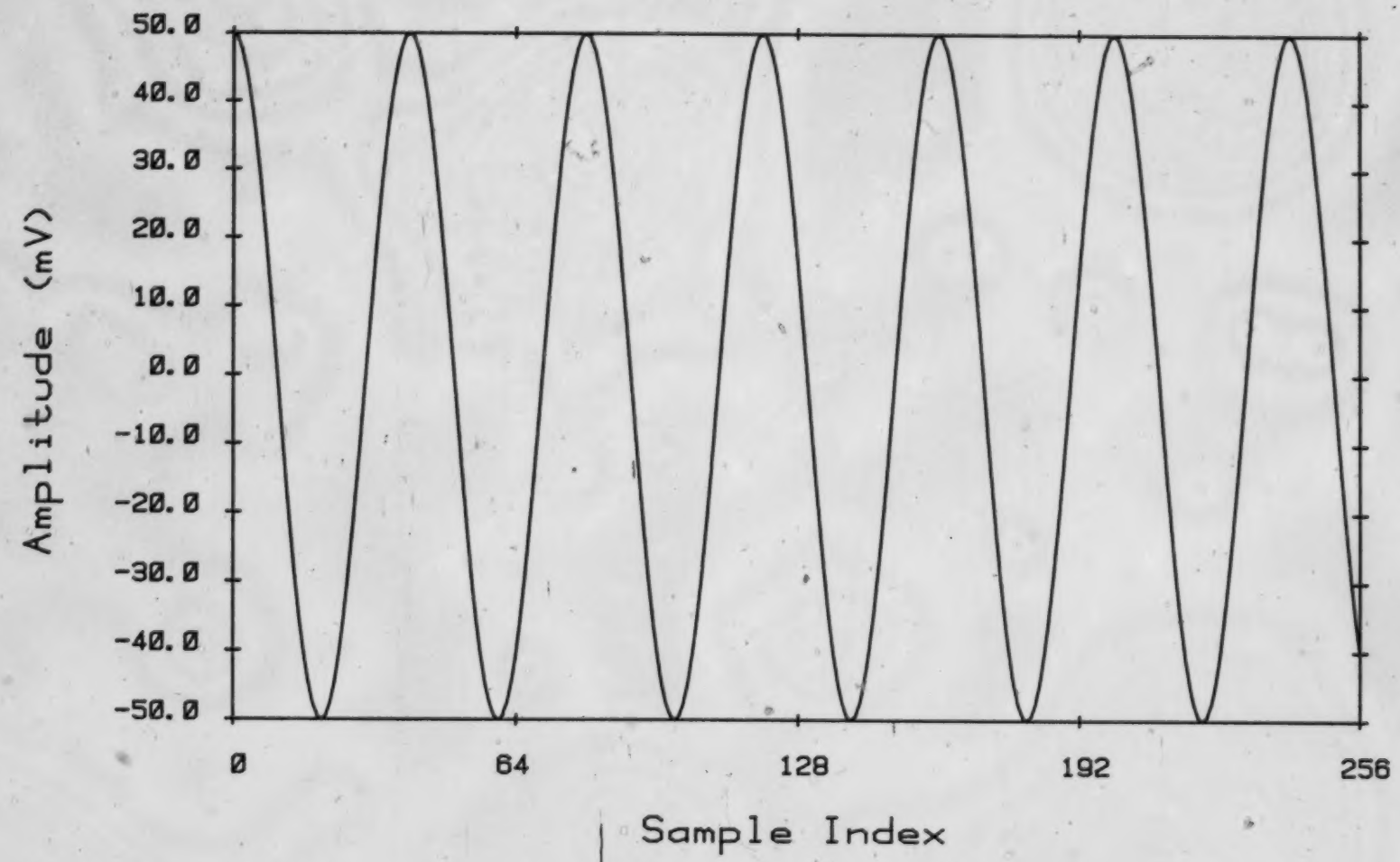


Fig. 3-6: A 3.0 cpm Sine Wave

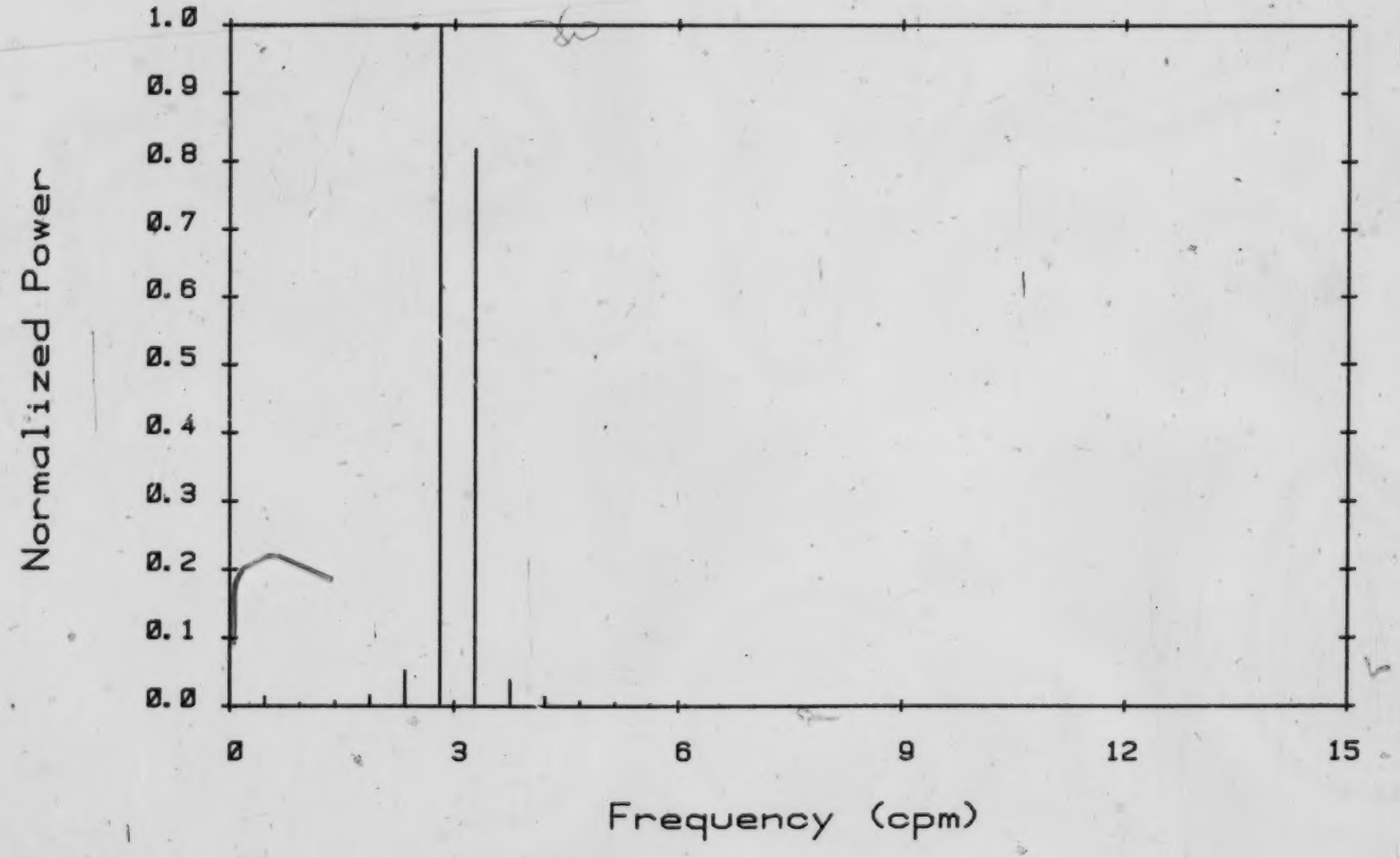


Fig. 3-7: Magnitude Spectrum of Fig. 3-6

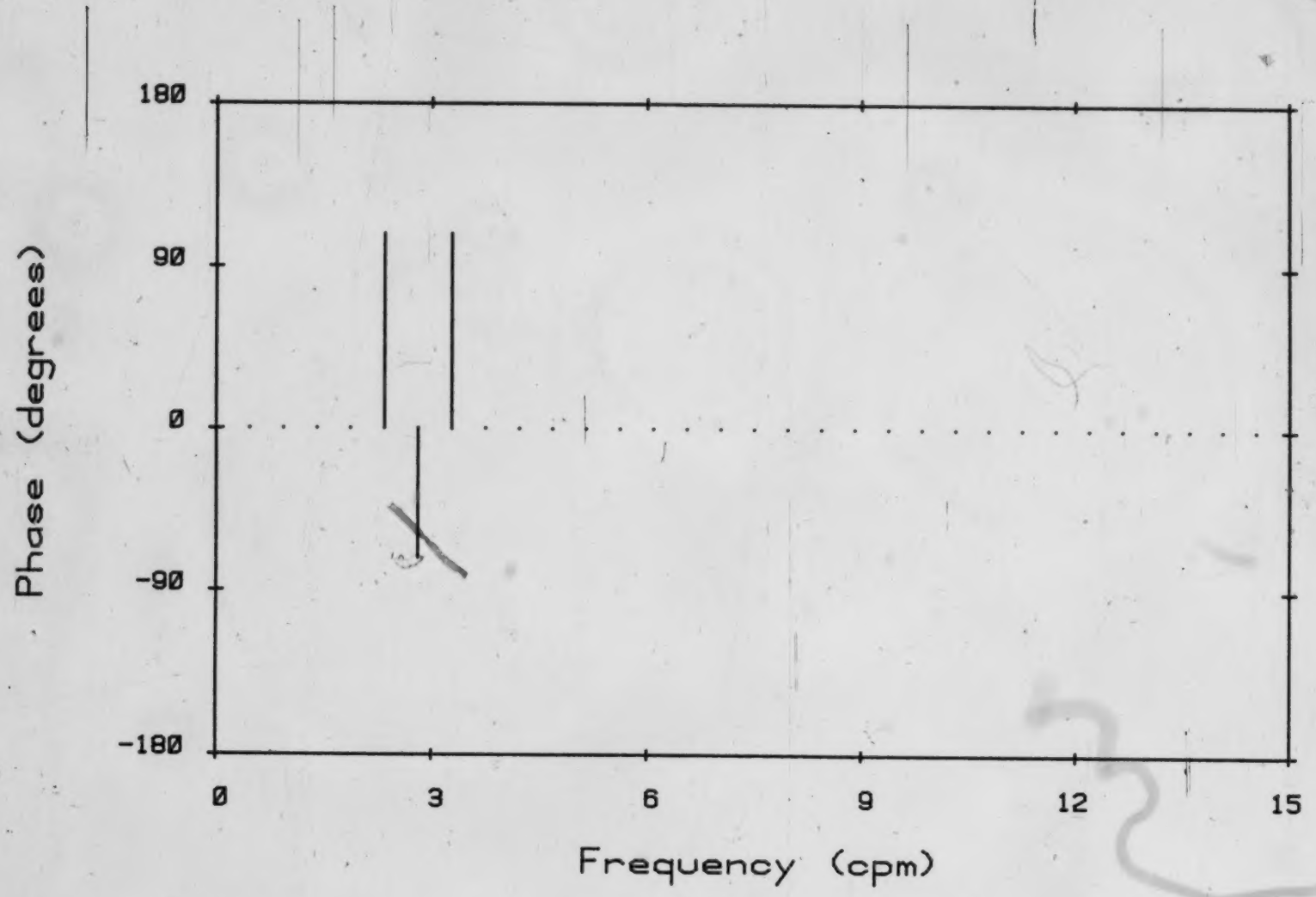


Fig. 3-8: Phase Spectrum of Fig. 3-6

reports the exact magnitude and phase of the sinusoid in the eighth bin of Figs. 3-4 and 3-5, respectively.

However, a sinusoid at 3.0 cpm falls between bin six ($f_6$ = 2.8125 cpm) and bin seven ($f_7$ = 3.28125 cpm). Therefore, the FFT will return misleading results. This case is illustrated in Figs. 3-6, 3-7 , and 3-8. The parameters of the sine wave are listed in Table 3-3. The magnitude and phase spectra of this sinusoid do not accurately define the parameters of the actual sinusoid.

Another aspect of this phenomenon, which is commonly referred to in the signal-processing literature as the "picket-fence effect", becomes important in waveshape analysis because it is necessary to obtain detailed information about the parameters of each harmonic in a signal. Again, we consider the case of a sinusoid that falls exactly into a bin. If we now add to the sinusoid one of its harmonics, (3.1) requires that the frequency of the harmonic must also fall exactly into one of the bins (as long as its frequency is less than one half of the sampling frequency). Therefore, the FFT will report the exact magnitude and phase for each component in the composite signal.

However, if the frequency of the fundamental sinusoid does not satisfy (3.1), then the frequency of the harmonic probably will not fall into one of the bins either (although it could). Let the fundamental frequency be designated by the symbol $f_1$ and the harmonic frequency at

n times $f_4$ be given the symbol $f_n$. If $f_1$ is $\Delta f$ Hertz lower (higher) than the nearest bin frequency $f_{b1}$

$$f_1 = f_{b1} \pm \Delta f \tag{3.3}$$

then $f_n$ will be $n\Delta f$ Hertz lower (higher) than the bin frequency $f_{bn} = nf_{b1}$

$$\begin{aligned} f_n = nf_1 &= n(f_{b1} \pm \Delta f) \\ &= nf_{b1} \pm n\Delta f \\ &= f_{bn} \pm n\Delta f \end{aligned} \tag{3.4}$$

Of course, the FFT can only report the magnitude and phase at the frequencies given by (3.1). Therefore, we know the magnitude and phase at $f_{b1}$ and $f_{bn}$, but not at $f_1$ and $f_n$. In fact, the ratio of the magnitudes of the components at $f_1$ and $f_{b1}$ will be different than the corresponding ratio of the components at $f_n$ and $f_{bn}$.

Hence, the condition that must be satisfied if the FFT is to yield accurate results is that the frequency of each component of the signal under consideration must satisfy (3.1). This condition can be met in some cases by increasing the size of the FFT, but for biological signals this solution could require a very large (and impractical) window size. In many applications, (3.1) represents an unnecessarily stringent restriction. To accurately reconstruct a waveshape, however, it is an important consideration.

### 3.4. Spectral Comparison

The most obvious method of determining whether a signal has been distorted by filtering is to compare the spectra of the input and output signals. Comparing the magnitude spectra (at the same point in time), for example, will reveal the changes (if any) in the magnitude of each component of a signal. Similar comparison of the phase spectra could also be made.

Unfortunately, this technique is not very useful for waveshape analysis. The reason for this is simple. Consider the case of a sine wave distorted by additive random noise, and assume that at the time under consideration a noise component exists at the same frequency as the sinusoid. If the FFT is now computed, the bin corresponding to the frequency of the sinusoid (and the noise) will report the magnitude and phase of the total signal.

Now assume that the noise has been completely removed by some ideal filter that does not affect the sine wave. The FFT of the output will then report the actual magnitude and phase of the sinusoid in the same bin. Comparison of the spectra before and after filtering will indicate changes in the magnitude and phase of the signal. Even though the sinusoid was unaffected by the filter, the spectral information could be interpreted as an indication of distortion.

This argument can be extended to the case of EGG

signals. In Chapter 1 it was shown that the magnitudes of the third and fourth harmonics can be comparable to the magnitude of the interference. It is easy to see that the spectral comparison technique can not be used to analyze the distortion of these components when they are buried in noise. Of course, this problem is even more serious given that a ideal noise-cancelling filter does not exist.

### 3.5. Apparent Phase Shift

There is another aspect of the picket-fence effect that becomes important when analyzing a signal. The phase angle of a signal as reported by the FFT is measured relative to the time at which the FFT window starts. This is no problem for sinusoids at the frequencies defined by (3.1), because each of these $f_i$ corresponds to a period that divides into the FFT window an integer number of times (cf. Fig. 3-3). Therefore, FFT's computed at windows starting $\pm N$, $\pm 2N$, $\pm 3N$, etc., will always report the same magnitude and phase. However, sinusoids at frequencies not given by (3.1) will not divide into the N sample window an integer number of times (cf. Fig. 3-6). Therefore, the FFT's computed in adjacent windows will report different phase spectra for the signal, even in cases where the actual phase is constant. Since the phase spectrum in this case is somewhat difficult to interpret anyway (because the frequency does not correspond to a

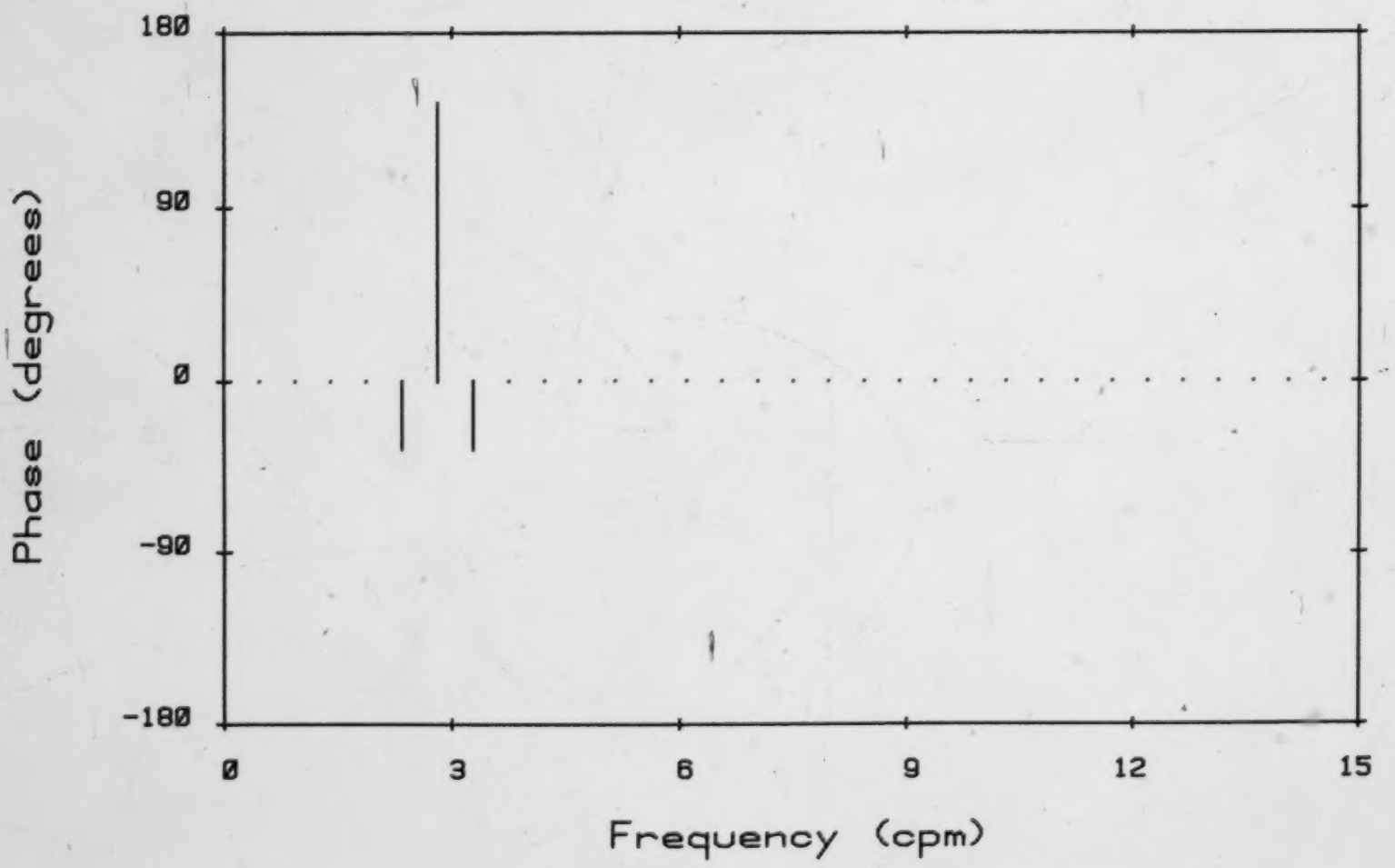


Fig. 3-9: Phase Spectrum in the Next Window

bin), the results can be quite misleading.

This situation is illustrated by comparing the phase spectrum of Fig. 3-8 with that of Fig. 3-9, which shows the phase of the sinusoid of Fig. 3-6 in the "next" 256-sample window (starting 256 samples after the start of the first 256-sample window). Each graph reports a different phase spectrum for the signal, even though the phase angle of the sinusoid is actually constant. The magnitude spectrum, of course, remains constant since it is independent of the time of observation, and will always appear as shown in Fig. 3-7 for this particular signal.

This "apparent phase shift" is a predictable constant in each bin because it depends only upon the size of the observation window and the period (and hence the frequency) of the actual signal. For a signal of constant frequency, the apparent phase shift can be calculated using the relation

$$\Delta\phi = T_L * 360^{\circ} \qquad (3.5)$$

where $T_L$ is the "lost" portion of a complete period (the portion of the last cycle that is truncated by the FFT window). This equation gives the number of degrees difference between the phase reported by the FFT in any

| Frequency (cpm) | Amplitude (mVpp) | Phase (degrees) |
|---|---|---|
| 3.0 | 50 | 0 |
| 6.0 | 50 | 0 |

Table 3-4: Signal Parameters for Table 3-5

two adjacent windows for the frequency component whose period is used to find $T_L$. Of course, (3.5) only applies to stationary periodic signals.

To investigate the apparent phase shift phenomenon, consider a test signal consisting of two components with the parameters given in Table 3-4. In this case, neither the fundamental nor the harmonic satisfy (3.1). Therefore, both components should exhibit an apparent phase shift. The phase angles reported by the FFT in bin six ($f_6$ = 2.8125 cpm) and bin twelve ($f_{12}$ = 5.625 cpm) are given in Table 3-5. These data are from the first seven 256-sample windows in the data file. In this table, $\phi_1$ ($\phi_2$) is the phase of the sinusoid at 2.8125 (5.625) cpm, and $\Delta\phi_1$ ($\Delta\phi_2$) is the apparent change in phase of $\phi_1$ ($\phi_2$) and is calculated as $\phi_1$ ($\phi_2$) in the current window minus $\phi_1$ ($\phi_2$) in the previous window.

As expected, the apparent phase shifts $\Delta\phi_1$ and $\Delta\phi_2$ are constant since the actual phase angles of the sinusoids do not change. The FFT reports a phase shift because the periods of the sinusoids do not divide evenly

| $\phi_1$ | $\phi_2$ | $\phi_2 - \phi_1$ | $\Delta\phi_1$ | $\Delta\phi_2$ |
|---|---|---|---|---|
| $-72^o$ | $-144^o$ | $-72^o$ | | |
| $144^o$ | $-72^o$ | $-216^o$ | $216^o$ | $72^o$ |
| $0^o$ | $0^o$ | $0^o$ | $216^o$ | $72^o$ |
| $-144^o$ | $72^o$ | $216^o$ | $216^o$ | $72^o$ |
| $72^o$ | $144^o$ | $72^o$ | $216^o$ | $72^o$ |
| $-72^o$ | $-144^o$ | $-72^o$ | $216^o$ | $72^o$ |
| $144^o$ | $-72^o$ | $-216^o$ | $216^o$ | $72^o$ |

Table 3-5: Results of Apparent Phase Shift Test

into the 256-sample FFT window. Equation (3.5) can be used to verify the experimental values in Table 3-5. The 3.0 cpm sinusoid has a period of $T_1$ = 20 seconds = 40 samples when $f_s$ = 120 cpm. Therefore, 256 / 40 = 6.4 periods will fit into the 256-sample window. The window truncates 60% of the incomplete period, so from (3.5) the apparent phase shift is

$$\Delta\phi_1 = 0.6 \text{ periods} * 360^\circ/\text{period} = 216^\circ \qquad (3.6)$$

which is the experimental result. The harmonic at 6.0 cpm has a period of $T_2$ = 10 seconds = 20 samples. In this case, 256 / 20 = 12.8 periods fit the FFT window. Again, we use (3.5) to compute the apparent phase shift :

$$\Delta\phi_2 = 0.2 \text{ periods} * 360^\circ/\text{period} = 72^\circ \qquad (3.7)$$

which confirms the experimental result.

Similar results were obtained for a triangle wave generated as the sum of three sinusoids. The signal parameters are given in Table 3-6. As was the case for the previous signal, the apparent phase shifts of the 3.0 cpm and 6.0 cpm sinusoids are $216^\circ$ and $72^\circ$ ($432^\circ = 360^\circ + 72^\circ$), respectively. (The apparent phase shifts are again measured in bins six and twelve.) However, in this case the actual phase angles of the sinusoids are not zero. More important is the fact that the sinusoids are not in phase. The conclusion drawn from this is that the apparent phase shift is independent of the actual (relative) phase angles of the components.

From Table 3-6, we see that the sinusoid at 9.0 cpm

exhibits an apparent phase shift of $-72^{\circ}$. The period of this component (for $f_s$ = 120 cpm) is $T_3 \simeq 6.67$ seconds $\simeq$ 13.13 samples. Therefore, about 19.2 cycles will fit into the 256-sample FFT window. From (3.5), the apparent phase shift is

$$\Delta\phi_3 = 0.8 \text{ periods} * 360^{\circ}/\text{period} = 288^{\circ} \qquad (3.8)$$

and $288^{\circ} = 360^{\circ} - 72^{\circ}$, which agrees with Table 3-6.

Another interesting aspect of this is that the apparent phase shift of a harmonic at n times the fundamental frequency is n times the apparent phase shift of the fundamental. For example, from Table 3-6 we have $\Delta\phi_2 = 2 * \Delta\phi_1 = 432^{\circ} = 360^{\circ} + 72^{\circ}$. Also, $\Delta\phi_3 = 3 * \Delta\phi_1 = 648^{\circ} = 720^{\circ} - 72^{\circ}$.

From these experiments, the following conclusions can be made:

a) Windowing a signal prior to computing the FFT causes an apparent phase shift. This is due to the truncation of a portion of the last cycle in the window.

b) This apparent phase shift is constant in each window, and is independent of the actual relative phase shifts of the harmonics. It depends on the size of the —

| Frequency (cpm) | Amplitude (mVpp) | Phase | $\Delta\phi$ |
|---|---|---|---|
| 3.0 | 100 | $-135^{\circ}$ | $216^{\circ}$ |
| 6.0 | 35 | $180^{\circ}$ | $72^{\circ}$ |
| 9.0 | 12 | $135^{\circ}$ | $-72^{\circ}$ |

Table 3-6: More Apparent Phase Shift Results

FFT window and the period of the sinusoid under consideration.

It might seem possible at this point to determine whether or not a waveform has been distorted by monitoring the apparent phase shift of each component of a signal both before and after filtering. However, this technique simply does not work. When a white noise signal with an amplitude of only 10 mVpp is added to the signal defined in Table 3-4, the phase angles reported by the FFT can vary dramatically. This is due to the fact that a noise component with a small magnitude can have large phase angle. As a result, the apparent phase is no longer constant, and varies in an unpredictable fashion. Measuring and analyzing the apparent phase shift in actual EGG signals turns out to be completely useless. Therefore, this technique can not be considered reliable enough to ensure that the EGG waveform is not altered by the filtering process.

### 3.6. Slope Identification

None of the spectral analysis techniques discussed in this chapter provide a good indication of the relative slopes of the leading and trailing edges of the EGG waveform. In most cases, inspection of graphs of the signals after filtering will clearly show this information. However, in some cases the amplitudes of the harmonics are very small, and the filtered EGG can appear

almost sinusoidal in shape. Also, if the patient record is badly distorted, the output of the filter might not be clean enough to provide conclusive information about the signal. Therefore, visual inspection can be difficult.

A very simple technique can be used to reduce or eliminate this problem. It involves comparing the number of sample intervals in which the slope of the waveform is positive ("plusses") to the number of intervals during which the slope is negative ("minuses"). The magnitude difference between the plusses and minuses (the "plus/minus difference") is an indication of which slope (positive or negative) predominates in the record. Dividing the plus/minus difference by the total number of samples gives the percentage of the record in which the dominant slope appears (the "plus/minus percentage").

Several examples will demonstrate the usefulness of this technique. First, consider a perfect sine wave. In exactly one cycle of any sinusoid, the plus/minus percentage must be exactly zero since there are an equal number of positive slope and negative slope intervals.

Next, consider the waveforms of Figs. 3-1 and 3-2. These graphs show two signals with similar but opposite slope trends. For the signal of Fig. 3-1, the plus/minus percentage for any number of samples greater than one cycle of the waveform is approximately 37.0%. This indicates that for this signal, the magnitude of the slope of the leading (rising) edge is less than that of the

trailing (falling) edge. Exactly the same conclusion can be drawn by visually examining the graph. Similar analysis for the signal of Fig. 3-2 yields a plus/minus percentage of approximately -37.0%, which indicates that the leading slope is steeper than the trailing slope. Again, this is confirmed by visual inspection of the corresponding graph.

Finally, consider a pseudo-white noise record (this record is used in several examples in Chapter 4 to demonstrate the applications of the ANC). Since the noise is random, in a large record the number of of plusses and minuses should be approximately equal. For this 7697 sample record, the plus/minus percentage is 0.51%. This low value suggests that there is no real trend in either the leading or trailing slopes of the signal, as we expected.

This technique is extremely simple, and provides only an indication of the trend of the slopes in a record. Nevertheless, it is an extremely useful tool in analyzing the human EGG.

### 3.7. Relevant Signal Components

Before the recovery of a waveform can be attempted, the question of how many signal components are relevant in determining the waveshape must be addressed. In some situations it may be possible or even necessary to recover all of the components. However, in many cases the major

features of the waveshape are determined by only a few of the largest components.

For the particular case of the human EGG, it has been found experimentally that only three components are required to accurately compare the relative slopes of the leading and trailing edges of the waveform. The magnitude of the fourth harmonic (at $4f_0$) is usually very small relative to that of the fundamental, and if its phase is varied from $0^\circ$ to $360^\circ$ the change in the waveshape is minor. Another consideration is that the frequency of the fourth harmonic is in the vicinity of 12 cpm, so it can be fairly close to the (usually) much stronger respiration signal. Finally, in many records the third harmonic is barely visible above the background noise, and the fourth harmonic is completely obscured. Therefore, the examples presented in this thesis will deal with the recovery of only three components of the EGG signal (the fundamental and the harmonics at $2f_0$ and $3f_0$).

# 4. Experimental Results

## 4.1. An Ideal Example of Convergence

The convergence of the adaptive filter can best be illustrated by a trivial example involving only sine waves. The adaptive filter is configured as an ANC, and is shown in Fig. 4-1. The training signal d is formed as the sum of two sine waves. A single sine wave is applied as the input signal x. Tables 4-1 and 4-2 list the data defining the input signals d and x respectively. For this example, the filter is configured with eight weights, and $\mu$ is set to $1.25 \times 10^{-6}$. The time domain signals applied to the d and x inputs are shown in Figs. 4-2 and 4-3, respectively.

According to the development of Section 2.2., we expect the output to be the least mean-squared error difference between d and x. Therefore, in this example

| Frequency (cpm) | Amplitude (mVpp) | Phase (degrees) |
|---|---|---|
| 3.75 | 100 | 0 |
| 7.50 | 50 | 90 |

Table 4-1: Signal Parameters for Fig. 4-2

| Frequency (cpm) | Amplitude (mVpp) | Phase (degrees) |
|---|---|---|
| 7.50 | 100 | 270 |

Table 4-2: Signal Parameters for Fig. 4-3

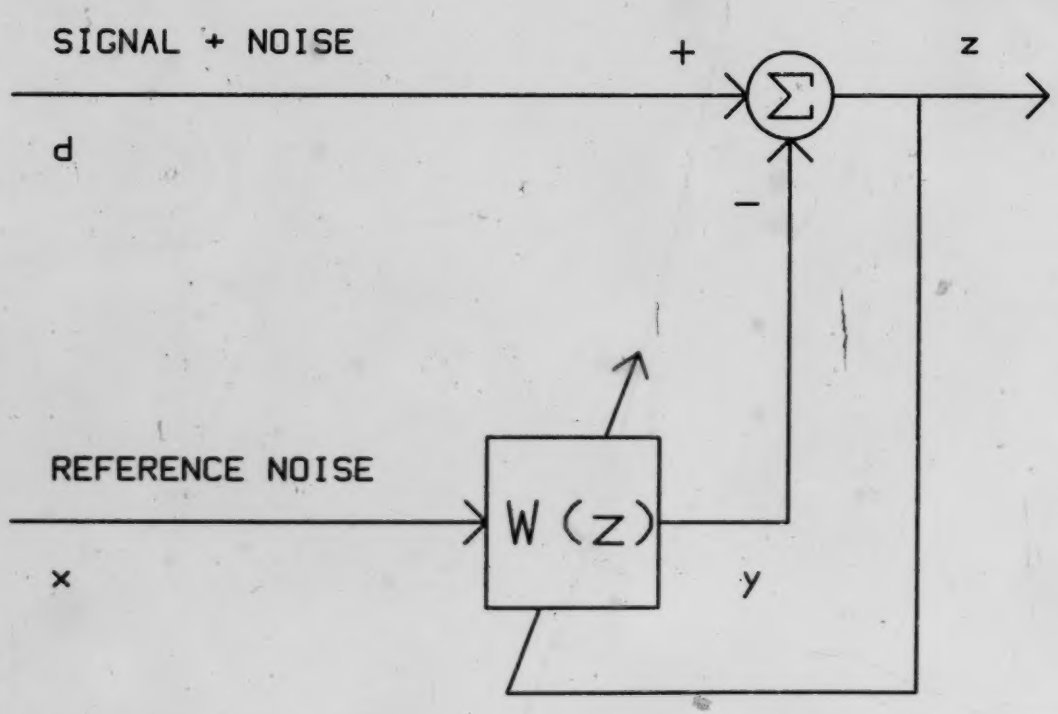


Fig. 4-1: Example of ANC Application

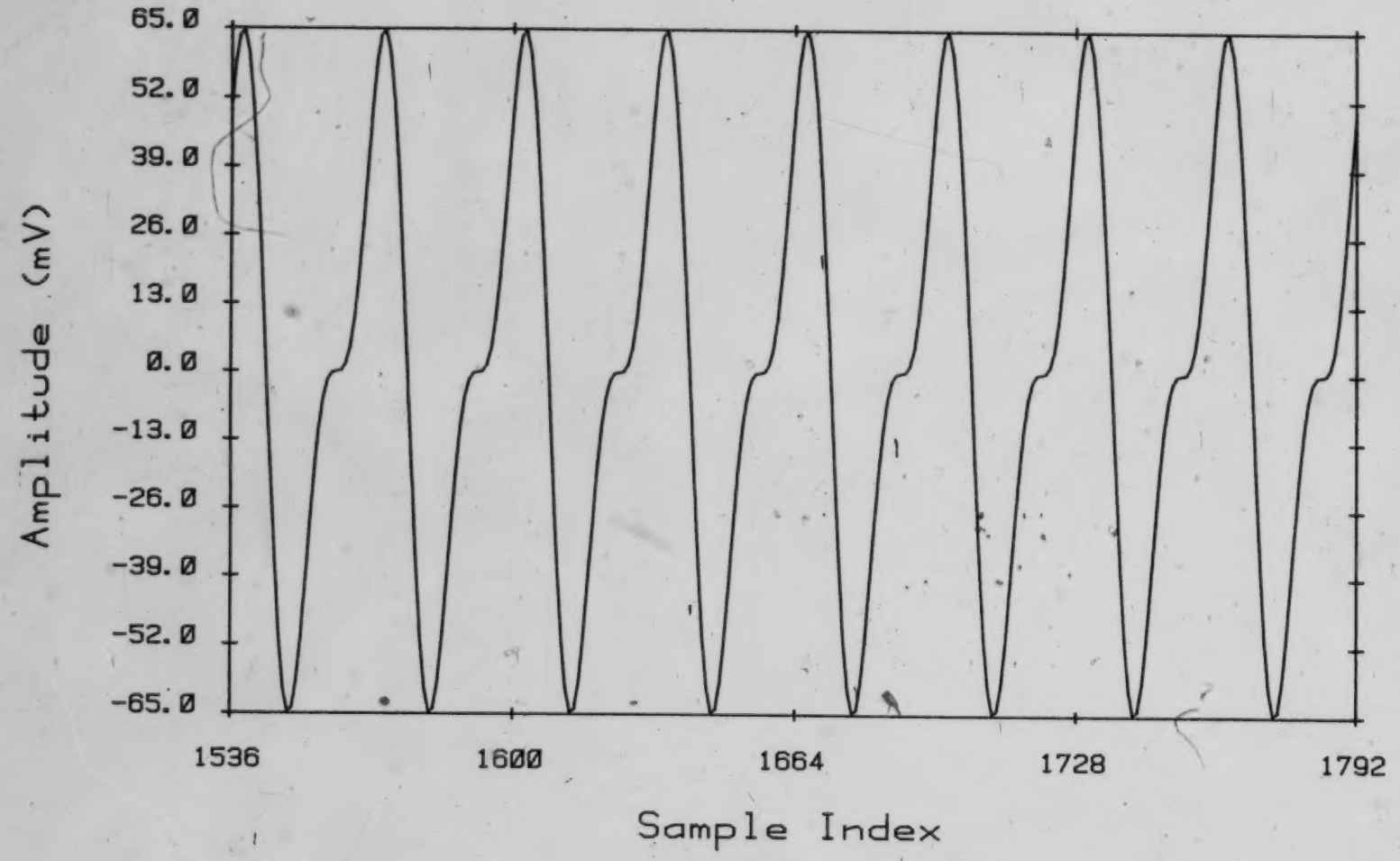


Fig. 4-2: The d Input Signal

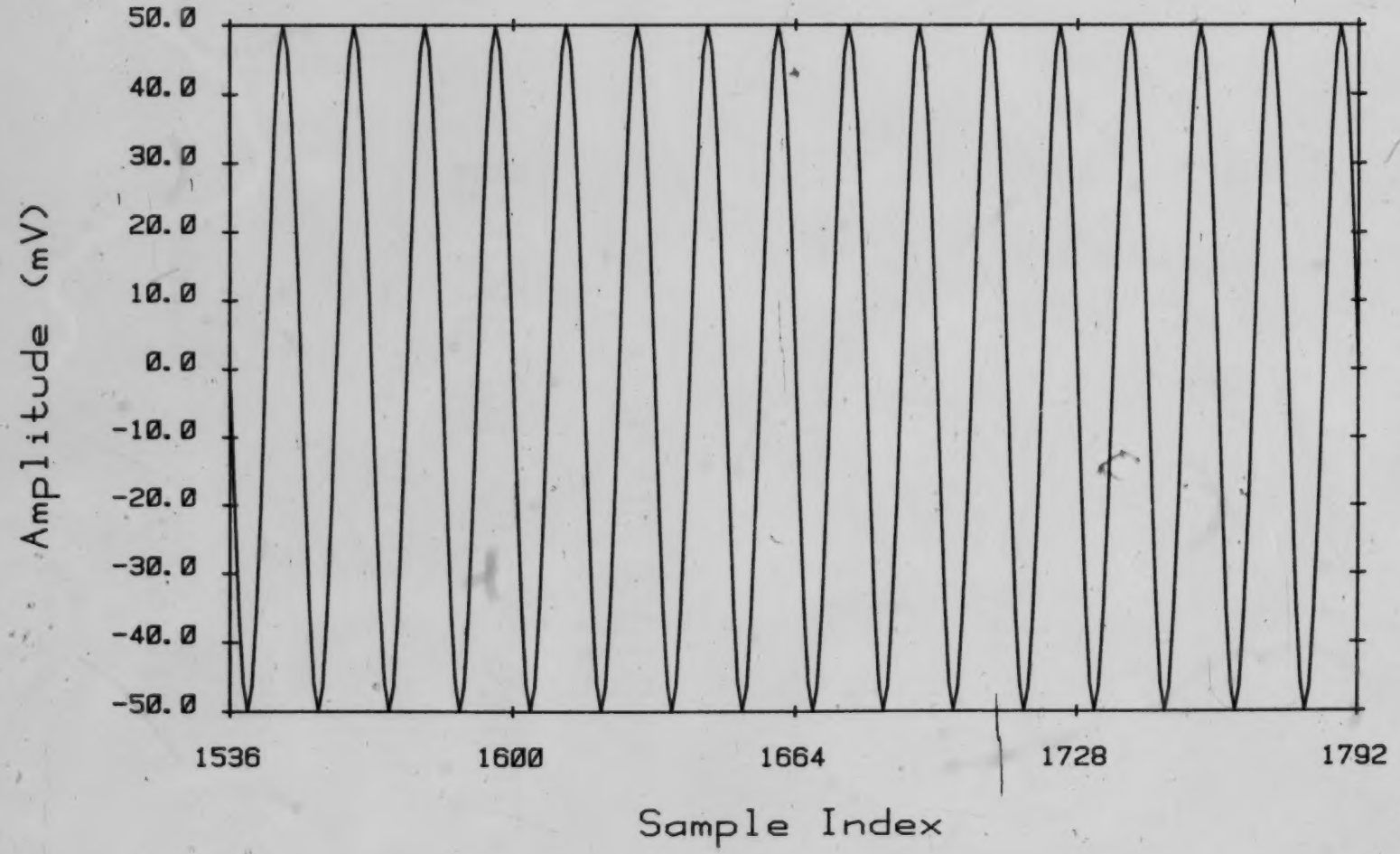


Fig. 4-3: The x Input Signal

the output signal z after convergence should strongly resemble a sine wave with the same parameters as the fundamental present at the d input. Effectively, the ALC will converge to an impulse response that will modify the sine wave applied to the x input such that the harmonic component at the d input will be cancelled.

The output signal signal is shown in Fig. 4-4, and the corresponding magnitude and phase spectra are shown in Figs. 4-5 and 4-6, respectively. As expected, the output signal is a 3.75 cpm sine wave with an amplitude of 100 mVpp and zero phase. Referring to Table 4-1, it is clear that the adaptive filter has modified the amplitude and phase of the sine wave applied to the x input such that the harmonic at the d input is cancelled.

In this case, the cancellation is exact because the inputs are perfect sine waves and the noise (the harmonic at 7.5 cpm) is completely additive. Also, the signal applied to the x input does not contain a component at the frequency of the signal (3.75 cpm). Therefore, the signals at the d and x inputs are uncorrelated and (2.16) is exactly satisfied. Also, the noise components at the d and x inputs are highly correlated since they differ only in magnitude and phase. Thus, this example is only useful to illustrate the convergence of the adaptive filter configured as an ANC since all of the conditions are "perfect".

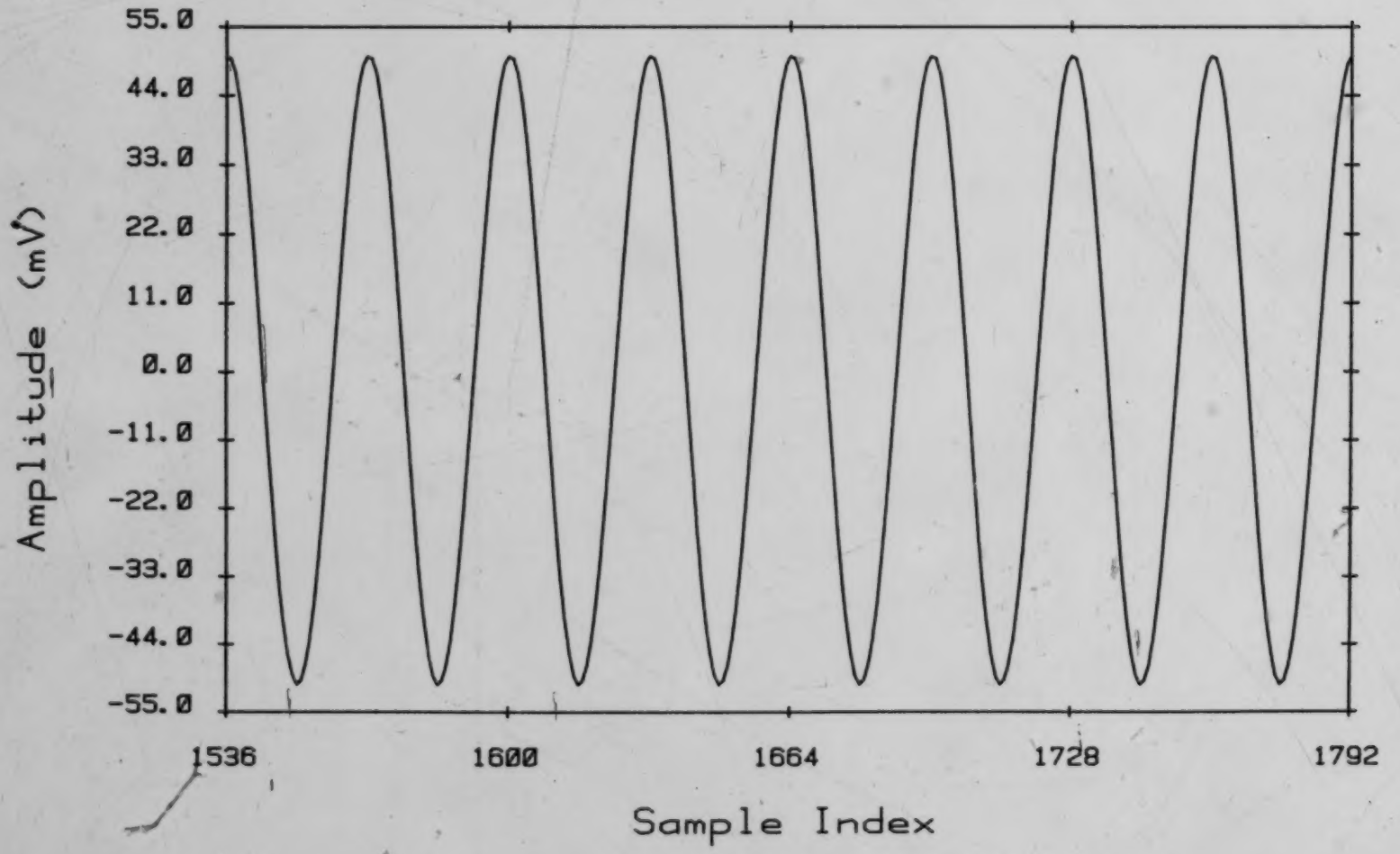


Fig. 4-4: The Output Signal After Convergence

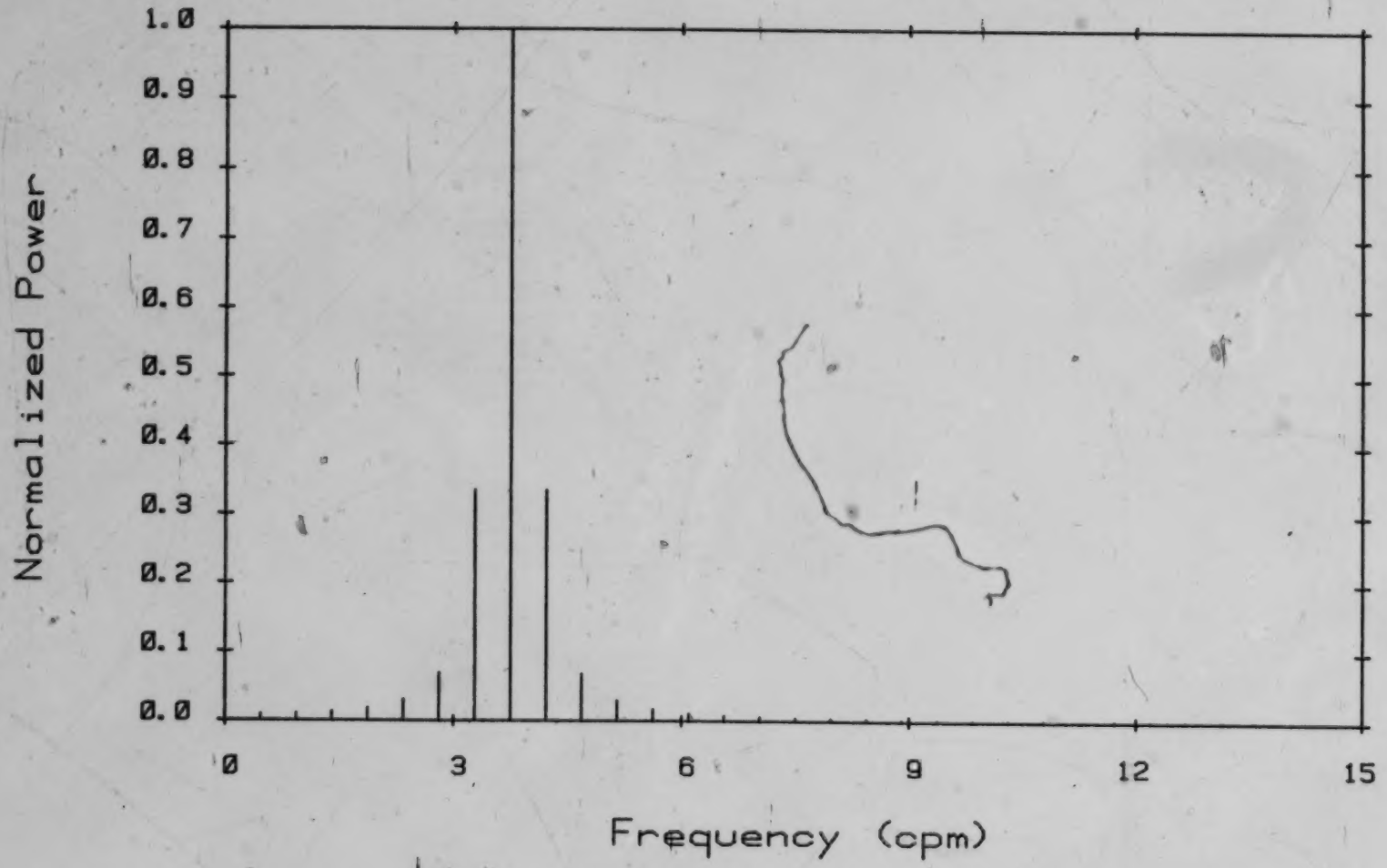


Fig. 4-5: Magnitude Spectrum of Fig. 4-4

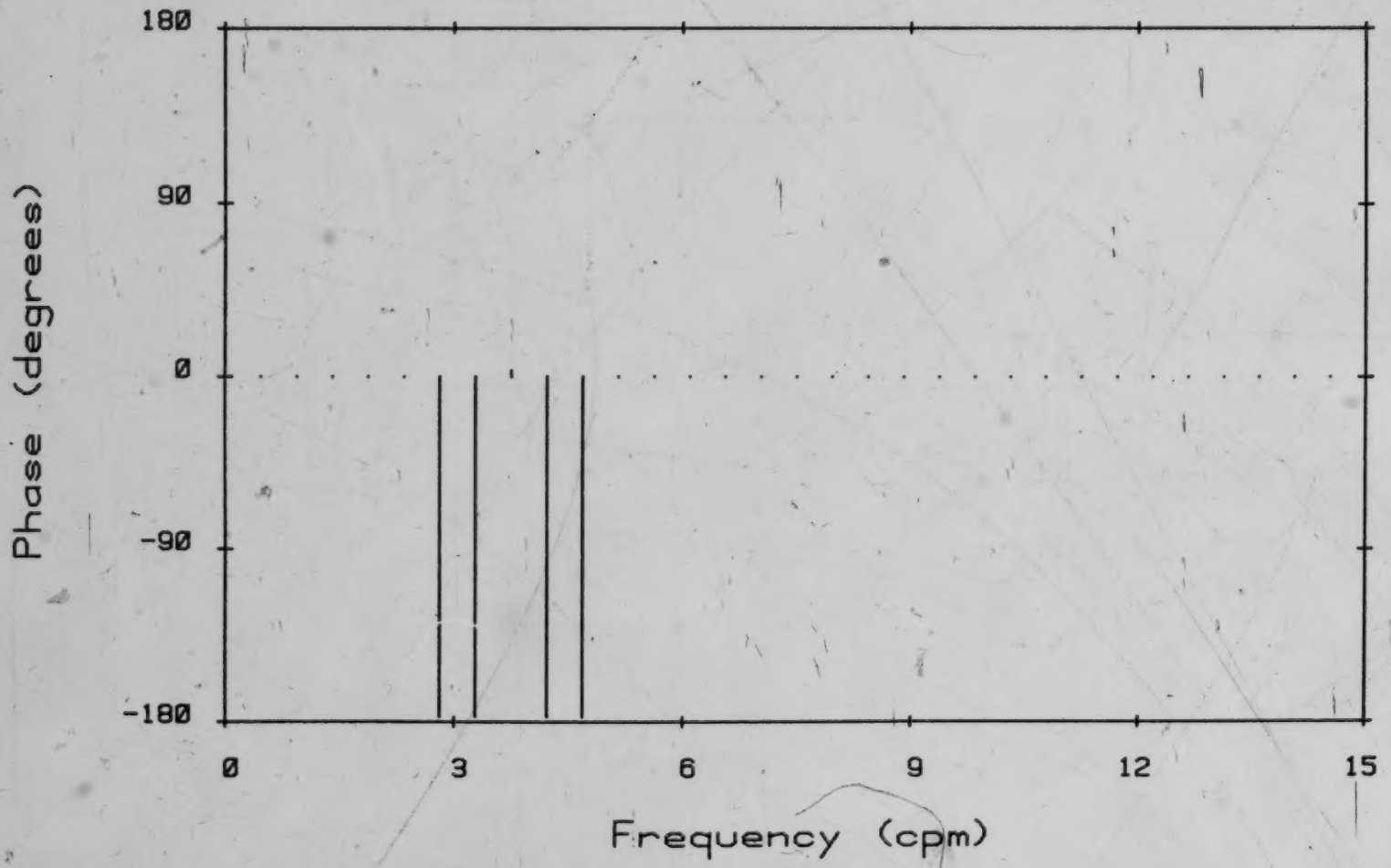


Fig. 4-6: Phase Spectrum of Fig. 4-4

## 4.2. A Non-ideal Example of Convergence

For a more practical example of convergence, the sine wave "noise signal" can be replaced by random white noise. The configuration remains the same as in the previous example. Thus, the noise cancelling operation will attempt to recover a sine wave distorted by white noise.

The "white noise" used in this experiment was generated using a Servomex Controls Ltd. Random Signal Generator type R.G.77. This unit generates a pseudo-white noise signal suitable for use in EGG experiments. The noise signal was sampled using the same procedure that is used to acquire patient records, and was stored in a data file on the computer. The noise signal can then be manipulated in the same manner as any of the patient records. It is hoped that using a sampled noise signal would provide a "whiter" spectrum than would computer-generated random numbers since no artificial "seeds" are required.

The signal applied to the d input in this example is formed by adding a sine wave to the white noise record. The average magnitude spectrum of this signal is shown in Fig. 4-7, and the sinusoid parameters are given in Table

| Frequency (cpm) | Amplitude (mVpp) | Phase (degrees) |
|---|---|---|
| 3.75 | 25 | 0 |

Table 4-3: Signal Parameters for Fig. 4-7

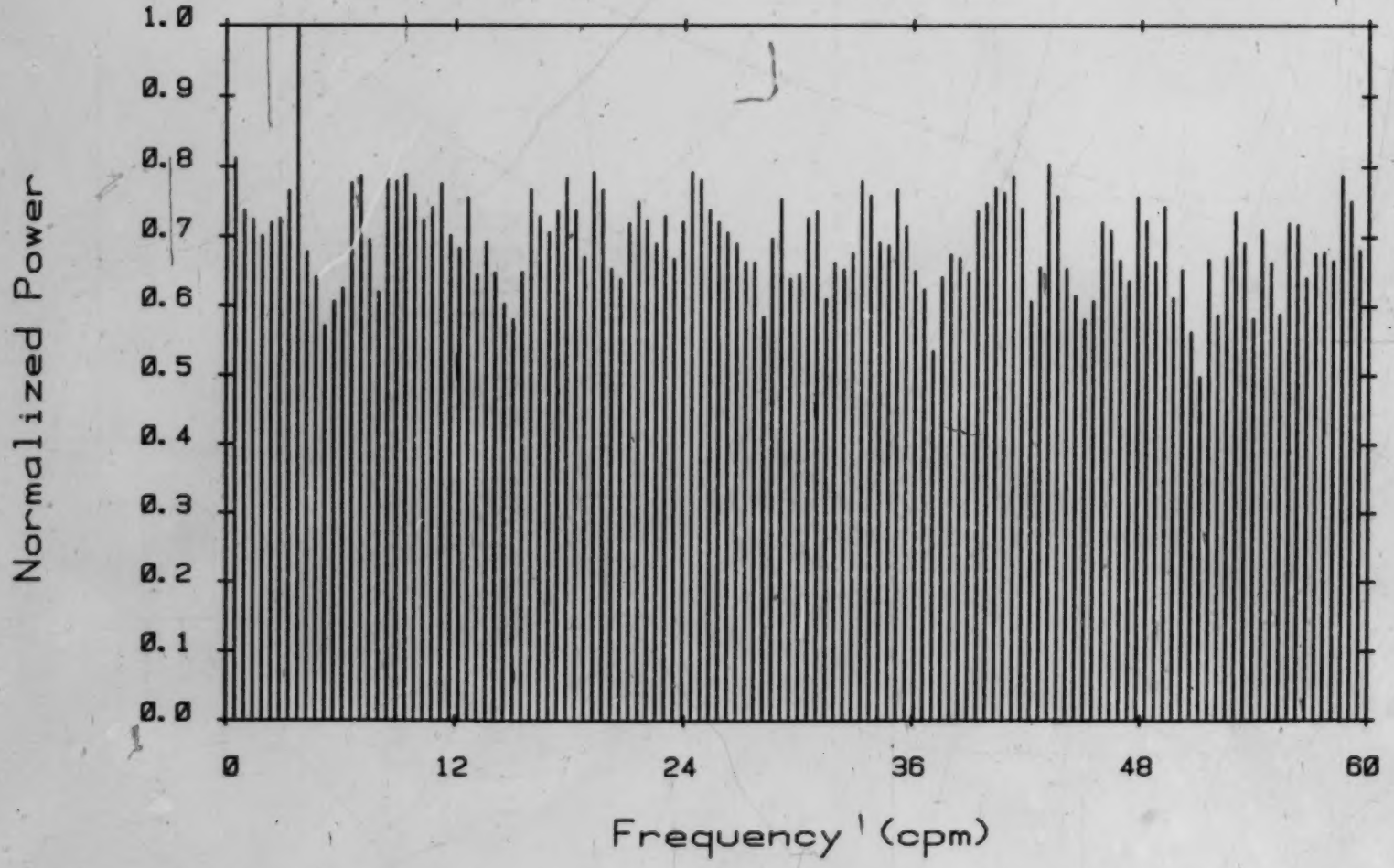


Fig. 4-7: The d Input Signal

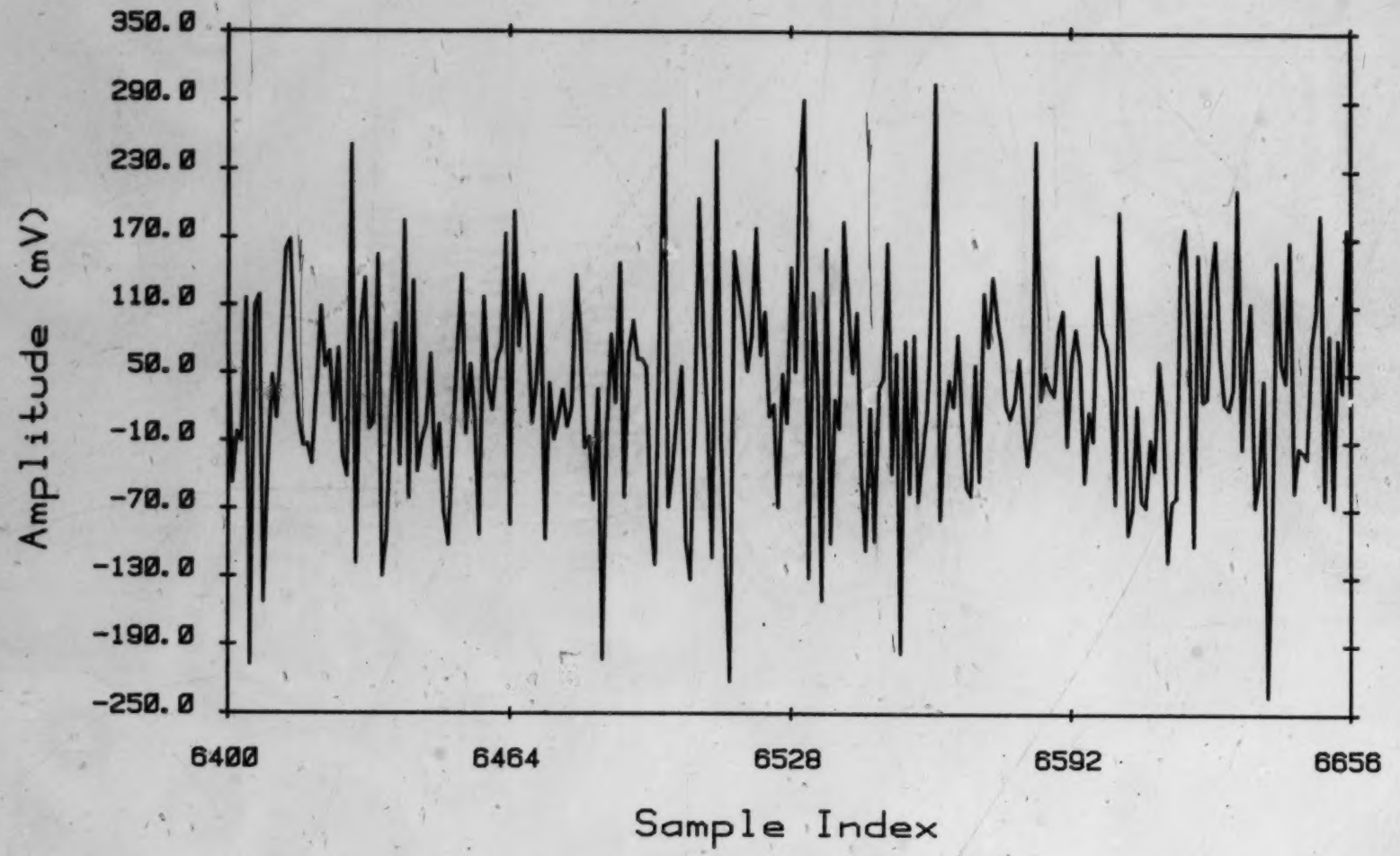


Fig. 4-8: The d Input Signal

4-3. The peak in this spectrum corresponds to the sine wave, and is barely visible above the white noise. The white noise is also amplified by 0.5 and applied to the x input. The adaptive filter is configured with 8 weights, and the convergence factor $\mu$ is set to $1.368 \times 10^{-7}$. With these parameters, the adaptive filter converges in approximately 2000 iterations.

Figs. 4-8 and 4-9 shows the input and output signals, respectively, after convergence. The output magnitude and phase spectra are shown in Figs. 4-10 and 4-11, respectively. As expected, the output signal is an approximation of the original sine wave, with a frequency of 3.75 cpm and a phase shift of zero degrees.

## 4.3. Adaptive Filter Versus Fixed Filter

The two preceding examples illustrate the performance of the ANC with both clean and noisy input signals. It is interesting at this point to compare the results of the second experiment with the performance of a simple fixed band-pass filter. The input signal is the same sine wave plus additive white noise that is plotted in Figs. 4-7 and 4-8, and is defined in Table 4-3.

| Order | Type | Ripple | Lower 3dB Cutoff | Upper 3dB Cutoff |
|---|---|---|---|---|
| 4 | Band Pass | 3 dB | 2.0 cpm | 5.5 cpm |

Table 4-4: Fixed Filter Parameters For Stationary Test

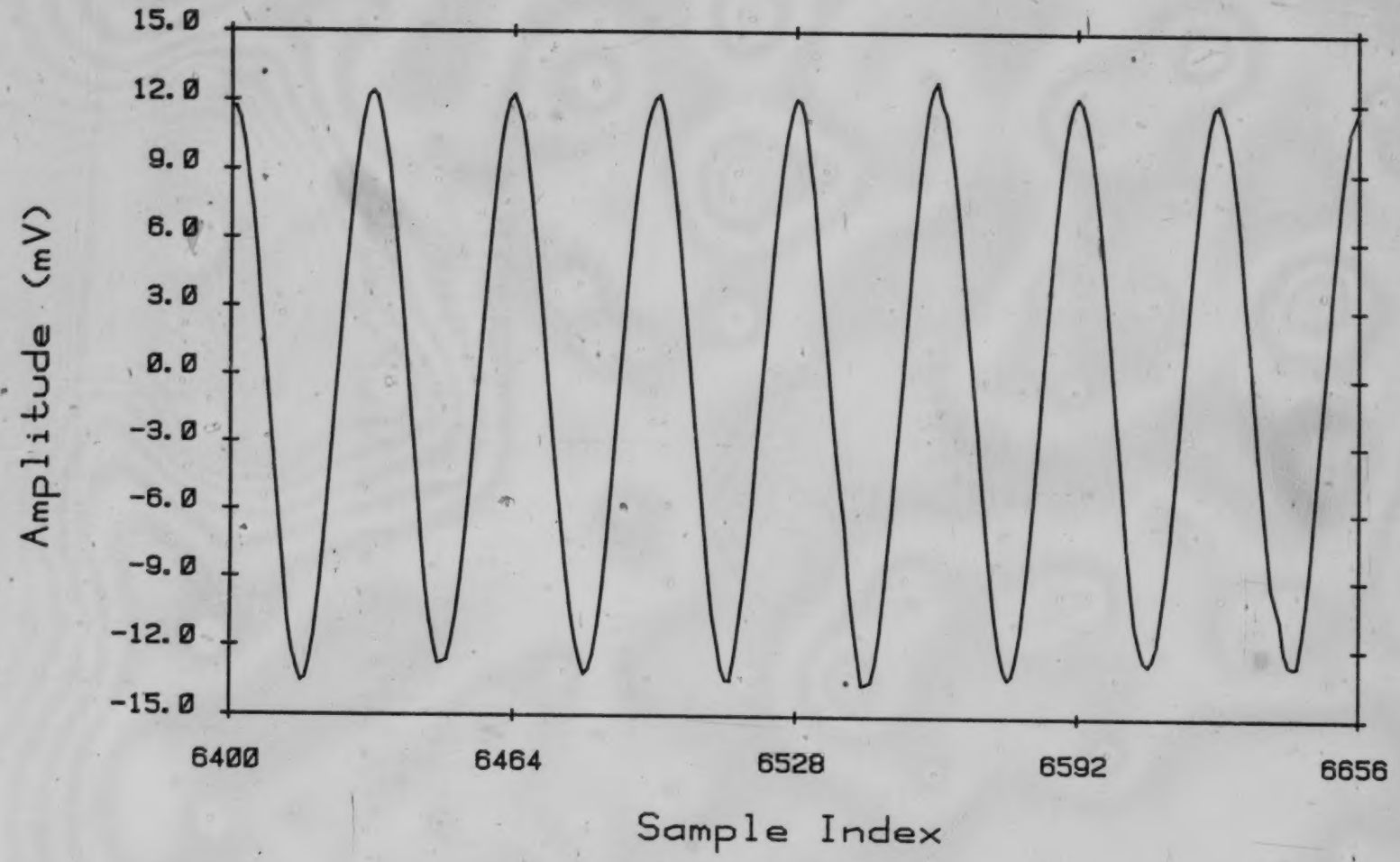


Fig. 4-9: The Output Signal After Convergence

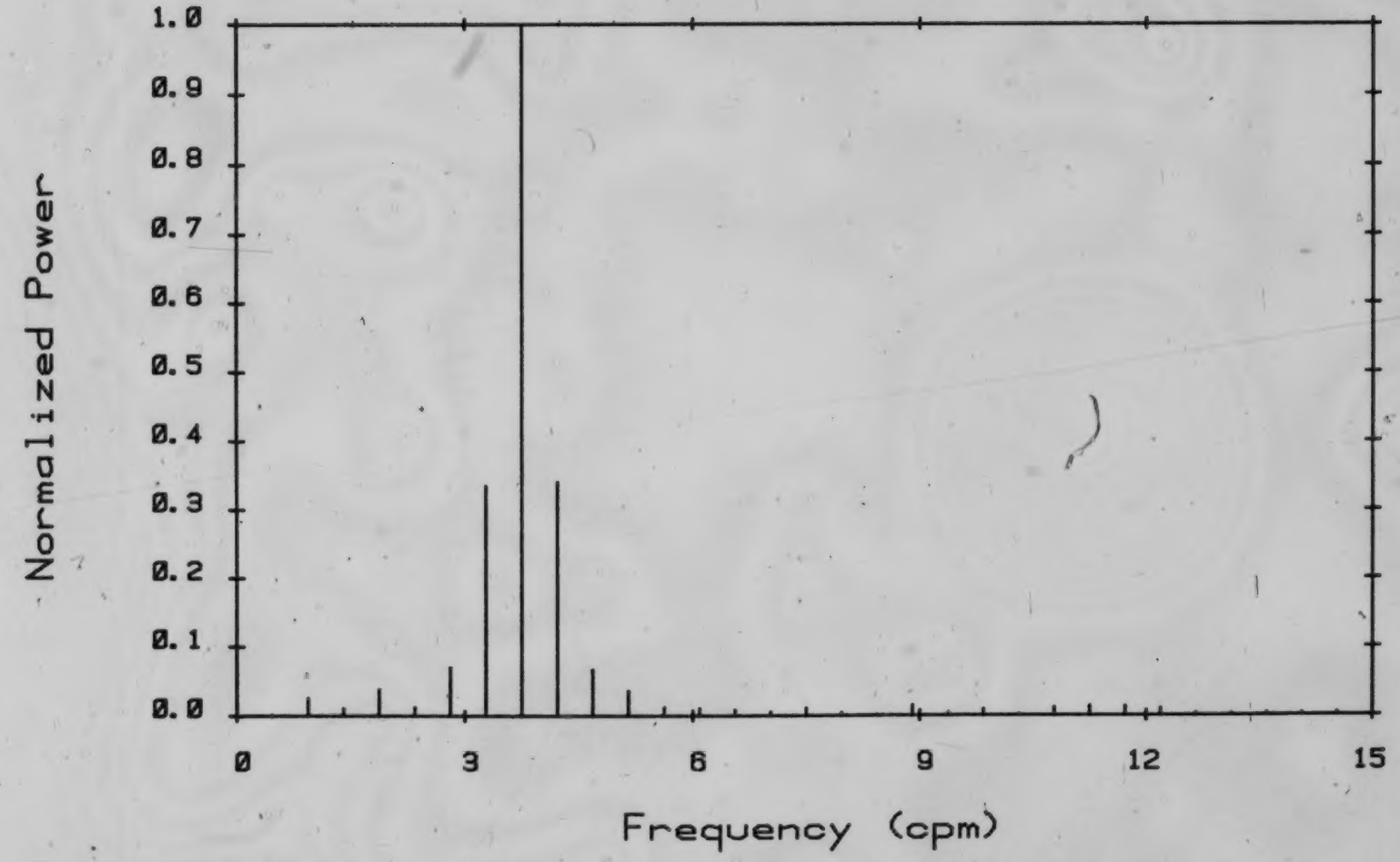


Fig. 4-10: Magnitude Spectrum of Fig. 4-9

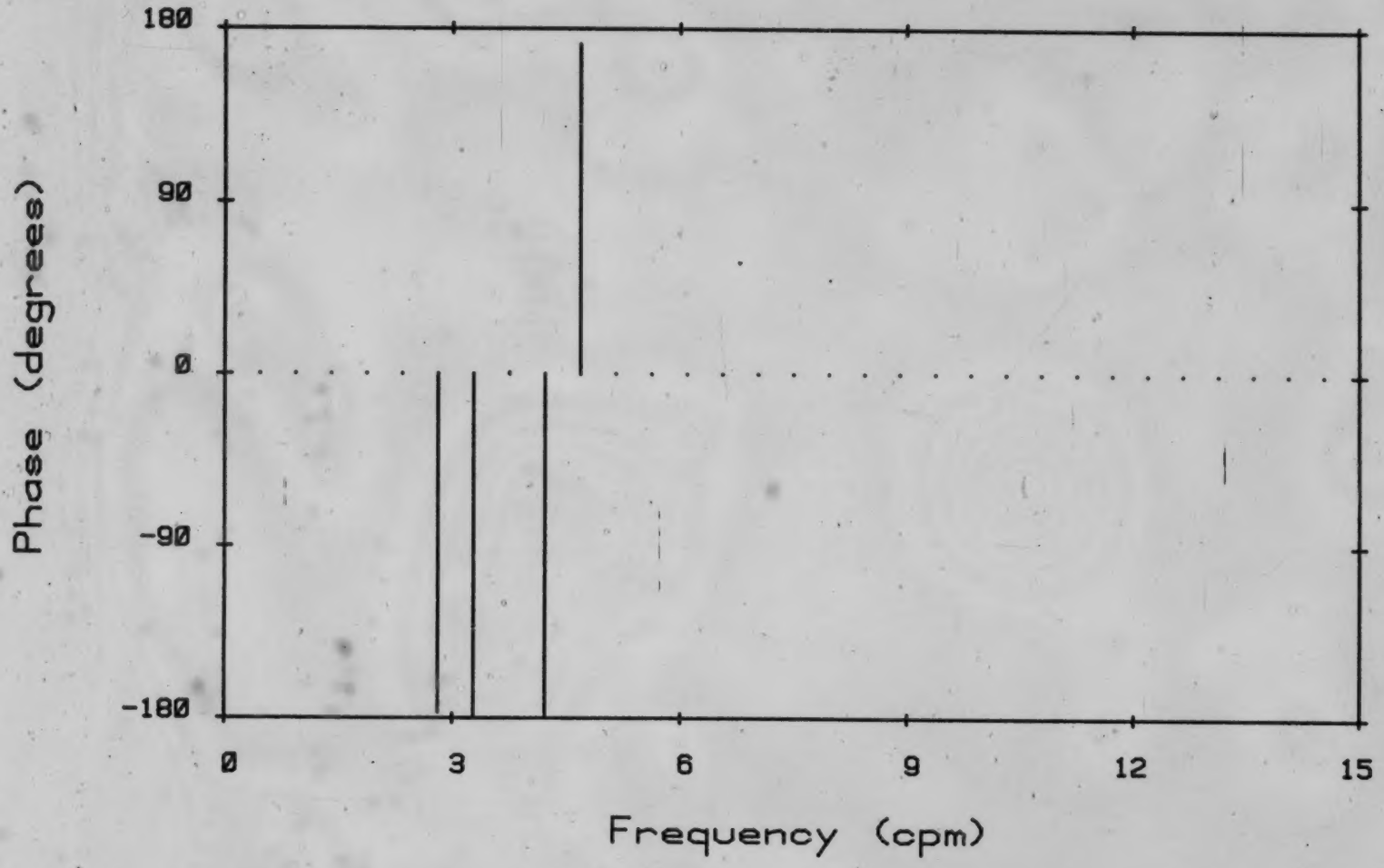


Fig. 4-11: Phase Spectrum of Fig. 4-9

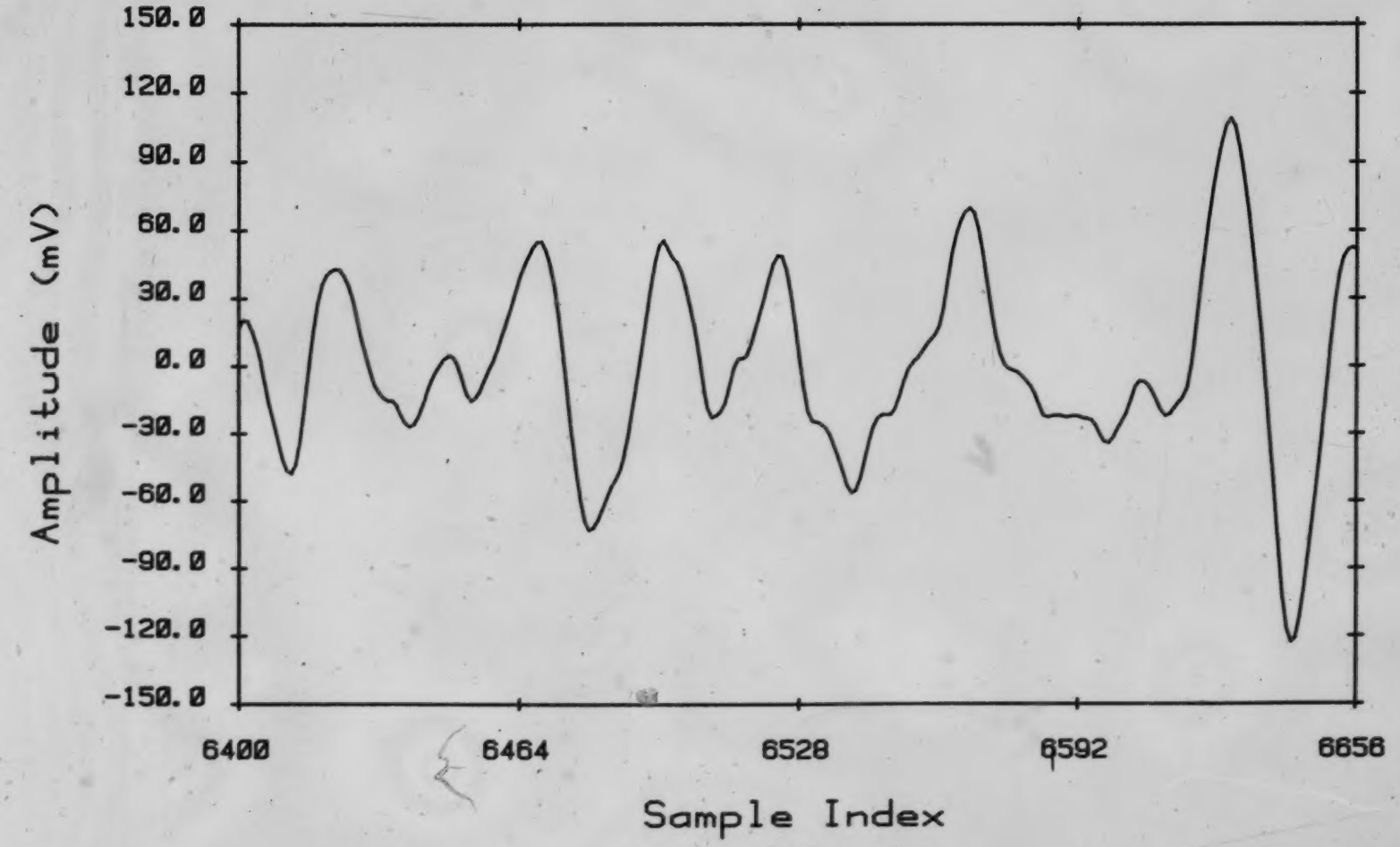


Fig. 4-12: Output of the Fixed Filter

The fixed digital filter is based on an analogue low-pass Chebyshev prototype, and is designed using the bilinear transformation [14]. Table 4-4 lists the filter parameters, which are experimentally found to provide the "best" results. No extensive attempt was made to optimize the filter because this comparison serves only to illustrate the differences between adaptive and fixed filters. The 3dB frequencies are chosen to center the sine wave within the passband.

The resulting output signal is plotted in Fig. 4-12. Comparison of this graph with Fig. 4-9 shows that the ANC produces far superior results in this application. There are three reasons for this. First, the ANC is capable of removing noise components present at the same frequency as the signal, while the fixed filter can not. Second, the fixed filter merely suppresses signal components at frequencies that fall in its rejection bands, and has little affect on signal components at frequencies within its passband. On the other hand, the ANC (as it is configured here) has no pass band or rejection band. Instead, it acts to completely remove noise from a signal. Finally, the fixed band-pass filter is subject to ringing, which is caused by strong signal components at frequencies in the vicinity of the 3dB cutoff frequencies. Again, this problem does not exist in an ANC because the adaptive filter does have either a pass band or a rejection band.

## 4.4. Signal Tracking

Another advantage of the adaptive filter over fixed filters is that of automatic signal tracking. If the fundamental frequency of the signal changes with time (ie. the signal "wanders"), the ANC can adjust its impulse response accordingly as long as the rate of change of frequency is sufficiently slow. The fixed filter, on the other hand, has a finite bandwidth. If the frequency of the signal moves out of the passband, the resulting output will be useless. Again, if the frequency of the signal is in the vicinity of the 3dB frequencies of the filter, ringing will add distortion to the output.

To illustrate the application of the ANC to a non-stationary signal, the frequency of a sinusoid was swept from 3.75 cpm to 7.5 cpm. The resulting signal was added to the same white noise record that was used in the two preceding examples. Table 4-5 lists the signal parameters before and after the frequency sweep. The rate of change of the frequency was set so that the sweep would occur over an interval of 4000 samples (2000 seconds). The adaptive filter was configured with eight weights and $\mu = 1.368 \times 10^{-7}$.

| Frequency (cpm) | | Amplitude (mVpp) | Phase (degrees) |
|---|---|---|---|
| initially | 3.75 | 100 | 0 |
| finally | 7.50 | 100 | 0 |

Table 4-5: Signal Parameters for Figs. 4-13 and 4-17

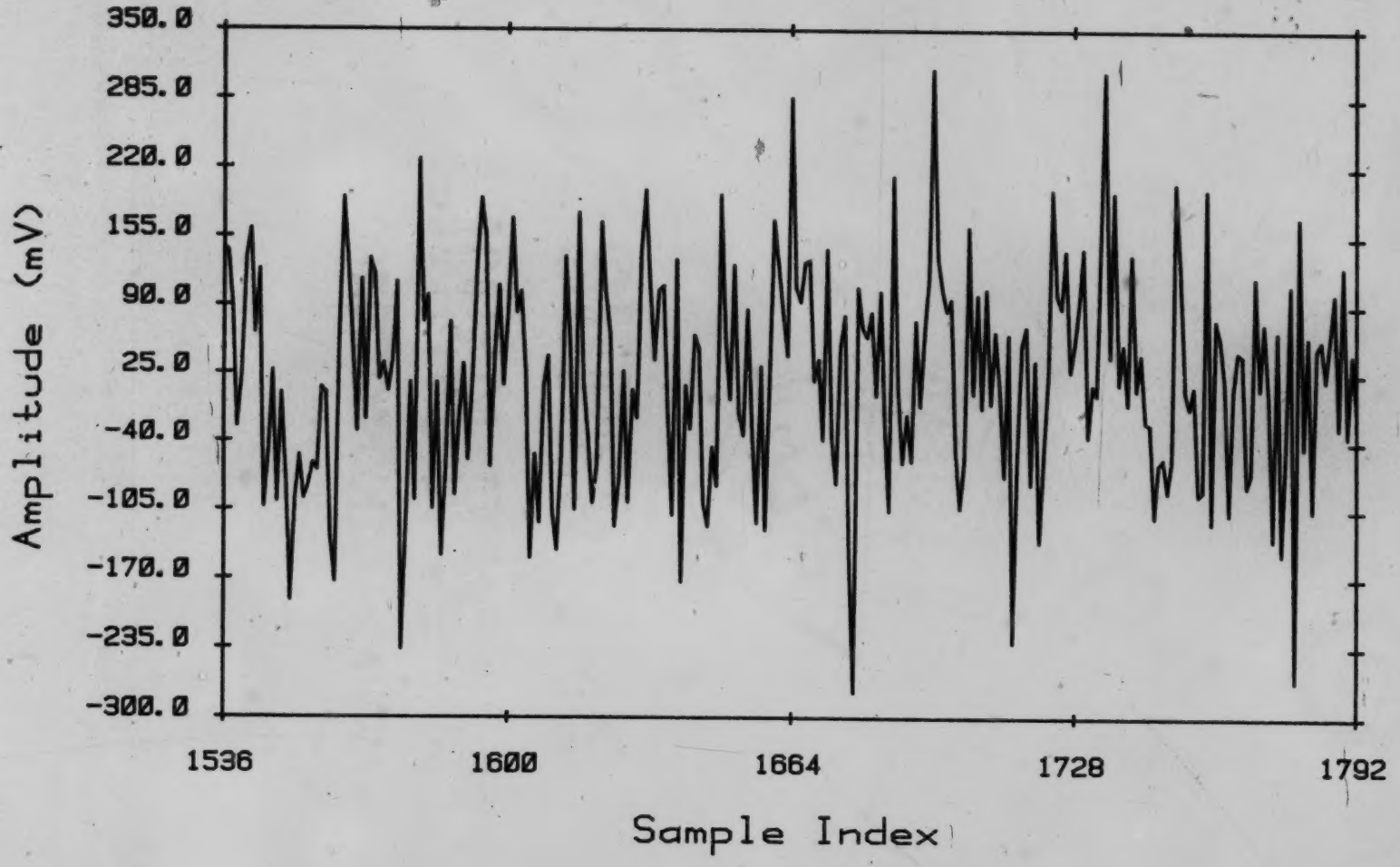


Fig. 4-13: Input Signal Before Linear Sweep

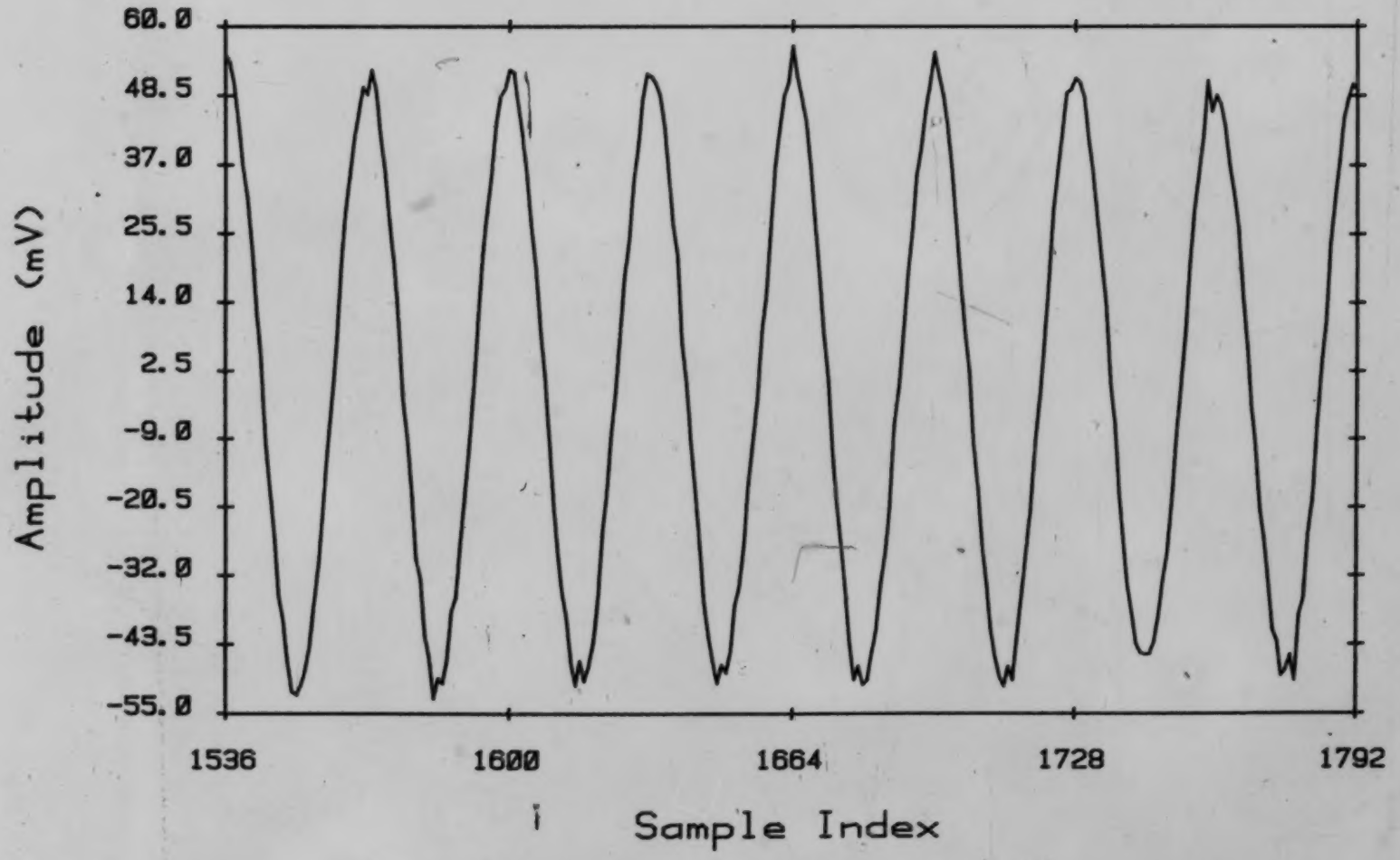


Fig. 4-14: Output Signal Before Linear Sweep

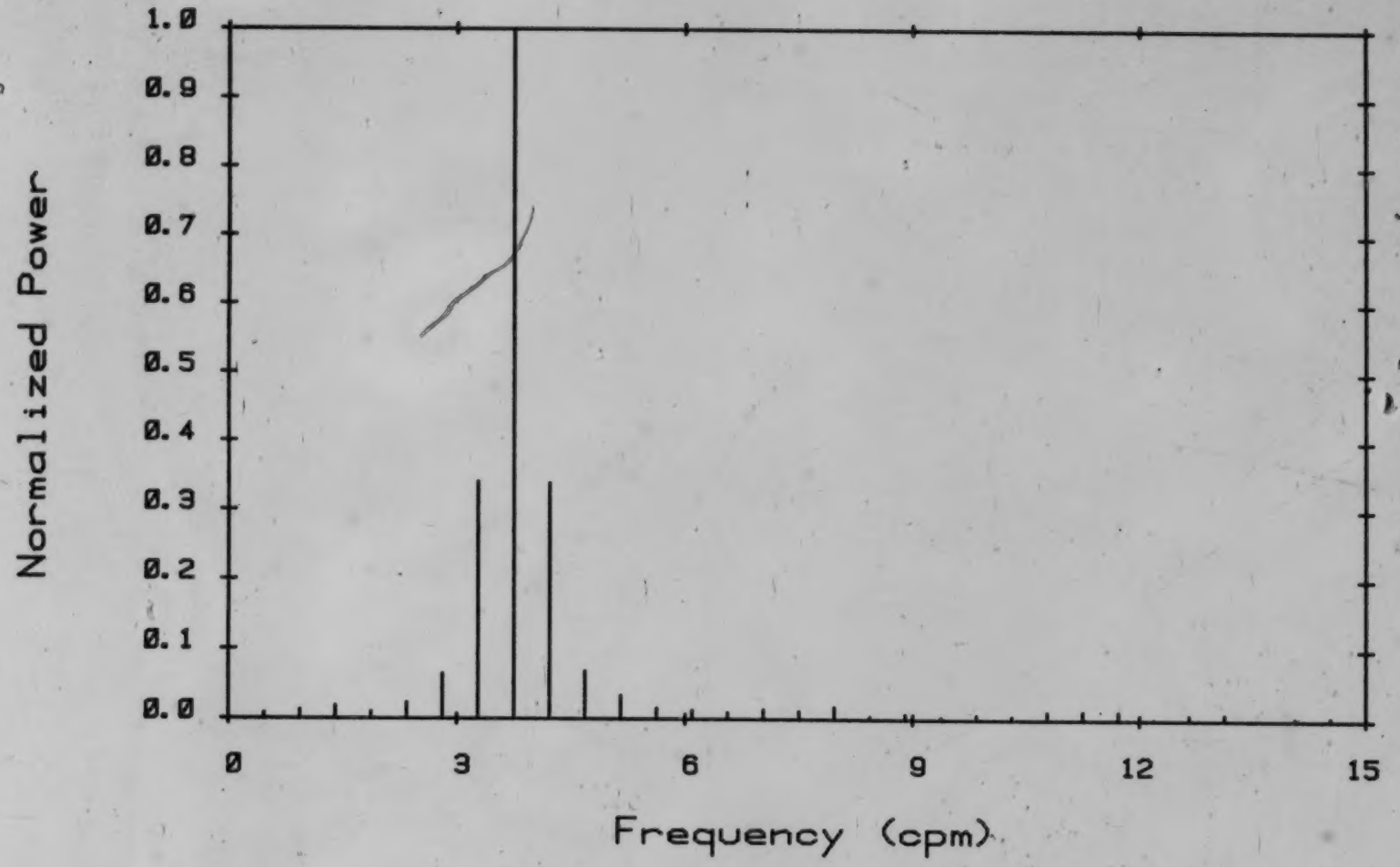


Fig. 4-15: Magnitude Spectrum of Fig. 4-14

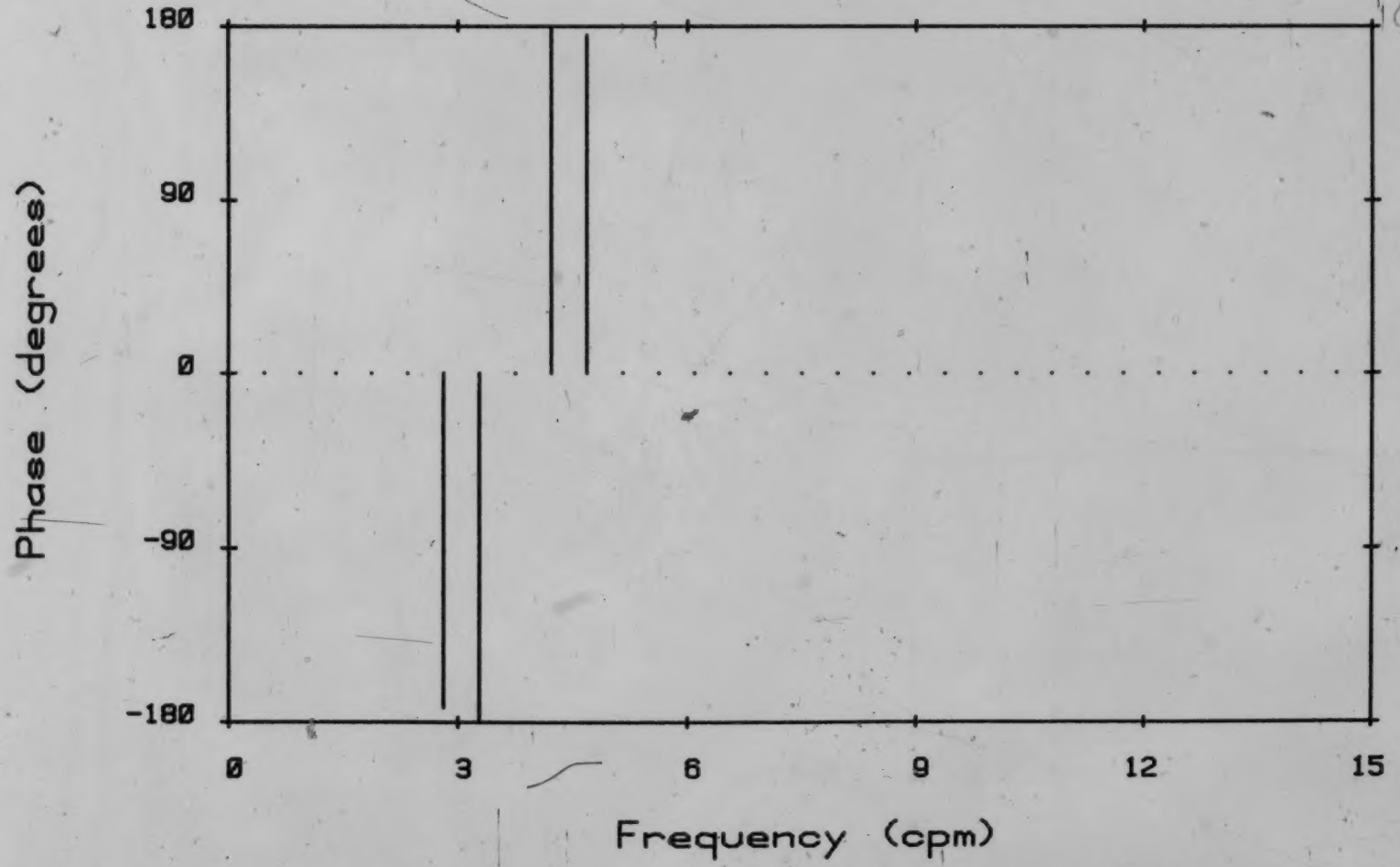


Fig. 4-16: Phase Spectrum of Fig. 4-14

Figs. 4-13 and 4-14 show the input and output, respectively, of the ANC at a time after convergence and before the frequency sweep begins. The output signal is the similar to that obtained in the second example in this chapter, because at this point both experiments are similar. The magnitude and phase spectra of the output signal are plotted in Figs. 4-15 and 4-16, and show that the output is a sine wave with a frequency of 3.75 cpm and zero phase.

Shortly after the point in time that this window represents, the frequency sweep begins. Figs. 4-17 and 4-18 show the input and output signals, respectively, after the sweep is complete. The magnitude and phase spectra of the output signal are plotted in Figs. 4-19 and 4-20, respectively. These graphs confirm that the the output is a sine wave with a frequency of 7.50 cpm and zero phase.

The only way that a fixed filter can be used to recover this signal is by designing a band-pass filter with sufficient bandwidth to pass the signal through the entire range of the frequency sweep. To illustrate this approach, a band-pass filter was designed with the

| Order | Type | Ripple | Lower 3dB Cutoff | Upper 3dB Cutoff |
|---|---|---|---|---|
| 4 | Band Pass | 3 dB | 3.0 cpm | 8.0 cpm |

Table 4-6: Fixed Filter Parameters For Sweep Test

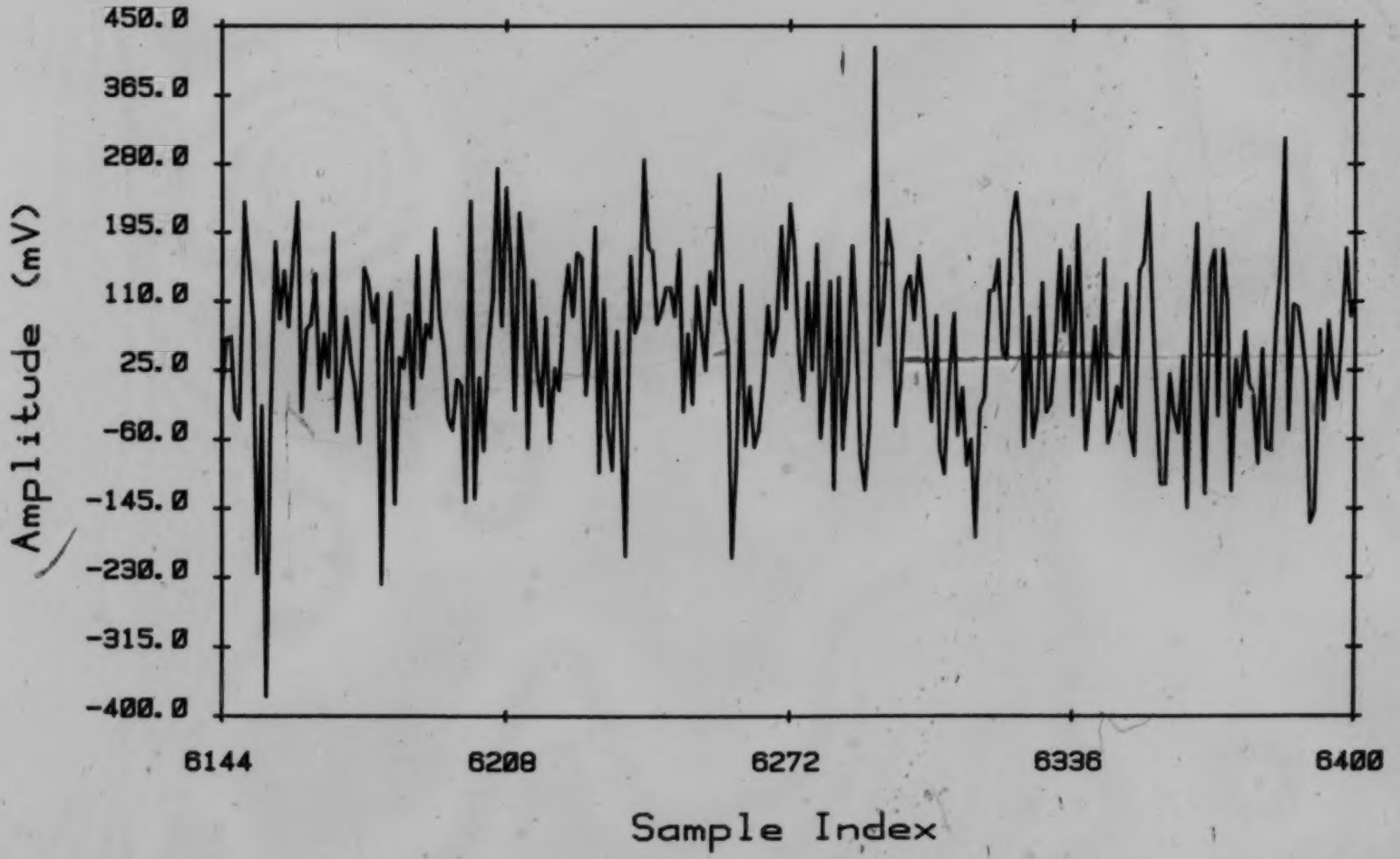


Fig. 4-17: Input Signal After Linear Sweep

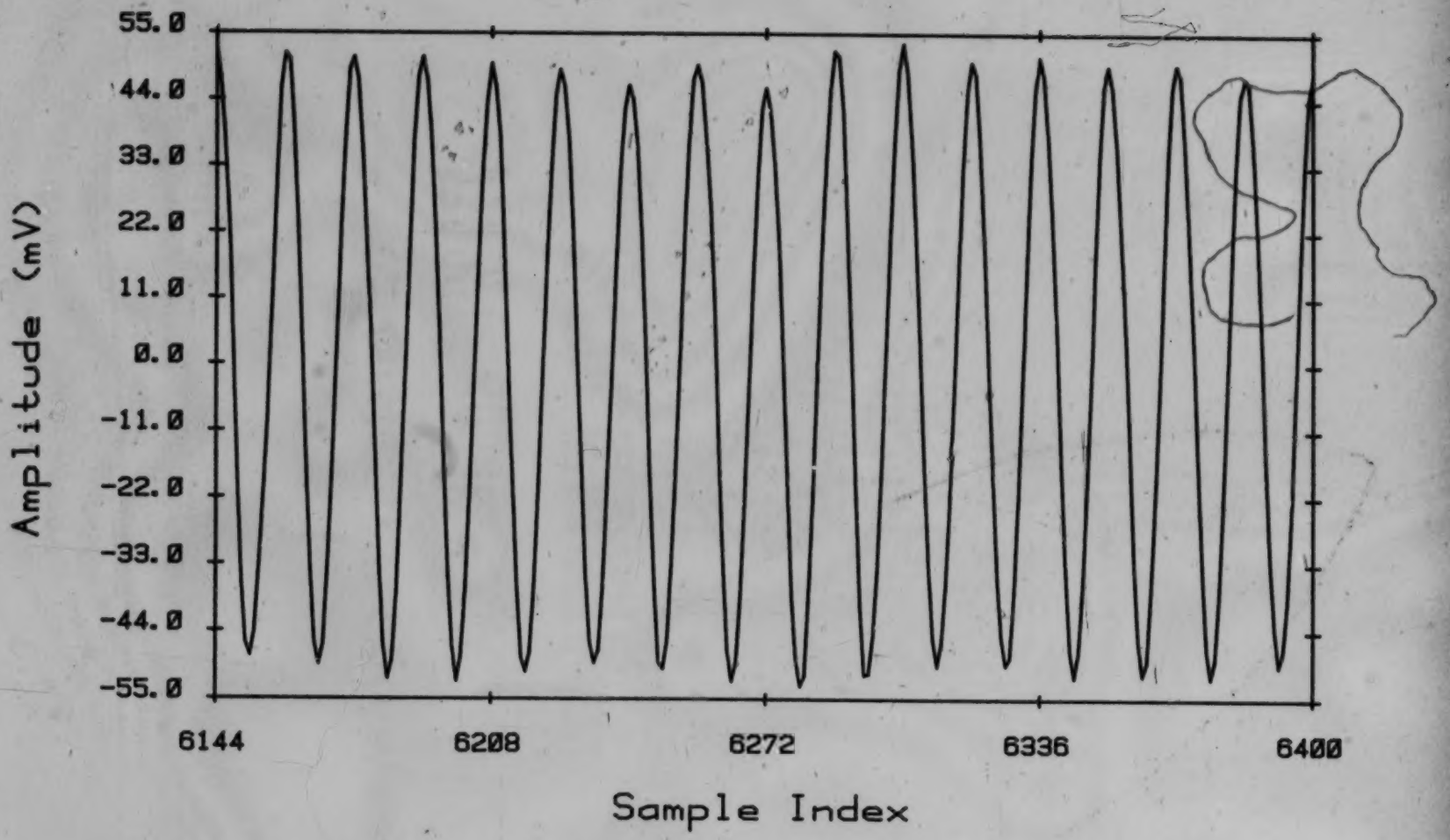


Fig. 4-18: Output Signal After Linear Sweep

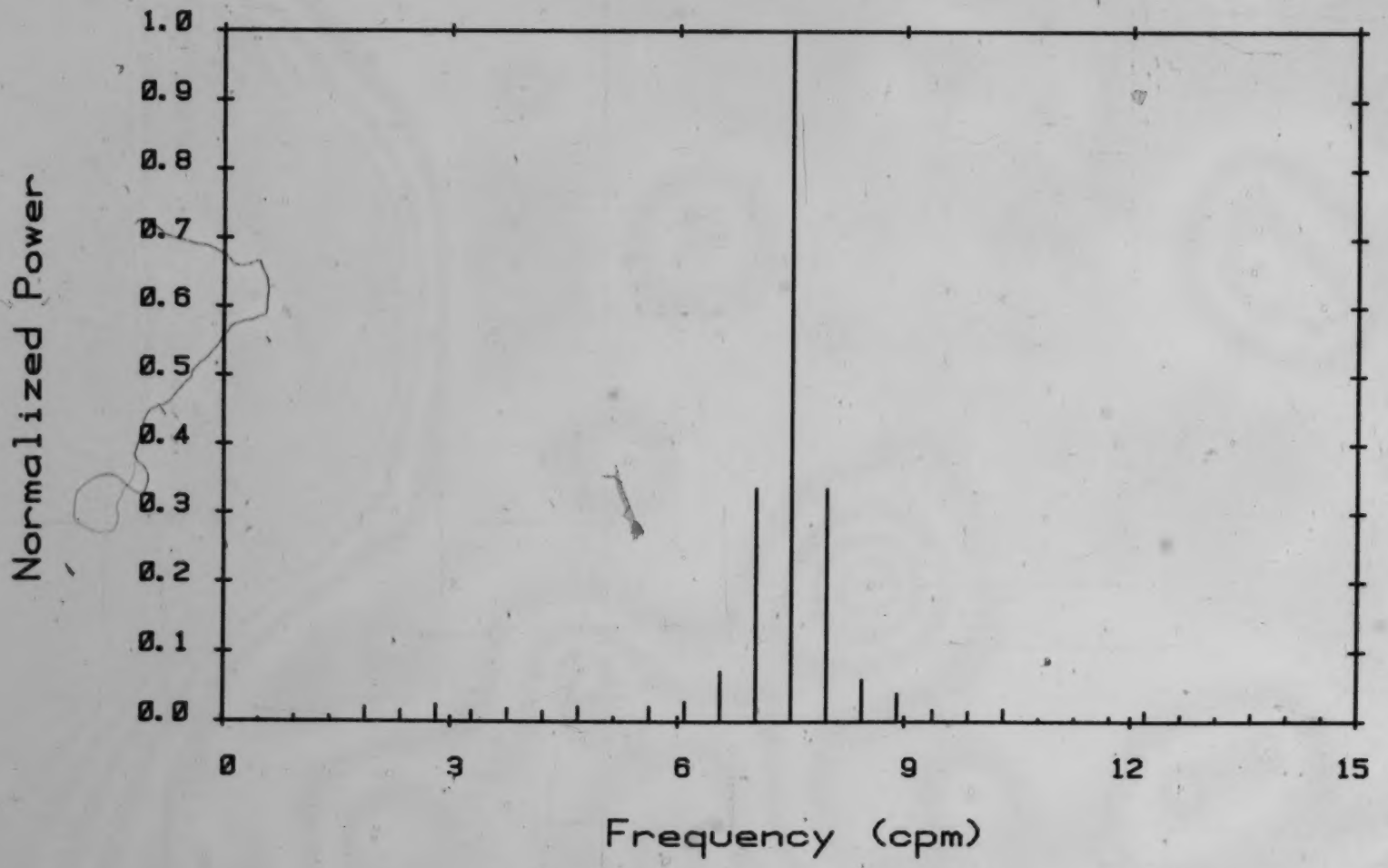


Fig. 4-19: Magnitude Spectrum of Fig. 4-18

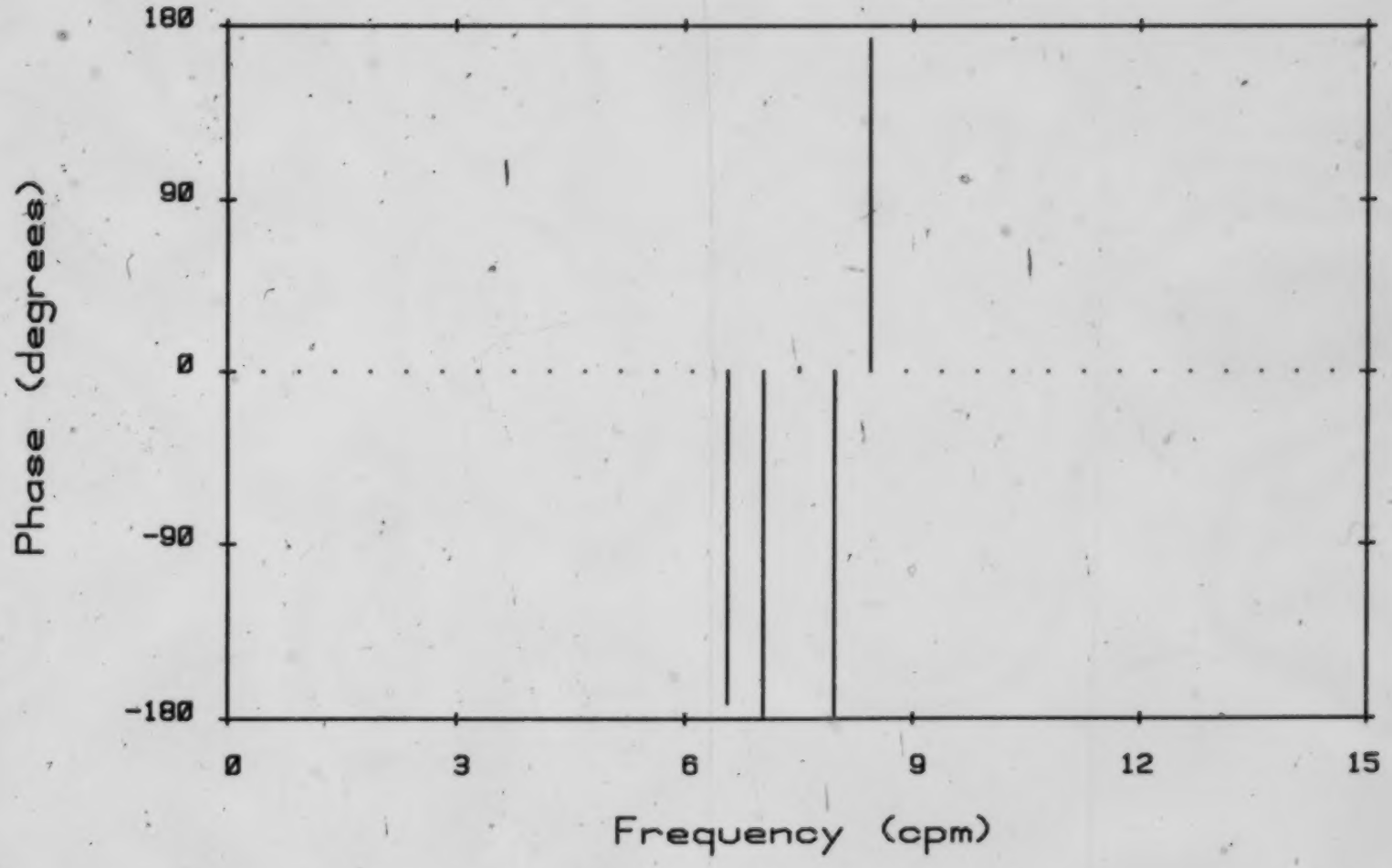


Fig. 4-20: Phase Spectrum of Fig. 4-18

parameters given in Table 4-6. This filter was designed using the bilinear transformation on a Chebyshev second order low-pass prototype [14]. The filtered signal at a time before the linear sweep begins is plotted in Fig. 4-21, and should be compared to the output of the ANC at the corresponding time (cf. Fig. 4-14). Fig. 4-22 shows the filtered signal after the linear sweep is completed. This graph can be compared to Fig. 4-18, which shows the output of the ANC at the same time.

These comparisons clearly show that the ANC provides superior results when filtering non-stationary signals. In a previous example, the ANC was also shown to be superior to fixed filters for filtering stationary signals that are corrupted by additive noise. These results provide the motivation for applying adaptive filtering techniques to the recovery of the EGG waveform in lieu of fixed digital filters.

Both of the examples performed using white noise in this chapter are idealized in the sense that the noise signals used at the d and x inputs differ by only a scale factor. Therefore, the ALC can be replaced by an amplifier and the noise can be directly subtracted from the noisy signal applied to the d input. These examples are intended to illustrate the operation of the adaptive filter. They are not "real-world" filtering problems. The examples in the next sections of this chapter deal with more realistic situations.

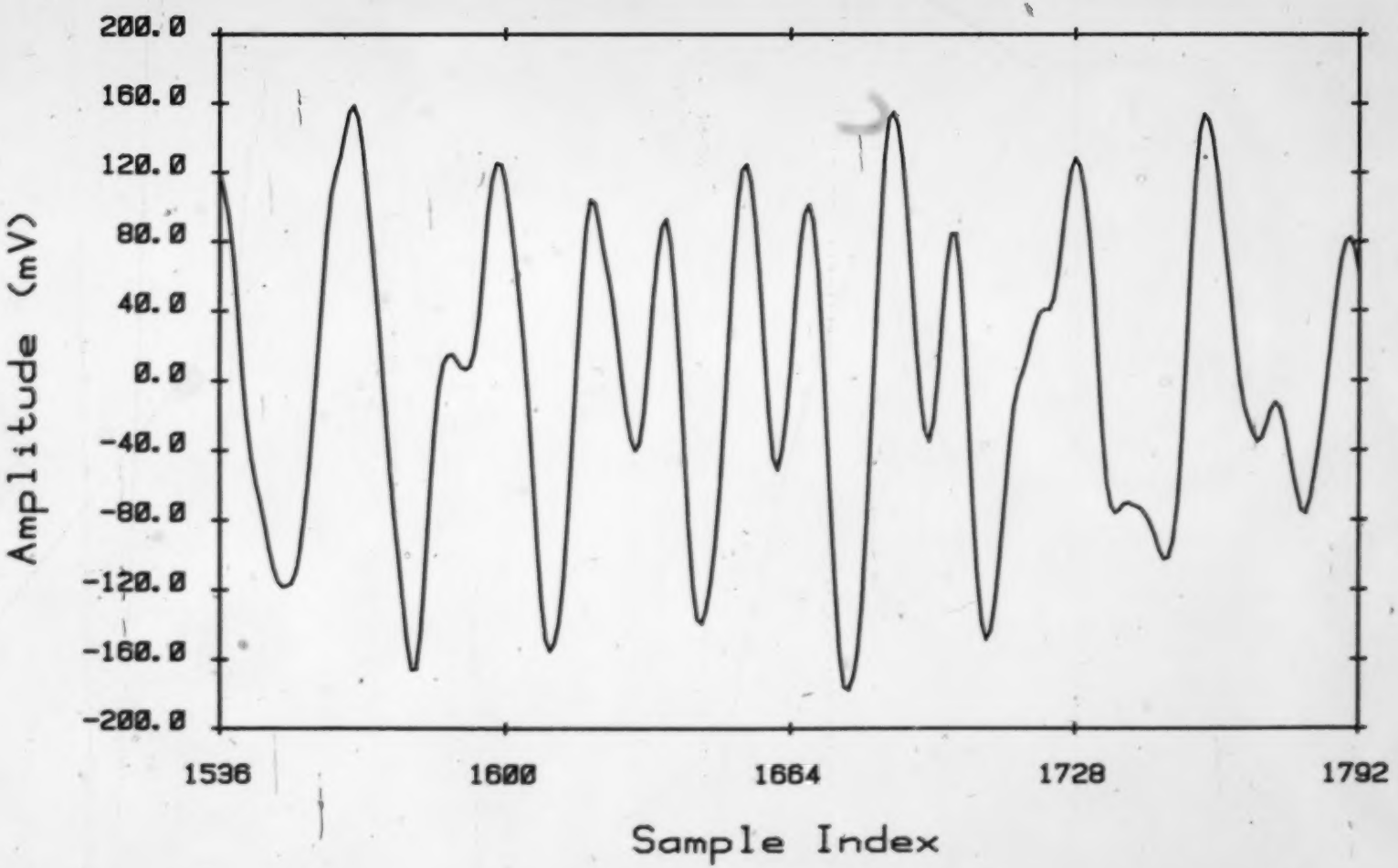


Fig. 4-21: Fixed Filter Output Before Linear Sweep

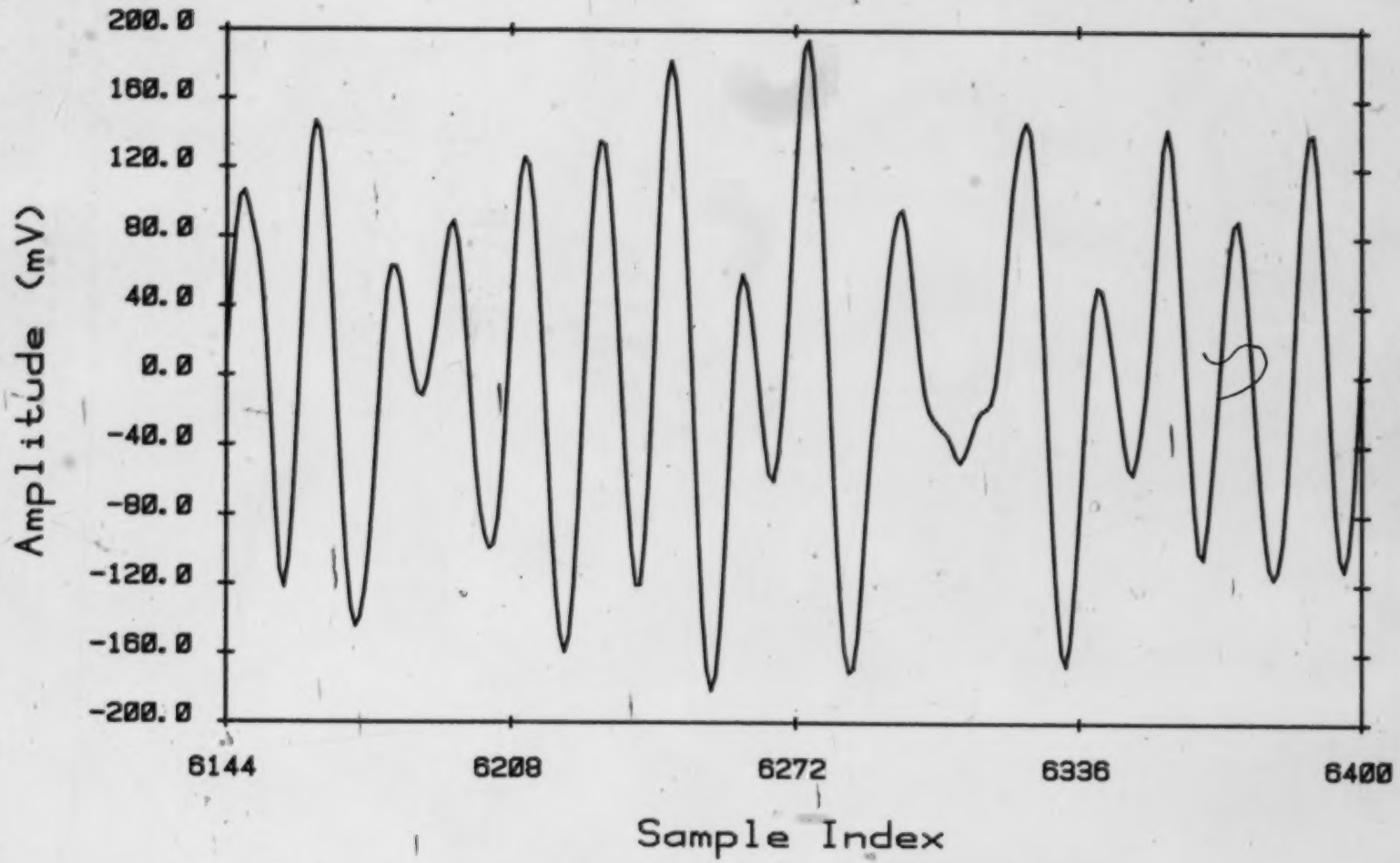


Fig. 4-22: Fixed Filter Output After Linear Sweep

## 4.5. Application of the Adaptive EGG Filter

In this section, the adaptive EGG filter of Fig. 2-5 will be applied to the recovery of a sine wave s corrupted by additive white noise ($n_d$). The signal parameters are given in Table 4-3. In this example, the noise signal $n_x$ applied to the x input is obtained by band-reject filtering the d input signal to suppress the sinusoidal component. The parameters of the filter H(z) are given in Table 4-7. The d input signal is plotted in Fig. 4-8. Note that the filter is of low order and has a bandwidth of only 0.6 cpm. The ANC is configured with four weights and $\mu = 5.572 \times 10^{-7}$.

In this situation, the signals are no longer ideal. The noise signal $n_x$ is only an estimate of the actual noise $n_d$, and $n_x$ also contains some of the signal component s. Both of these complications are caused by the non-ideal fixed filter H(z). Therefore, we can expect the the results obtained in this example will be worse than those obtained in Section 4.2.

The resulting output signal is plotted in Fig. 4-23, and the corresponding magnitude and phase spectra are plotted in Figs. 4-24 and 4-25, respectively. Comparison

| Order | Type | Ripple | Lower 3dB Cutoff | Upper 3dB Cutoff |
|---|---|---|---|---|
| 2 | Band Reject | 3 dB | 3.45 cpm | 4.05 cpm |

Table 4-7: Filter Parameters for H(z)

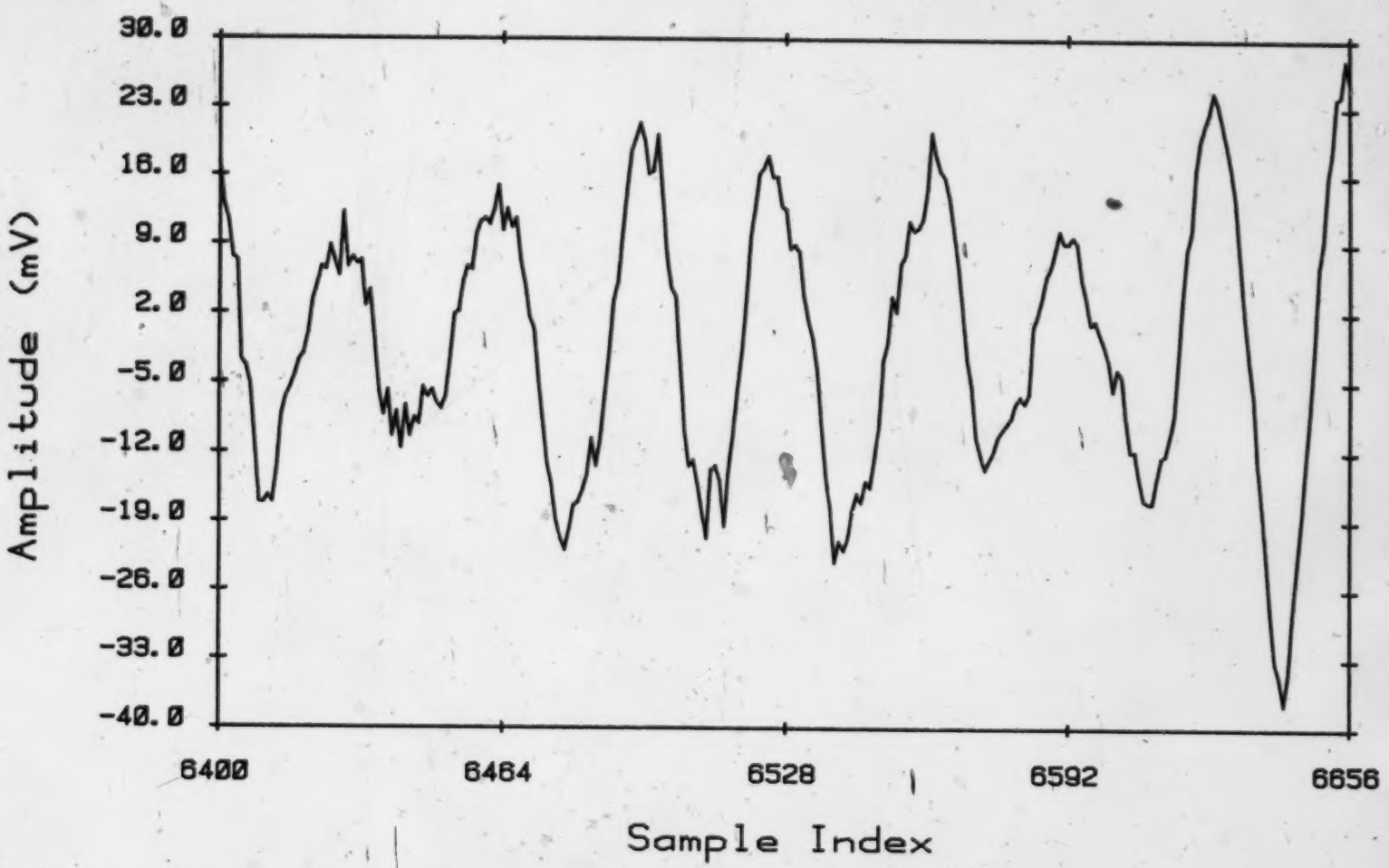


Fig. 4-23: The Output Signal After Convergence

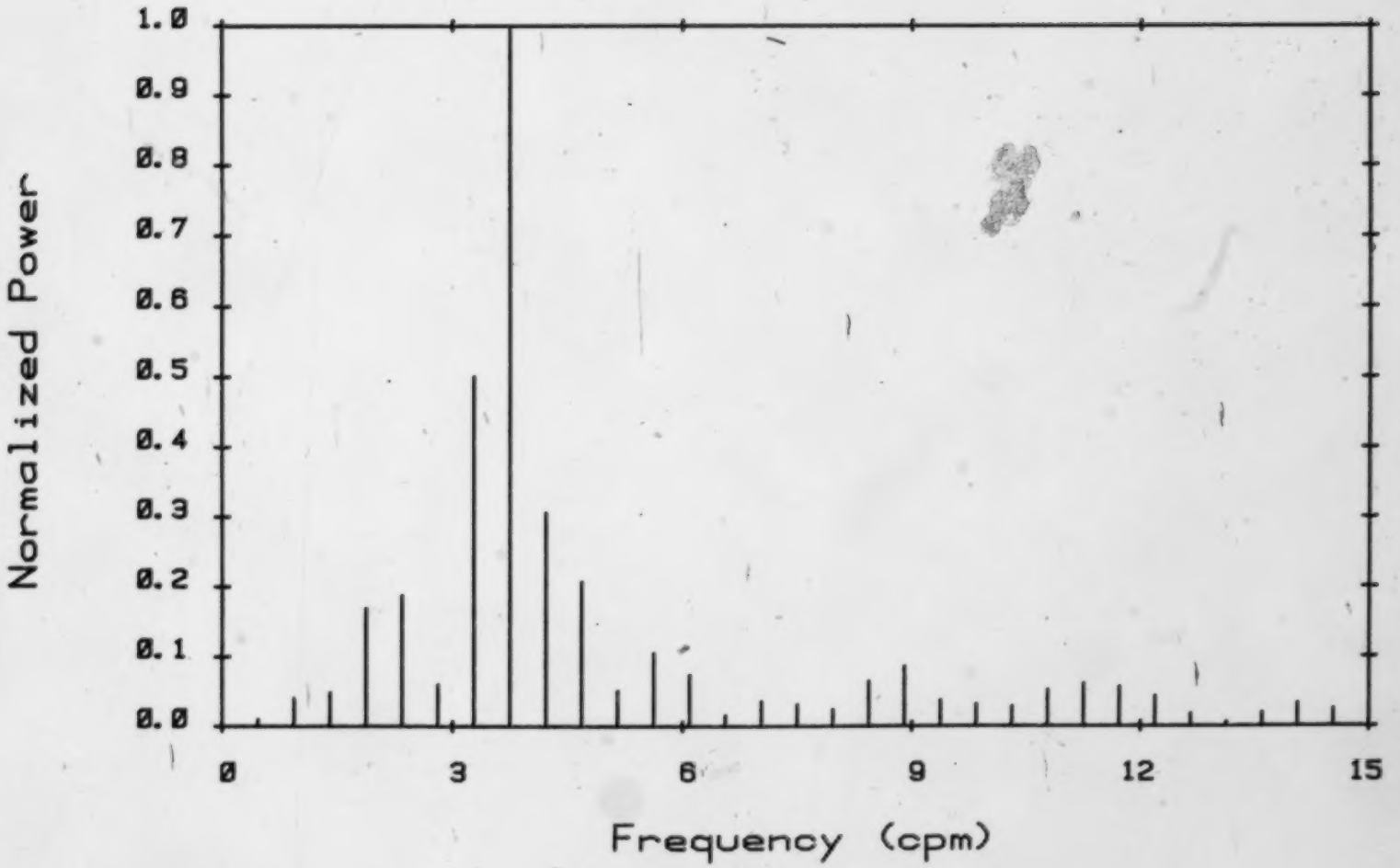


Fig. 4-24: Magnitude Spectrum of Fig. 4-23

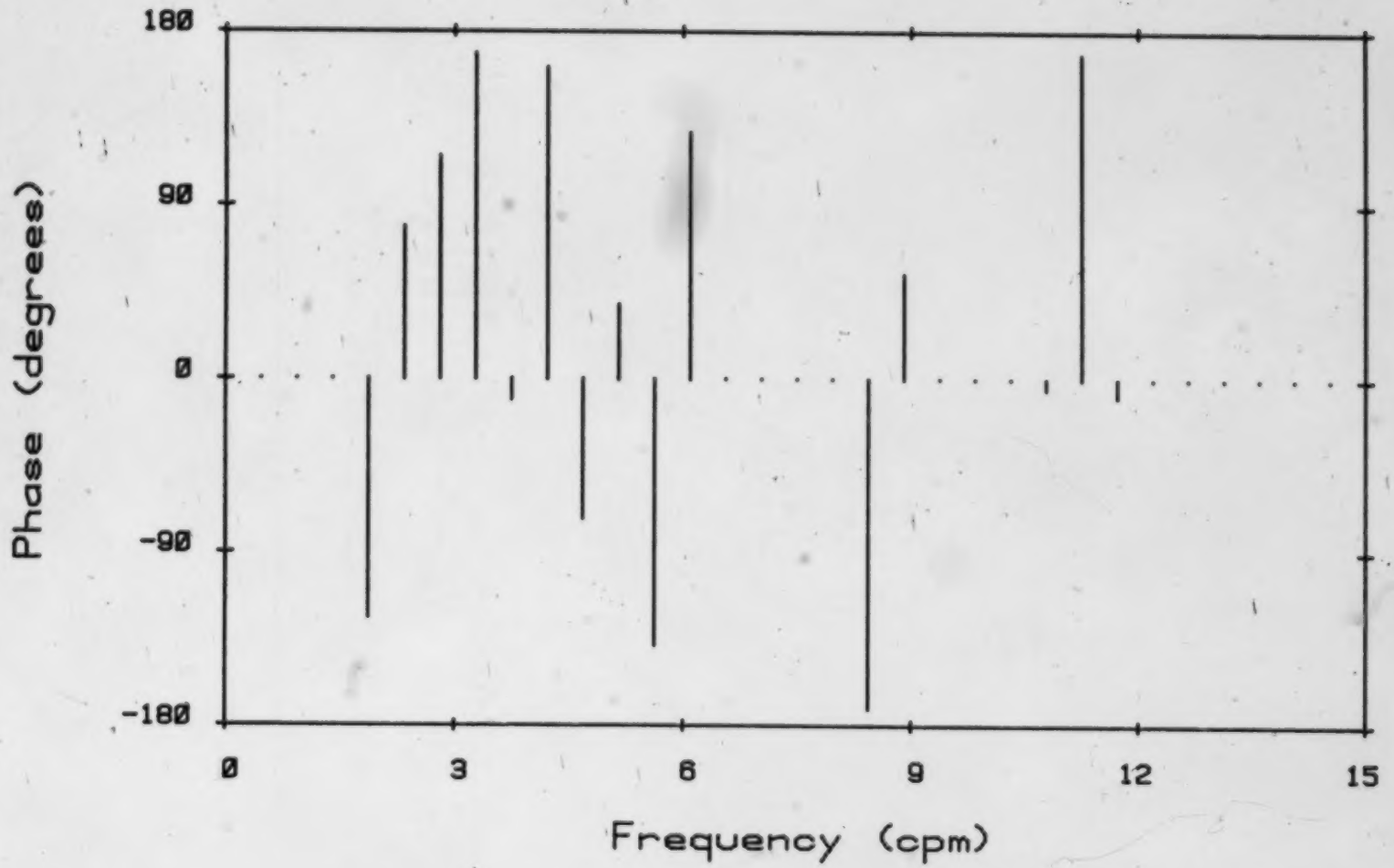


Fig. 4-25: Phase Spectrum of Fig. 4-23

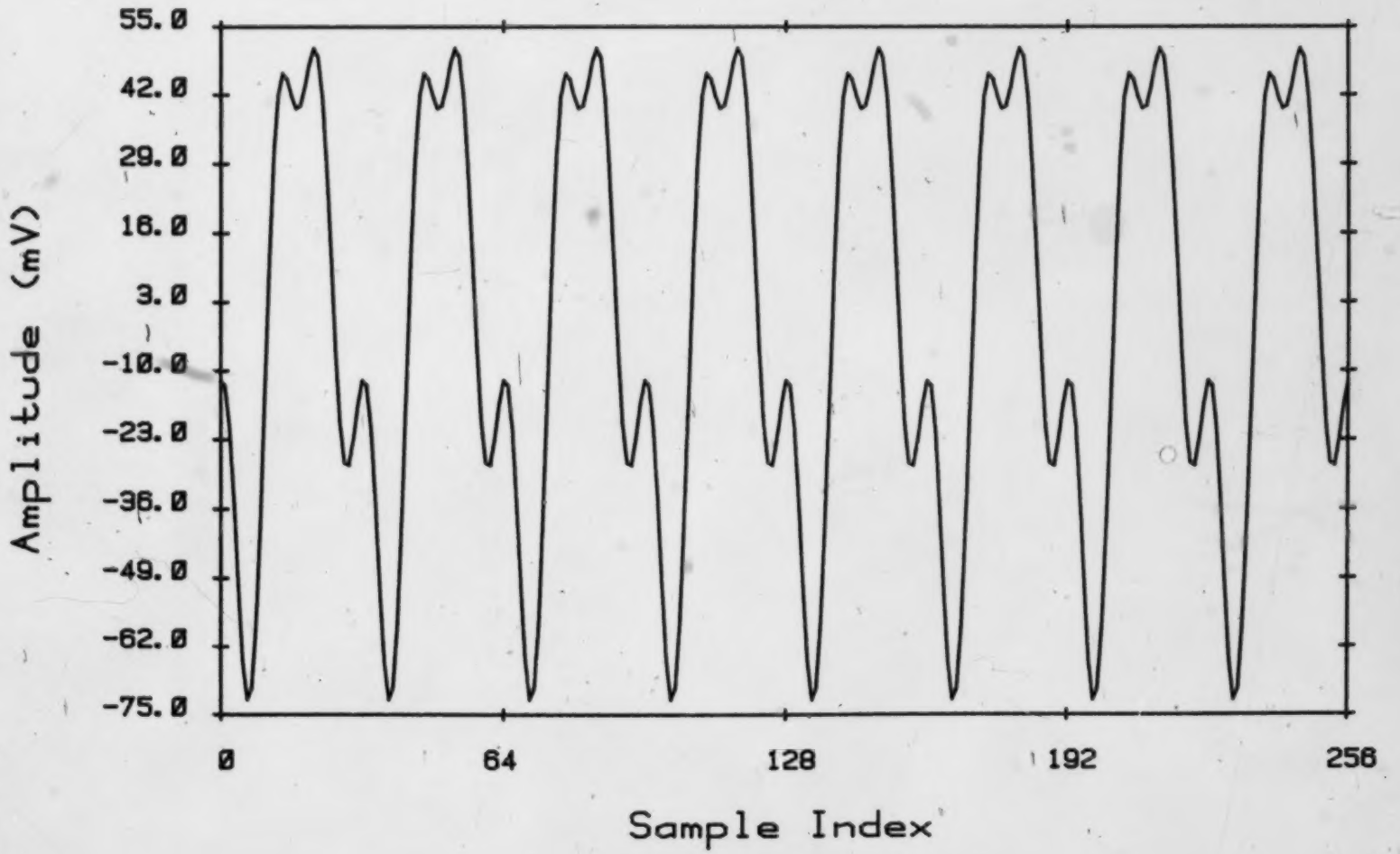


Fig. 4-26: Simulated Electrogastrogram

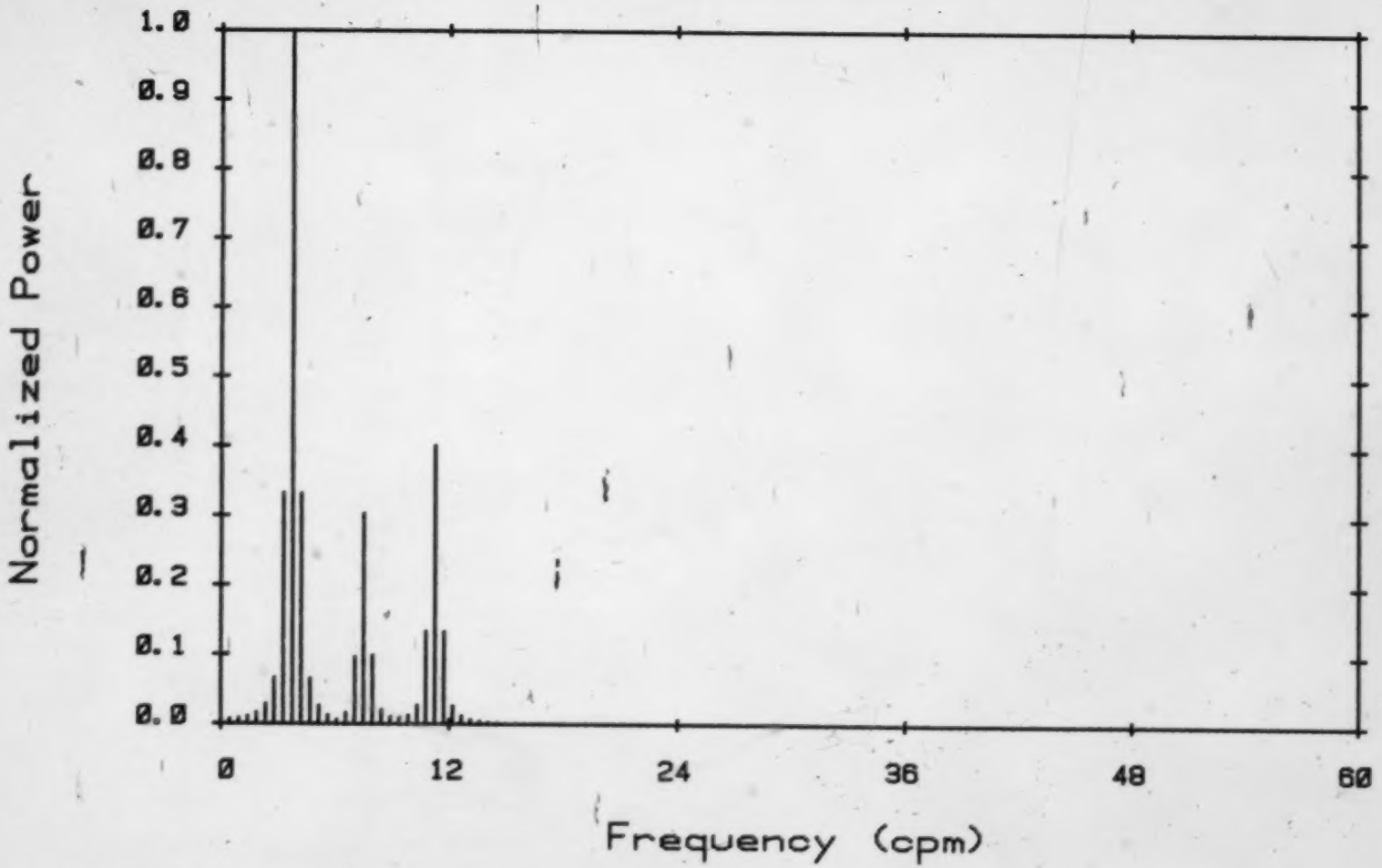


Fig. 4-27: Magnitude Spectrum of Fig. 4-26

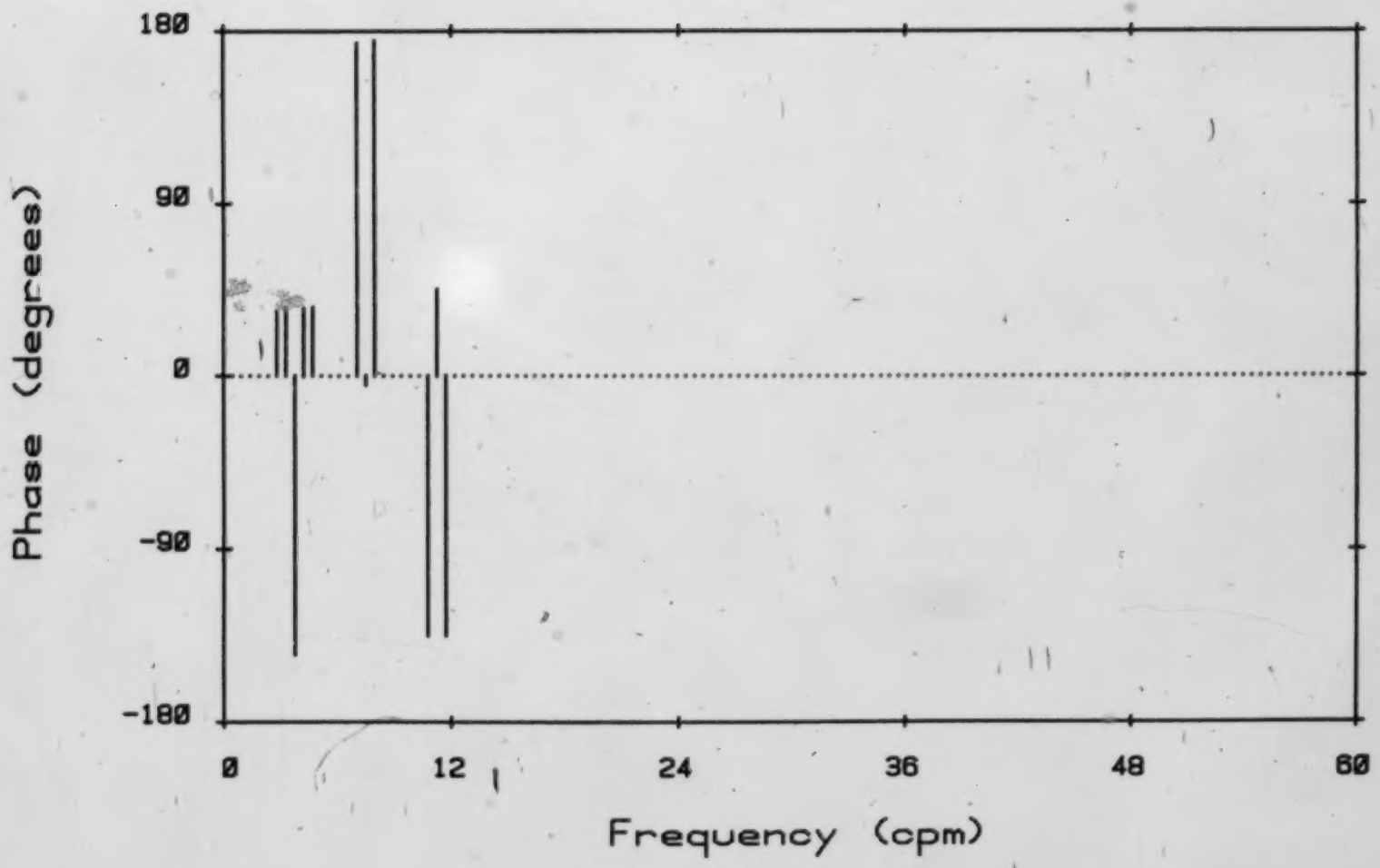


Fig. 4-28: Phase Spectrum of Fig. 4-26

of these graphs with Figs. 4-9, 4-10, and 4-11 indicates that the performance of the ANC has suffered because of the non-ideal filter H(z). However, the adaptive EGG filter used in this example produces an output that is closer to the original sinusoid than does the fixed filter (cf. Fig. 4-12) with similar input signals.

## 4.6. Recovering a Simulated EGG

The ANC of Fig. 2-5 can be used to recover several components of a waveform by using several cascaded band-reject filters for H(z), as was discussed in Section 2.3. To demonstrate this application, the waveform of Fig. 4-26 was generated. The parameters of this signal are given in Table 4-8. These parameters are intended to create a signal that closely resembles the EGG waveform. The magnitude and phase spectra are plotted in Figs. 4-27 and 4-28, respectively.

| Frequency (cpm) | Amplitude (mVpp) | Phase (degrees) |
|---|---|---|
| 3.75 | 100 | 145 |
| 7.50 | 30 | -5 |
| 11.25 | 40 | 45 |

Table 4-8: Signal Parameters for Fig. 4-26

| Frequency (cpm) | Amplitude (mVpp) | Phase (degrees) |
|---|---|---|
| 20.625 | 50 | 0 |

Table 4-9: Signal Parameters for Simulated Respiration

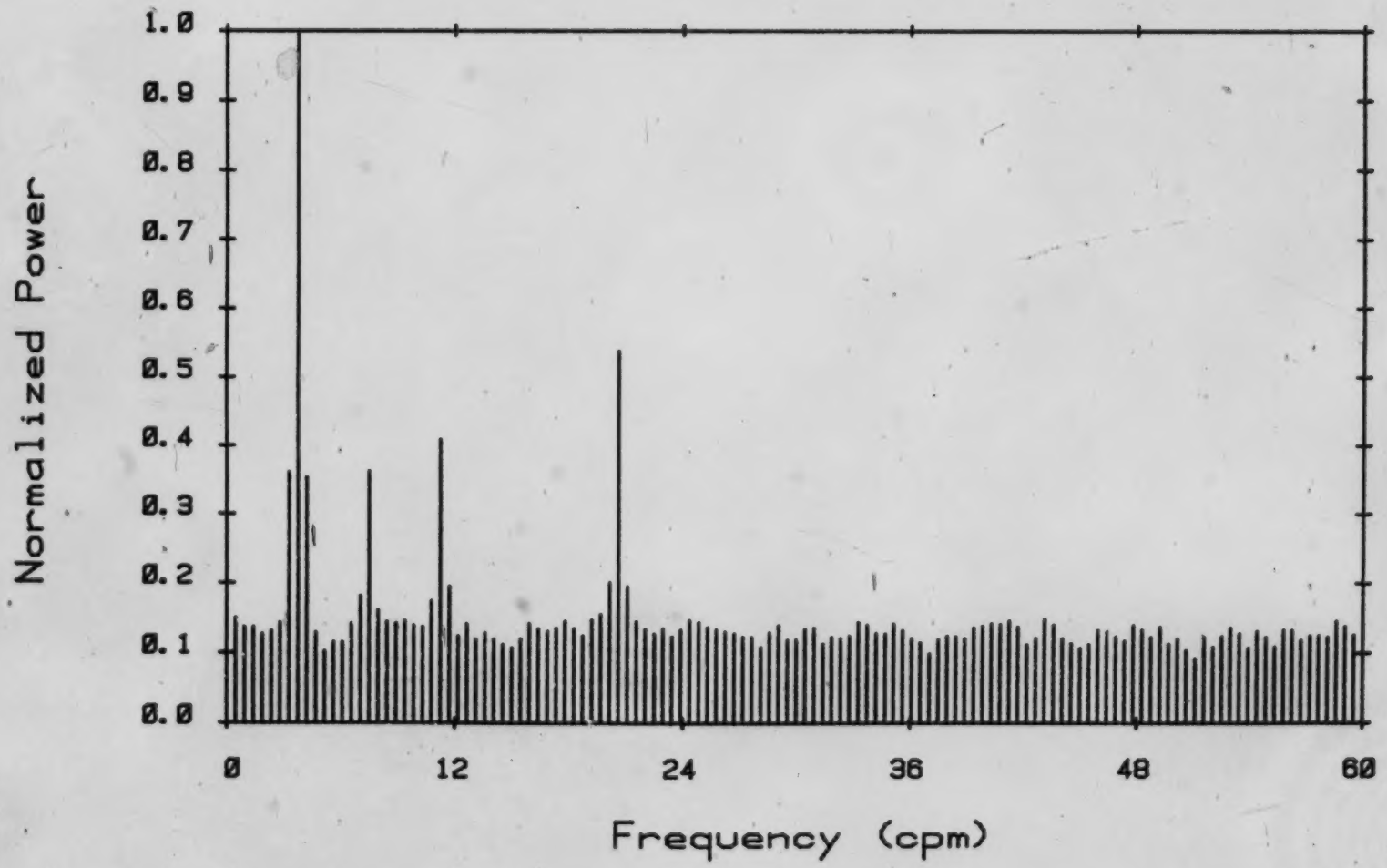


Fig. 4-29: Average Spectrum of the Simulated Signal

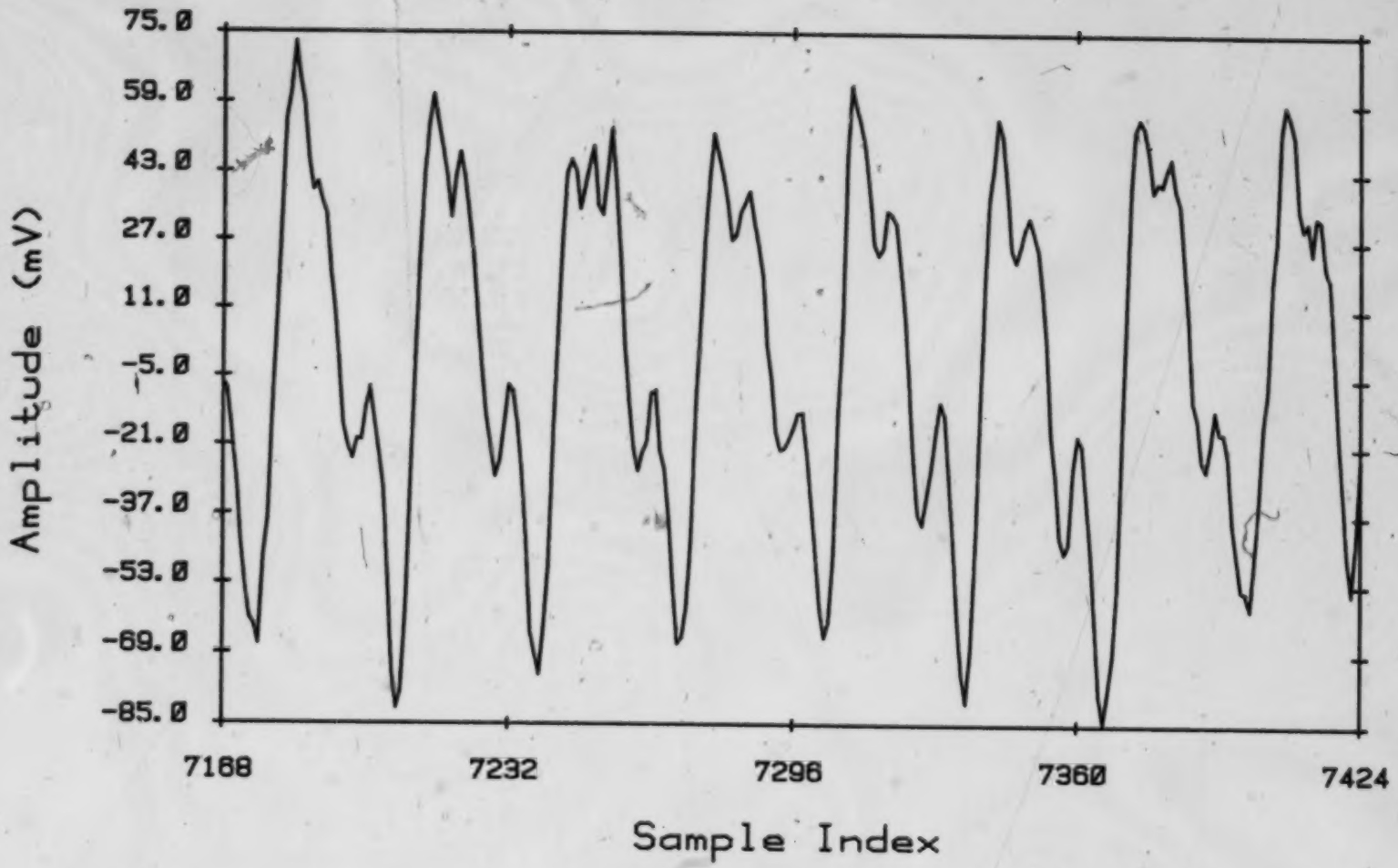


Fig. 4-30: The Output Signal After Convergence

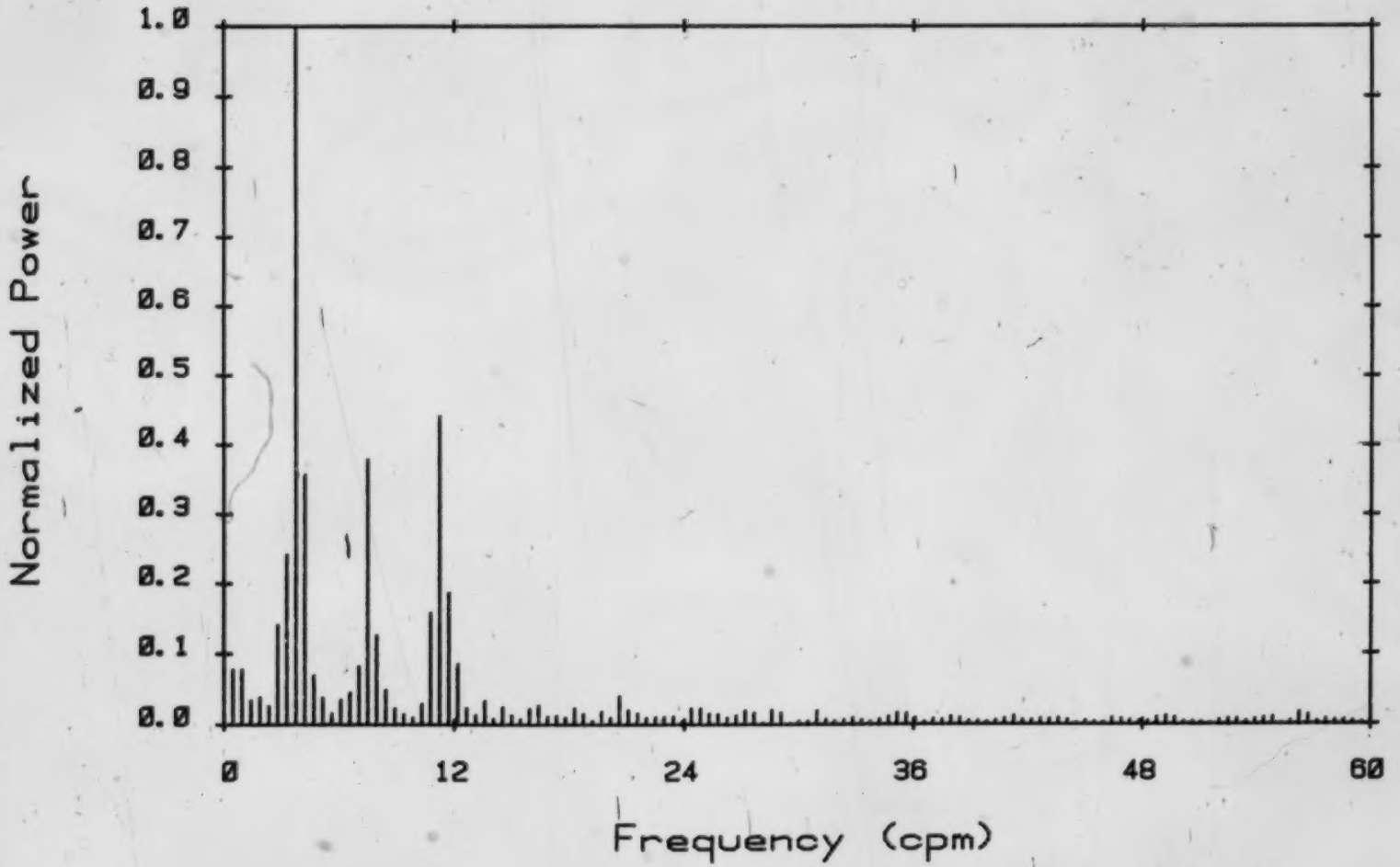


Fig. 4-31: Magnitude Spectrum of Fig. 4-30

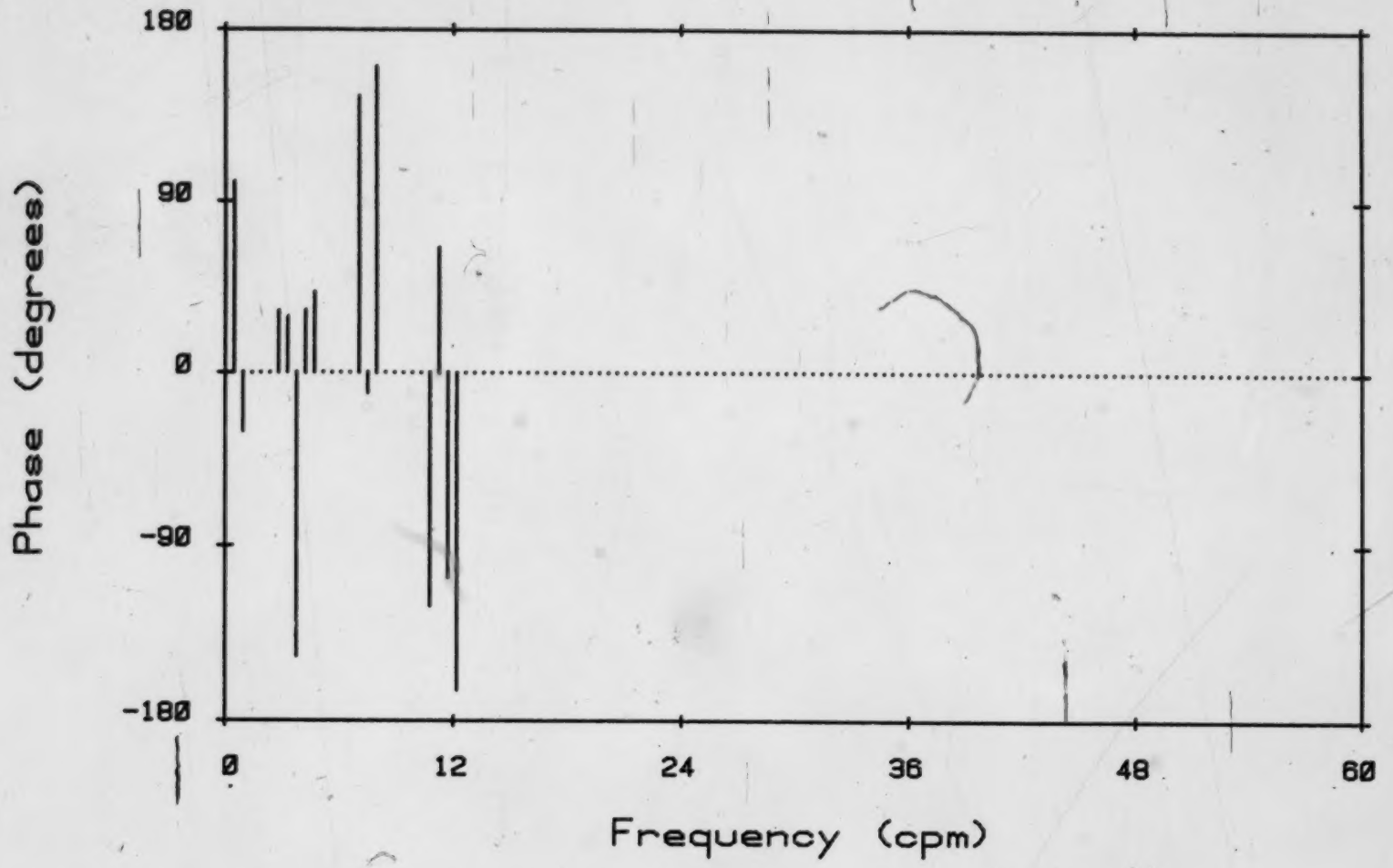


Fig. 4-32: Phase Spectrum of Fig. 4-30

To simulate the noise distorting the transcutaneous EGG, white noise (representing random interference) and a sinusoid (representing the respiration signal) with the parameters given in Table 4-9 are added to the signal of Fig. 4-26. The average magnitude spectrum of the resulting simulated transcutaneous EGG is plotted in Fig. 4-29. This is the signal that will be filtered in an attempt to recover the signal of Fig. 4-26.

The ANC used in this example was configured with four weights and $\mu = 2.067 \times 10^{-6}$. Three cascaded Chebyshev band-reject filters with the parameters given in Table 4-10 were used to suppress the desired signal components at the x input (cf. Fig. 2-5).

The resulting output signal after convergence is shown in Fig. 4-30, and the corresponding magnitude and phase spectra are given in Figs. 4-31 and 4-32, respectively. The output signal is evidently an approximation of the original input signal. Again we see that the non-ideal filters H(z) cause some slight distortion of the signal due to the limitations discussed

| Order | Type | Ripple | Lower 3dB Cutoff | Upper 3dB Cutoff |
|---|---|---|---|---|
| 2 | Band Reject | 3 dB | 3.45 cpm | 4.05 cpm |
| 2 | Band Reject | 3 dB | 7.20 cpm | 7.80 cpm |
| 2 | Band Reject | 3 dB | 10.95 cpm | 11.55 cpm |

Table 4-10: Filter Parameters for H(z)

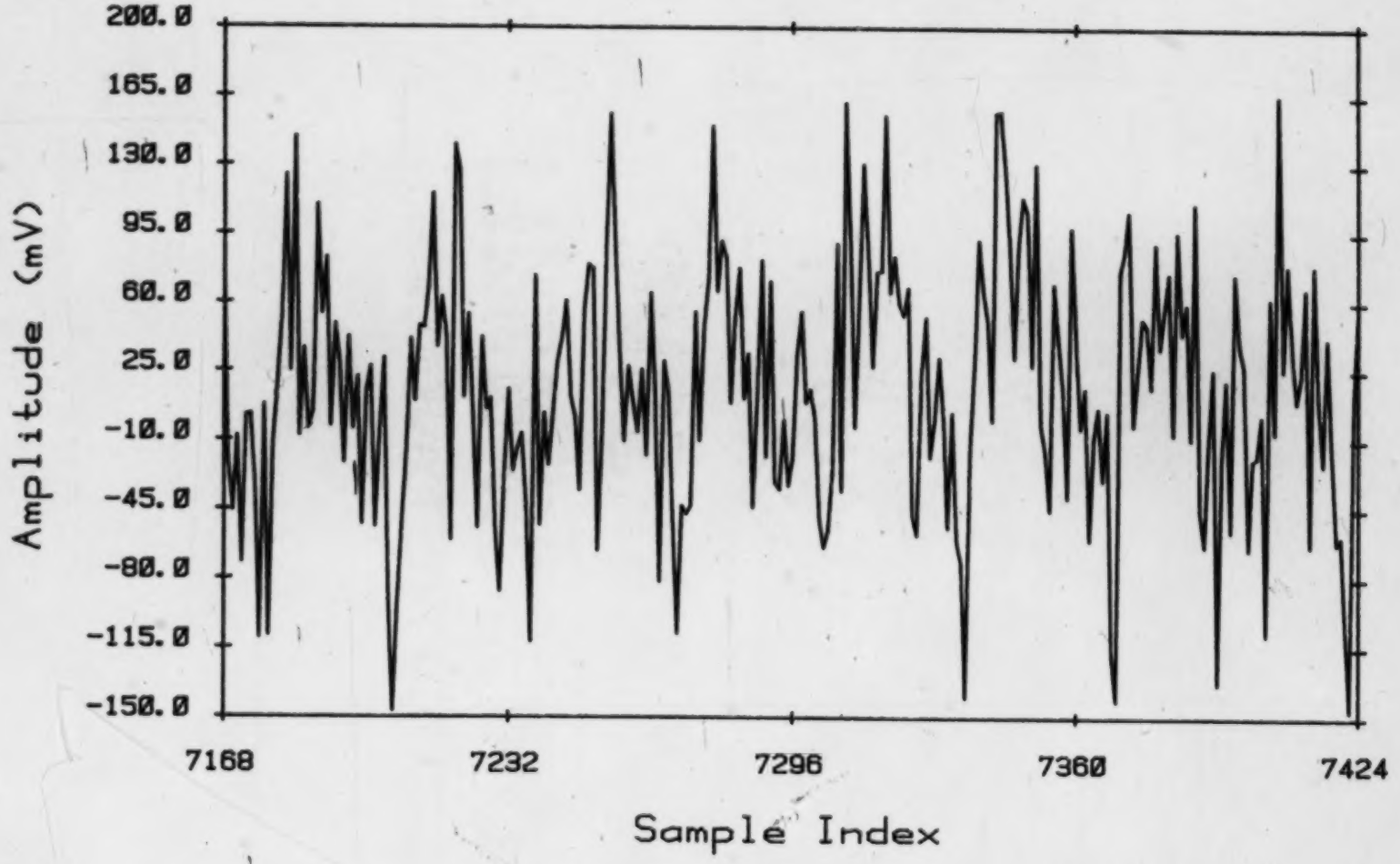


Fig. 4-33: The Simulated Transcutaneous EGG

in the previous section. However, the graphs clearly show that the output signal consists of three sinusoids with parameters approximating those in Table 4-8. Also, Fig. 4-30 confirms that the leading edge of the waveform exhibits a steeper slope than does the trailing edge. Thus, the useful information contained in the signal of Fig. 4-26 has been recovered even though the LMS approximation of the waveform is not exact.

It is also interesting to examine the plus/minus percentage of the signals involved in this example. For the simulated EGG of Fig. 4-26, the plus/minus percentage is computed as -77.1%. This means that the slope of the leading edge of the waveform is much steeper than the slope of the trailing edge. This result agrees with the previous conclusions.

The simulated transcutaneous EGG of Fig. 4-29 is distorted by white noise, so we can expect that the plus/minus percentage will be much lower than 77.1%. In fact, this is the case: the actual value is -1.3%. This low value indicates that the noise is obscuring the slope information. Visual inspection of this signal, which is shown in Fig. 4-33, does not reveal any significant information either.

After this signal is filtered, the plus/minus percentage is -6.6%. This confirms the previous conclusion that the slope of the leading edge is in fact steeper than the slope of the trailing edge, and agrees

with the observed characteristics of the actual signal.

## 5. Results Obtained From Patient Records

### 5.1. Patient Record #1

To introduce the application of the adaptive EGG filter to the recovery of actual human transcutaneous electrogastrograms, we will use an unusually noise-free patient record. The average magnitude spectrum of this record is shown in Fig. 5-1. This graph shows a strong fundamental component near bin six ($f_6$ = 2.8125 cpm), as well as harmonics near bins twelve ($f_{12}$ = 5.625 cpm) and eighteen ($f_{18}$ = 8.4375 cpm). A moderate amount of noise is visible between 10 cpm and 20 cpm, and the higher frequency noise is of low power. Since the fundamental and at least two harmonics are clearly visible above the background noise, we can expect the filter to produce a very good output signal.

A window taken from this record is shown in Fig. 5-2. The magnitude and phase spectra for this window are given in Figs. 5-3 and 5-4, respectively. Although noise is present, Fig. 5-2 clearly shows that the slope of the leading edge of the waveform is steeper than the slope of the trailing edge. This characteristic waveshape is not normally so distinct in a plot of the raw data.

The plus/minus percentage calculated for this record is -8.5%. This result confirms our conclusion arrived at by visual inspection, and indicates that the stomach contractions are travelling aborally. The analysis could

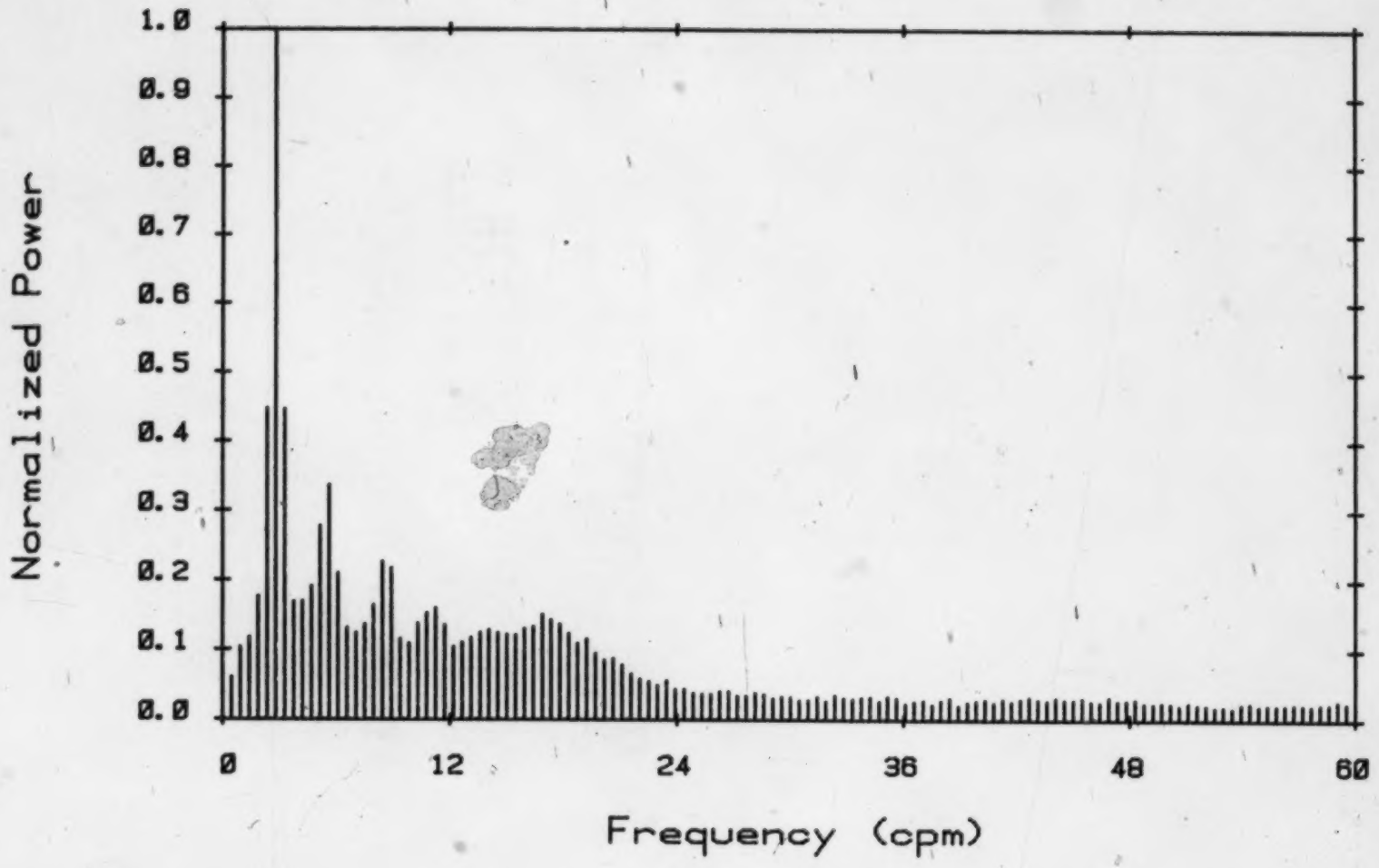


Fig. 5-1: Average Spectrum of Patient Record #1

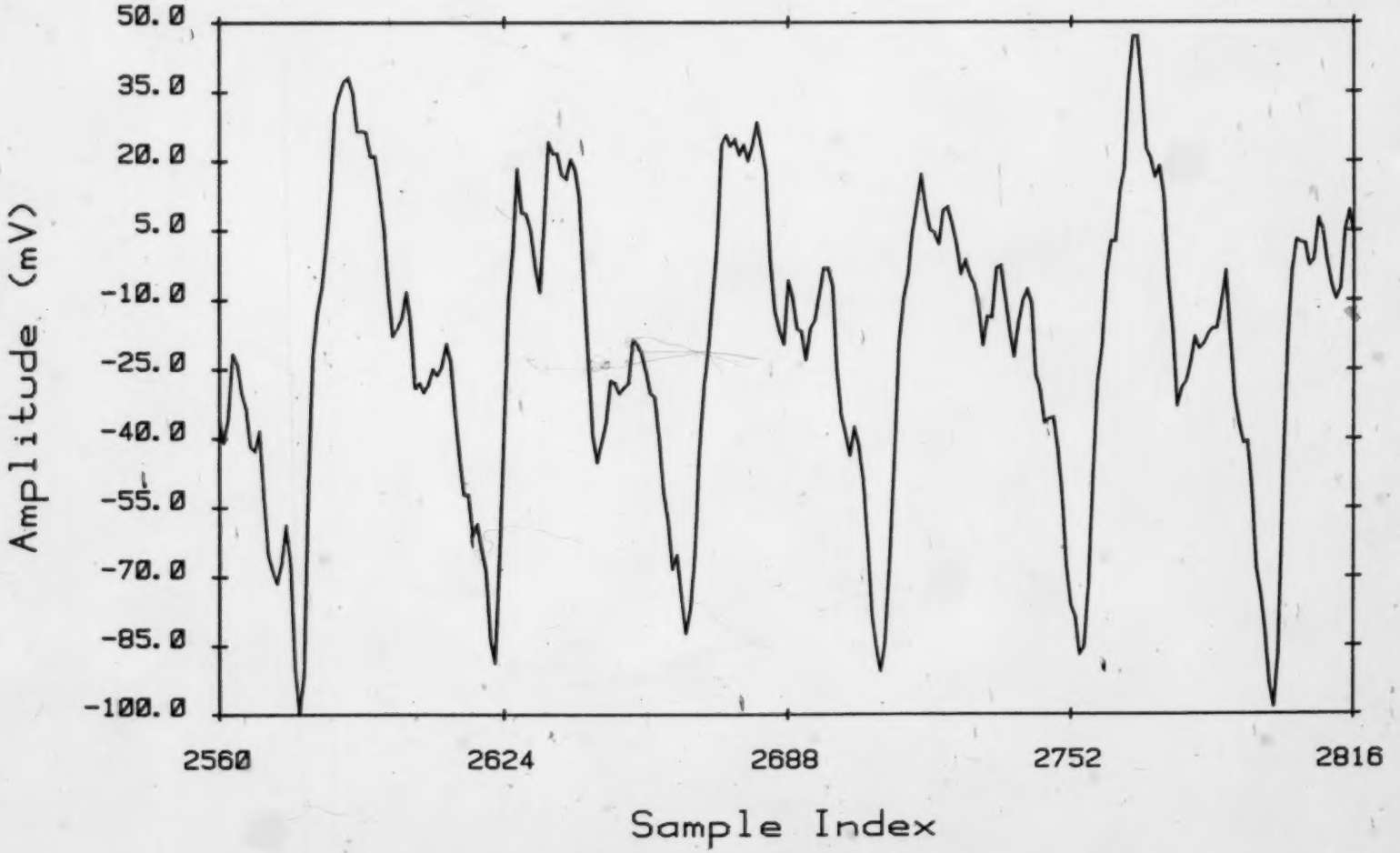


Fig. 5-2: A Window From Patient Record #1

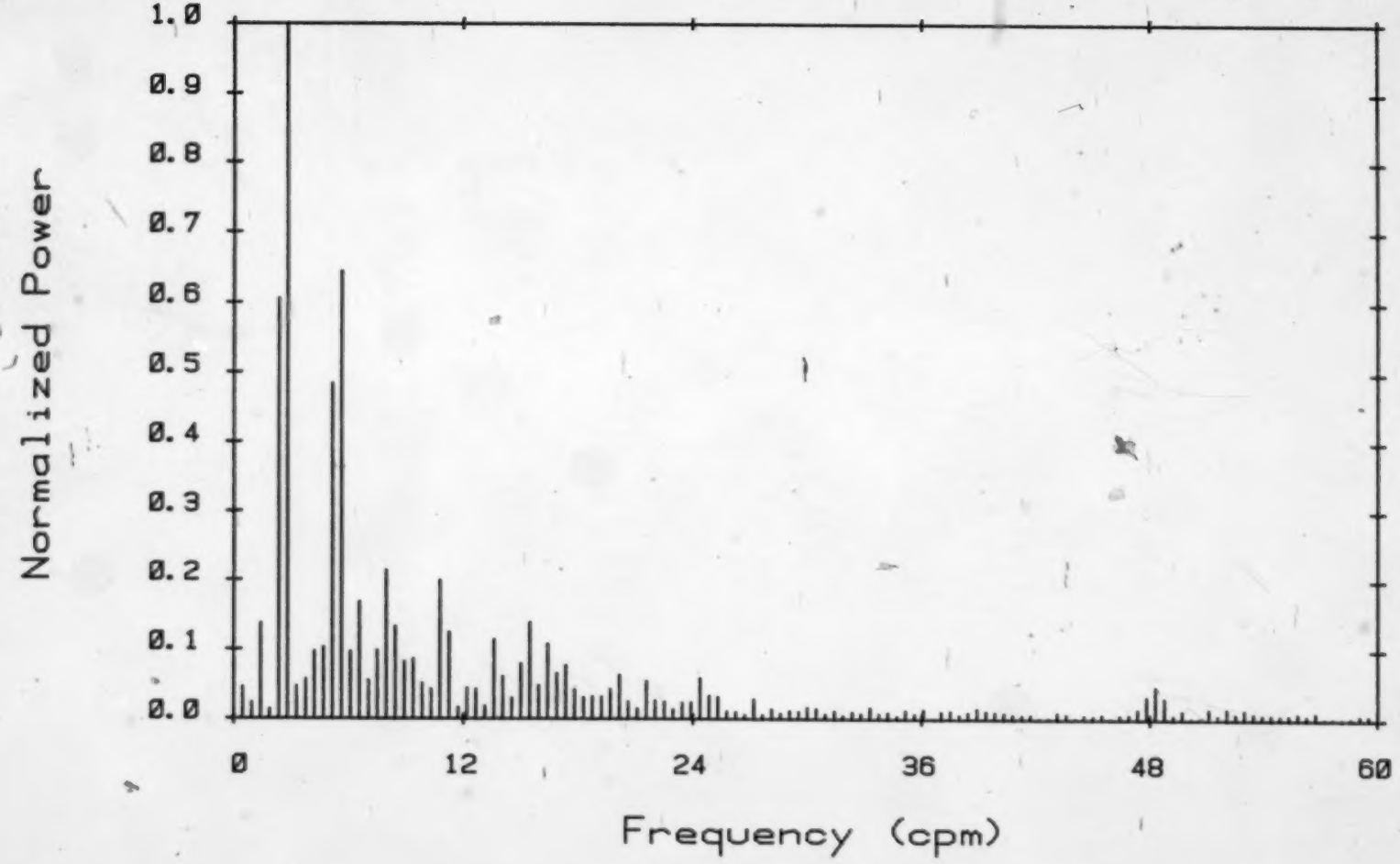


Fig. 5-3: Magnitude Spectrum of Fig. 5-2

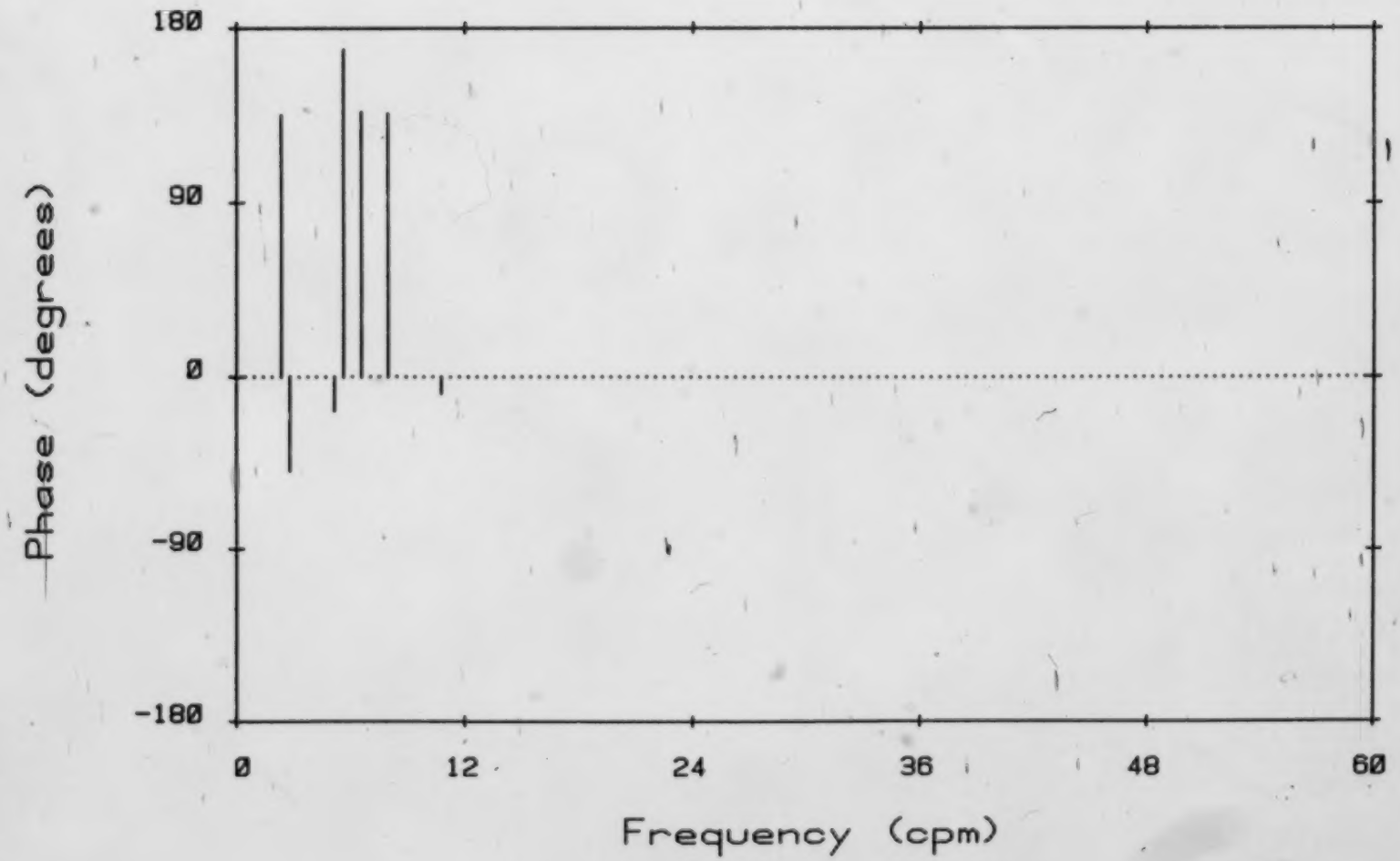


Fig. 5-4: Phase Spectrum of Fig. 5-2

now be considered complete because the pertinent information has been obtained directly from the original record. However, the adaptive filter can be used to clean up the record, and hence confirm these conclusions.

The adaptive filter is again configured as shown in Fig. 2-5. Four weights are used. On the two passes, $\mu$ is set to $5.4 \times 10^{-6}$ and $5.4 \times 10^{-7}$, respectively. The fixed filter H(z) is made up of a cascade of three Chebyshev band-reject filters with the parameters given in Table 5-1. The narrow bandwidth of each filter is made possible because the frequencies of the three signal components of interest can be found by inspection of Figs. 5-1 and 5-3. Note that all other components of the actual EGG are considered to be noise by the adaptive filter.

The average magnitude spectrum of the output signal is plotted in Fig. 5-5. Comparison of this graph with Fig. 5-1 shows a significant increase in the SNR of the data. Fig. 5-6 shows a window taken from the output record at a time corresponding to Fig. 5-2. Evidently, the conclusions drawn from the input signal are correct.

| Order | Type | Ripple | Lower 3dB Cutoff | Upper 3dB Cutoff |
|---|---|---|---|---|
| 2 | Band Reject | 3 dB | 2.5 cpm | 3.1 cpm |
| 2 | Band Reject | 3 dB | 5.3 cpm | 5.9 cpm |
| 2 | Band Reject | 3 dB | 8.1 cpm | 8.7 cpm |

Table 5-1: H(z) Parameters For EGG Recovery

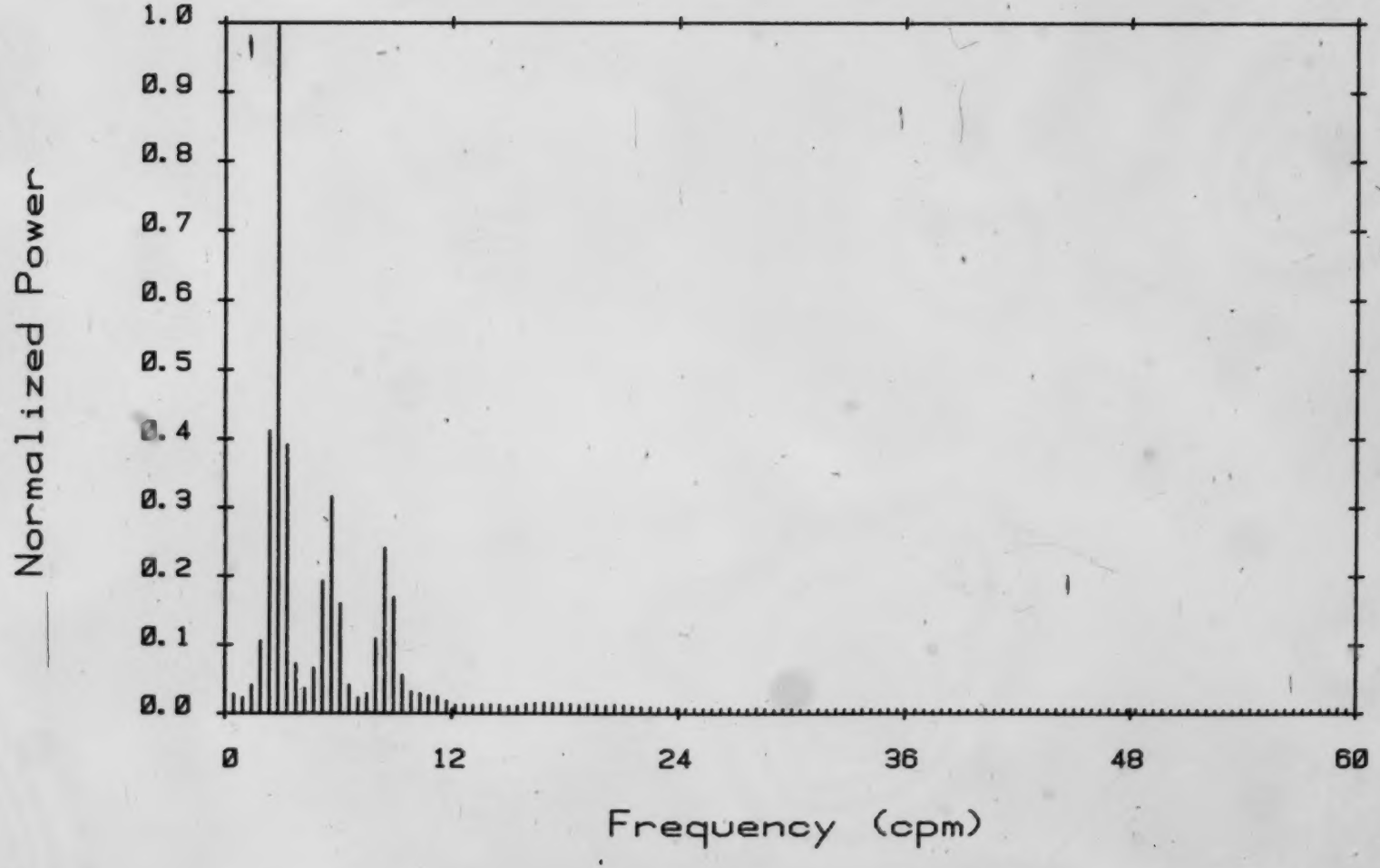


Fig. 5-5: Average Spectrum of Filtered Record #1

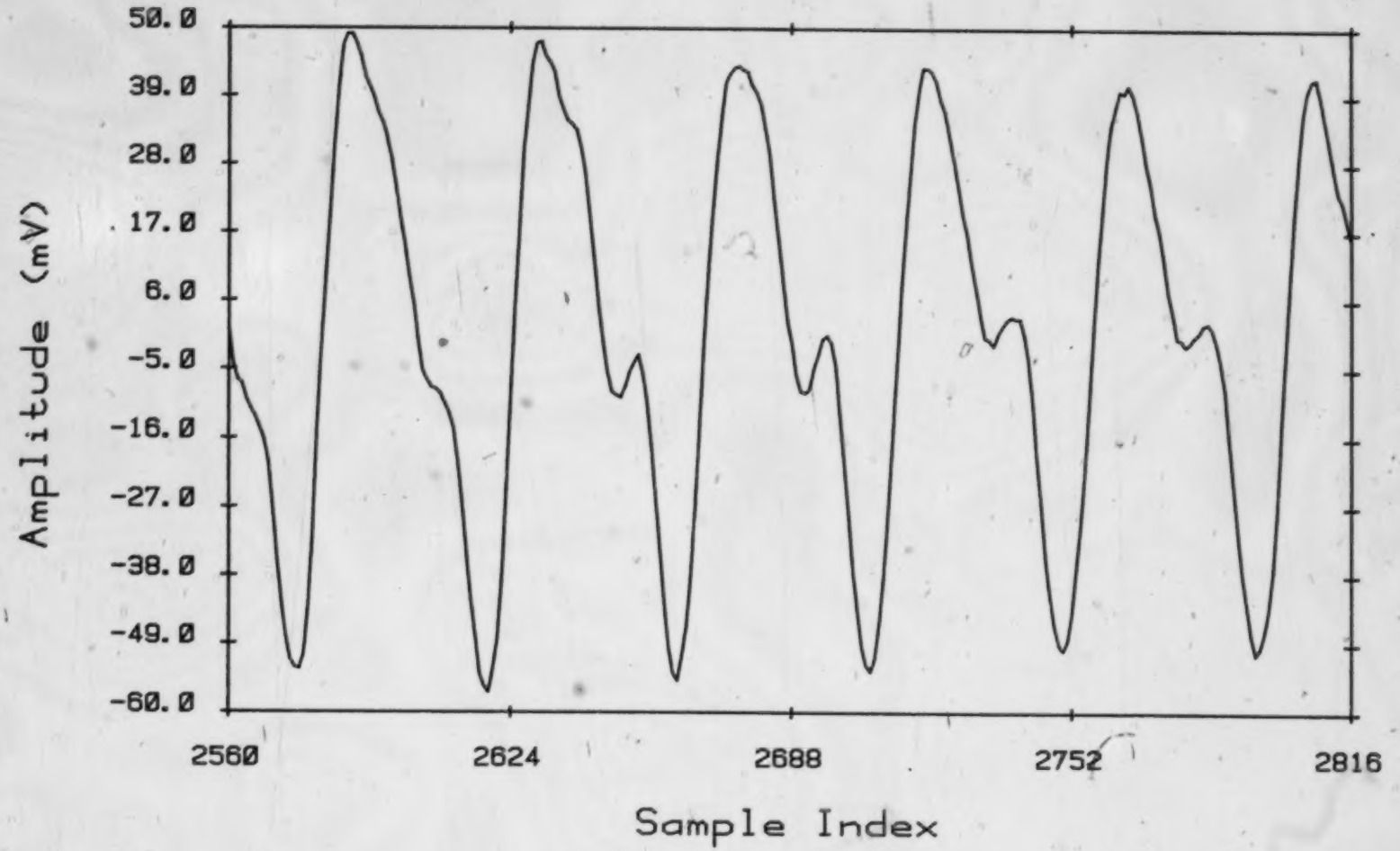


Fig. 5-6: The Output Signal After Convergence

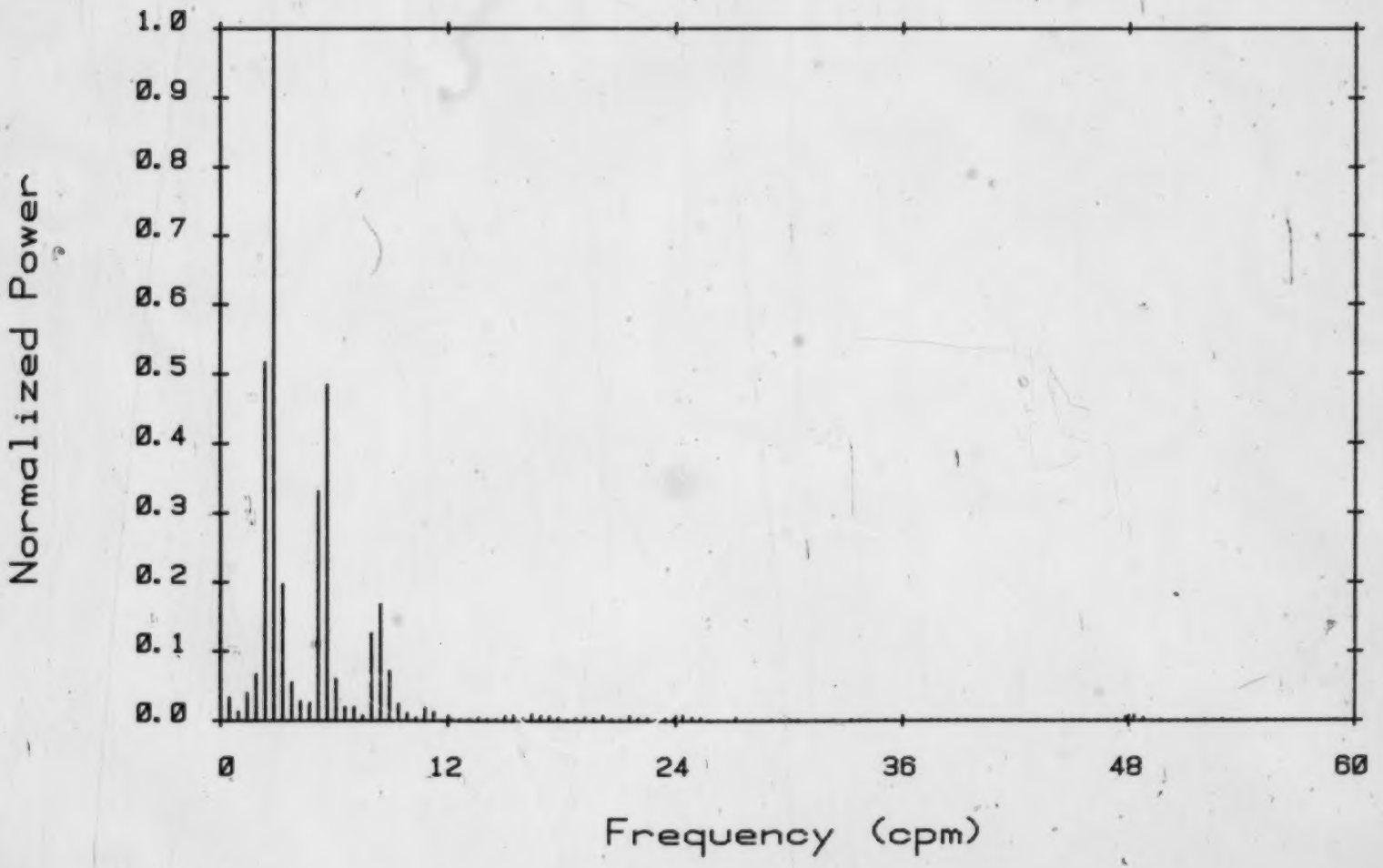


Fig. 5-7: Magnitude Spectrum of Fig. 5-6

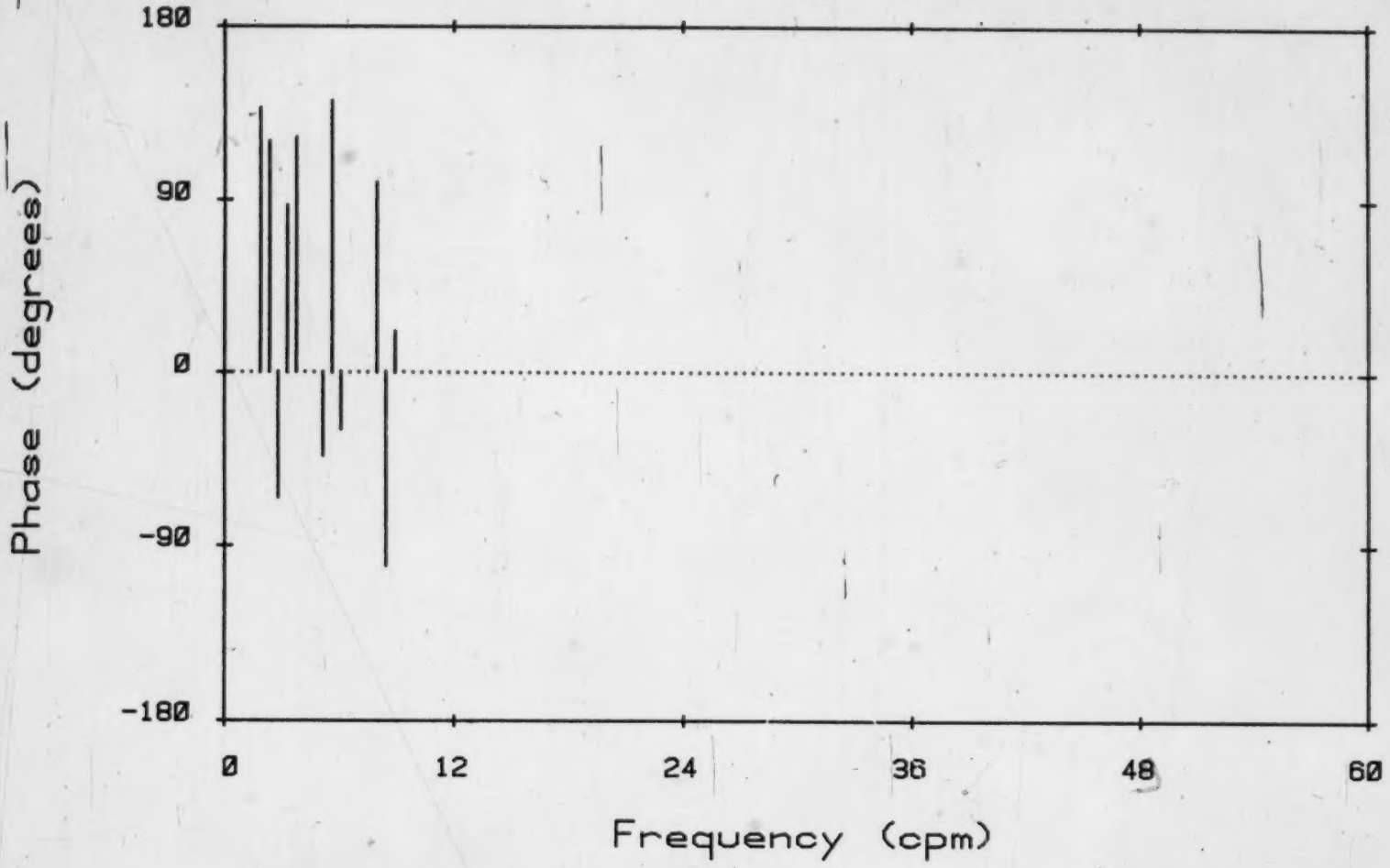


Fig. 5-8: Phase Spectrum of Fig. 5-6

However, Fig. 5-6 provides a more accurate indication of the actual shape of the EGG. The magnitude and phase spectra of Fig. 5-6 are plotted in Figs. 5-7 and 5-8, respectively.

The plus/minus percentage for the filtered signal is -13.2%. This agrees in sign with the result obtained for the original record, and is larger in magnitude because the noise has been largely suppressed. Again, the results of the initial analysis have been confirmed.

This example shows that the adaptive filter does not alter the medical information contained in the EGG. Instead, it enhances the reliability of the observations by suppressing the noise that obscures the waveform. Of course, the record used in this example is not a typical noisy signal. In the two examples that follow, noisier records will provide an indication of the usefulness of the adaptive filter in processing more typical signals.

## 5.2. Patient Record #2

The average magnitude spectrum of another patient record is plotted in Fig. 5-9. Comparison of this graph with Fig. 5-1 shows that this record contains slightly more power in the dc to 12 cpm range of frequencies than did the first. However, there is less power at higher frequencies in this record than in the previous case. Again, the fundamental appears near bin six, and at least three harmonics are visible above the background noise.

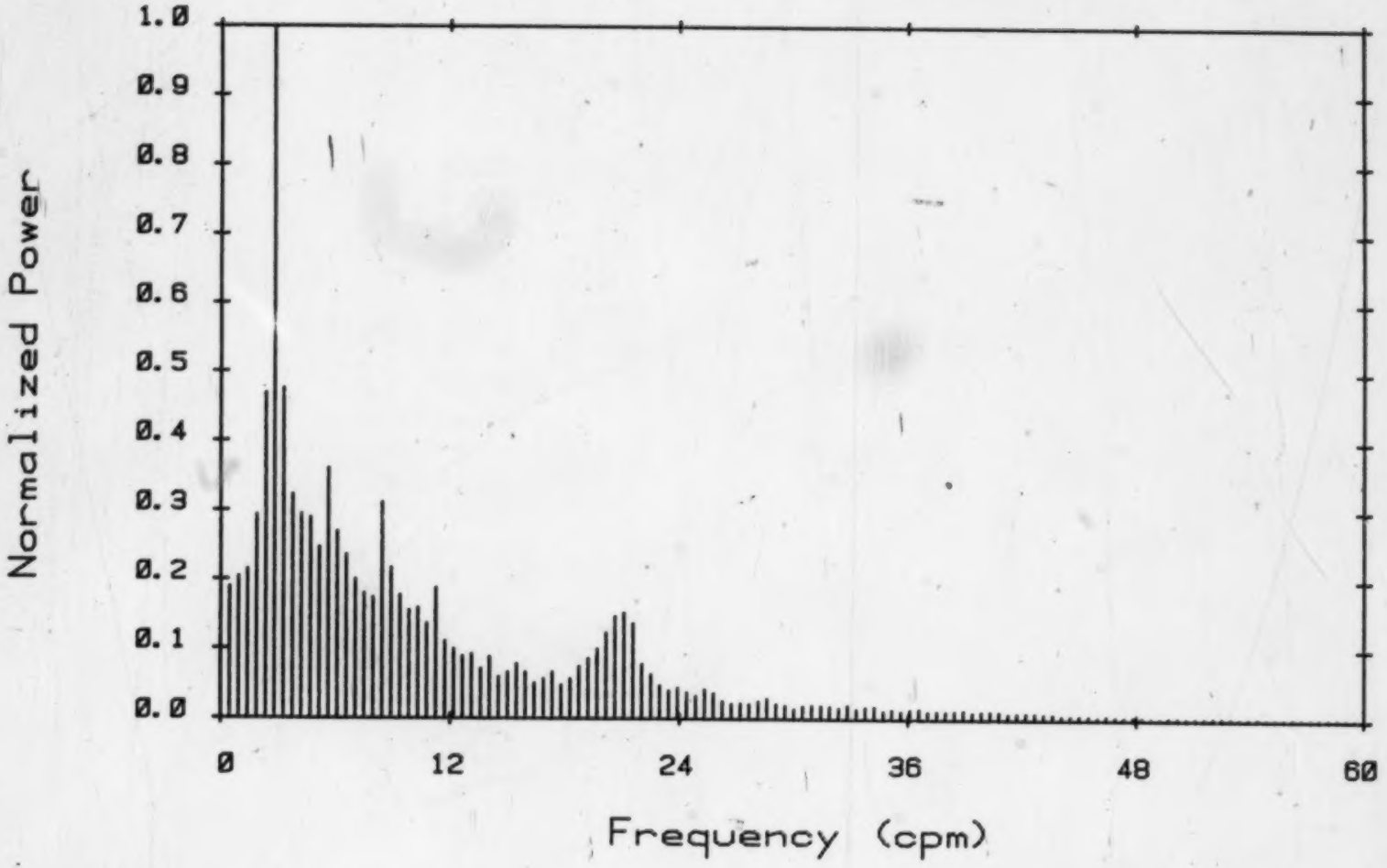


Fig. 5-9: Average Spectrum of Patient Record #2

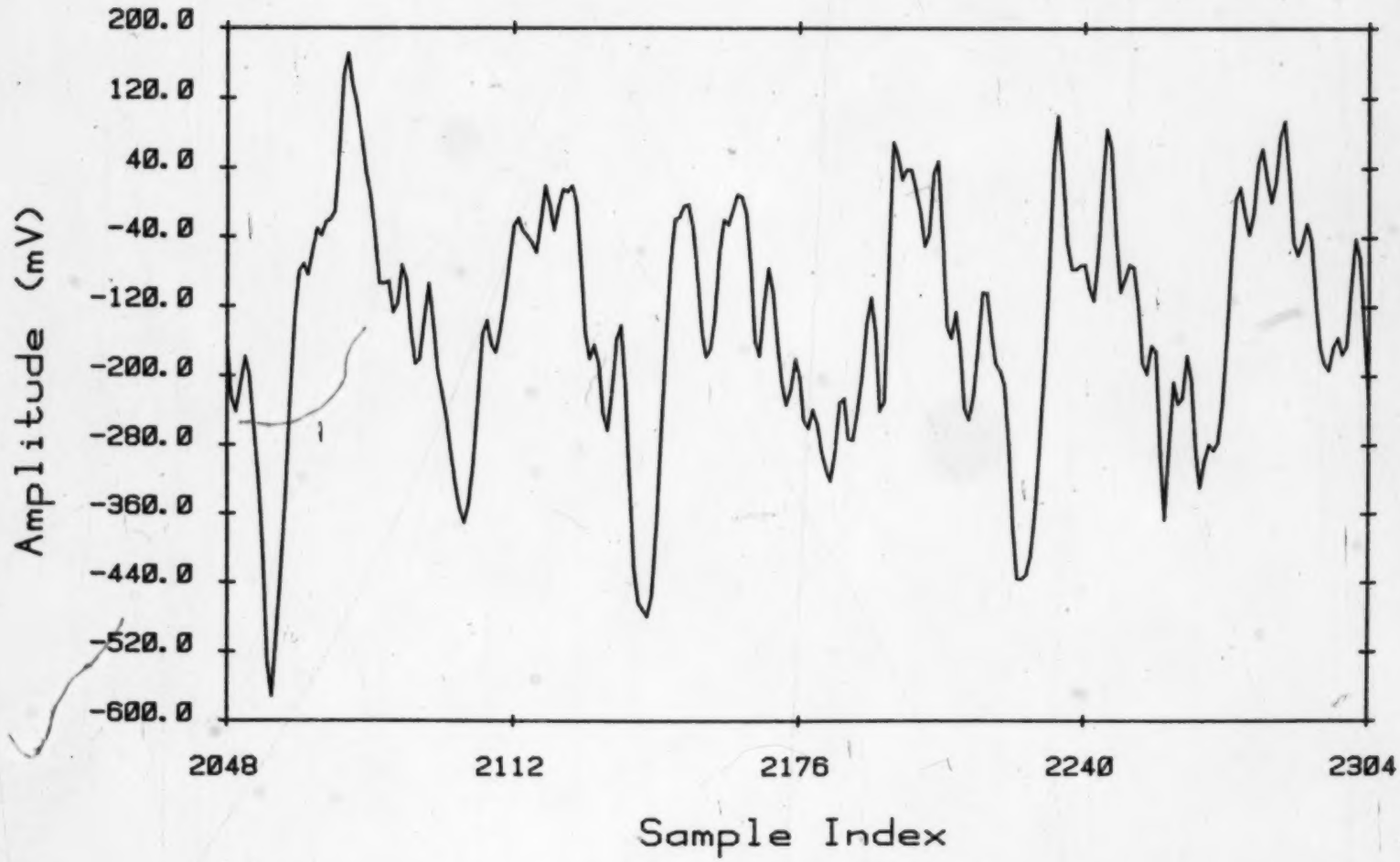


Fig. 5-10: A Window From Patient Record #2

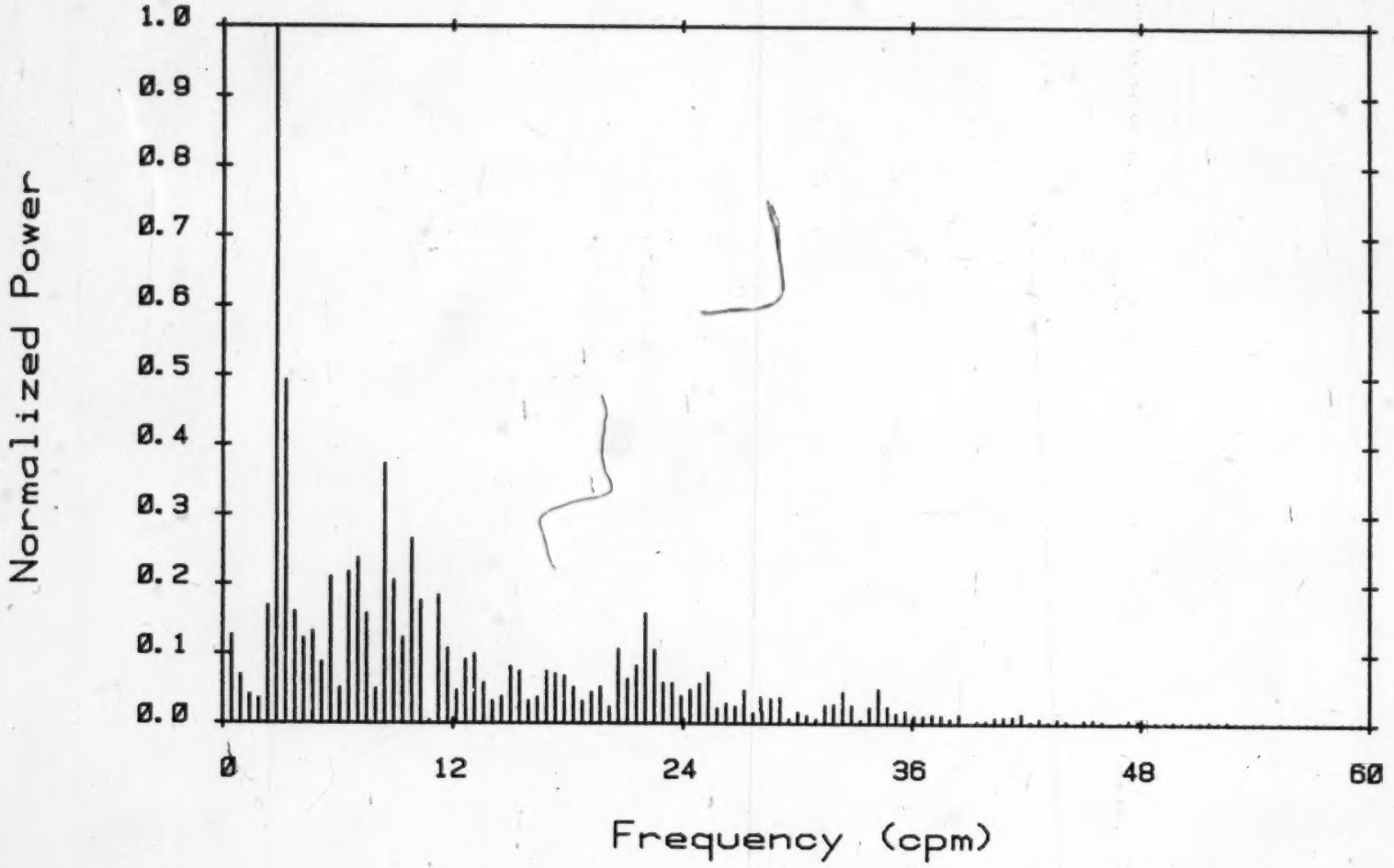


Fig. 5-11: Magnitude Spectrum of Fig. 5-10

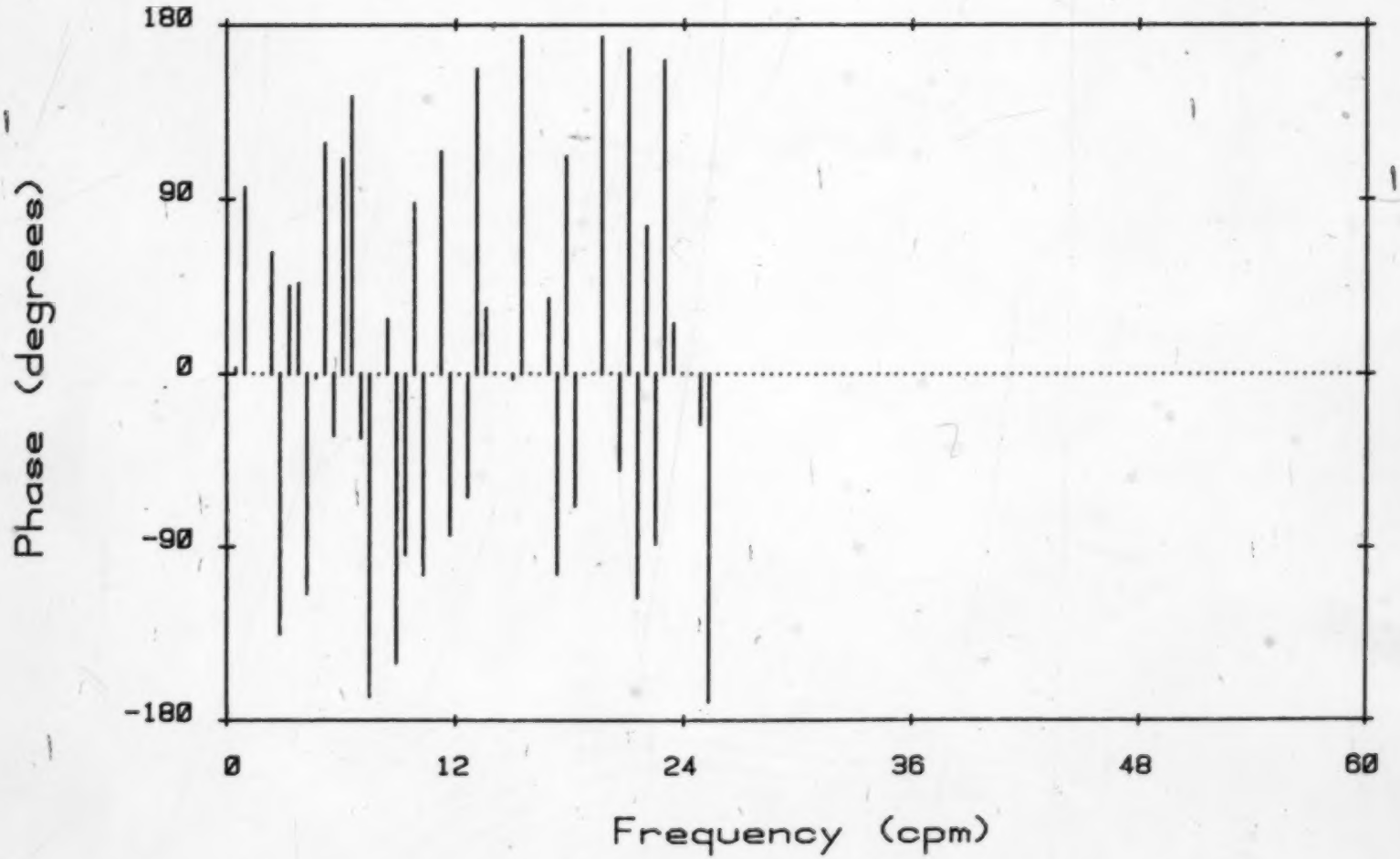


Fig. 5-12: Phase Spectrum of Fig. 5-10

A window from the record is shown in Fig. 5-10, and the corresponding magnitude and phase spectra are plotted in Figs. 5-11 and 5-12, respectively. No firm conclusions can be drawn from Fig. 5-10 about the relative slopes of the leading and trailing edges of the signal because of the significant distortion.

Analysis of this record reveals that the plus/minus percentage is virtually zero percent. This indicates that the ratio of the slopes is impossible to determine. Therefore, filtering of the record is required to extract the desired information.

The filter configuration is the same as in the previous example, except that the values of $\mu$ are set to $1.4 \times 10^{-7}$ and $1.4 \times 10^{-8}$, respectively, on the two passes. The average magnitude spectrum of the output signal is plotted in Fig. 5-13. Comparison of this graph with Fig. 5-9 shows that the filter has again achieved a significant reduction in the noise power in the record without affecting the three desired signal components.

A window from the output record at a time corresponding to Fig. 5-10 is shown in Fig. 5-14, and the corresponding magnitude and phase spectra are plotted in Figs. 5-15 and 5-16, respectively. While this signal is much cleaner than the original record, it is still difficult to visually determine the nature of the waveshape. The plus/minus percentage calculated for this signal is -3.4%, which indicates that the slope of the

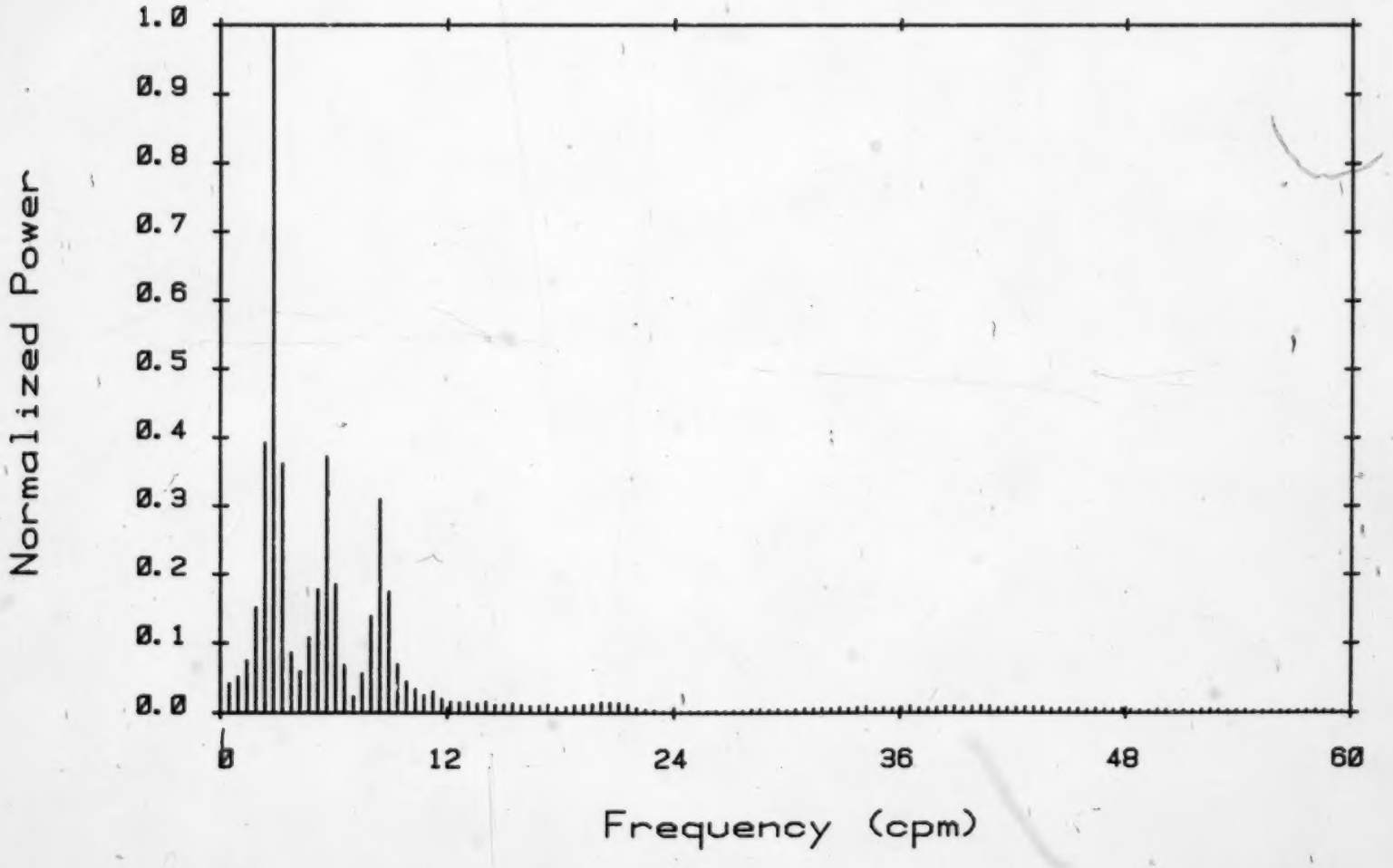


Fig. 5-13: Average Spectrum of Filtered Record #2

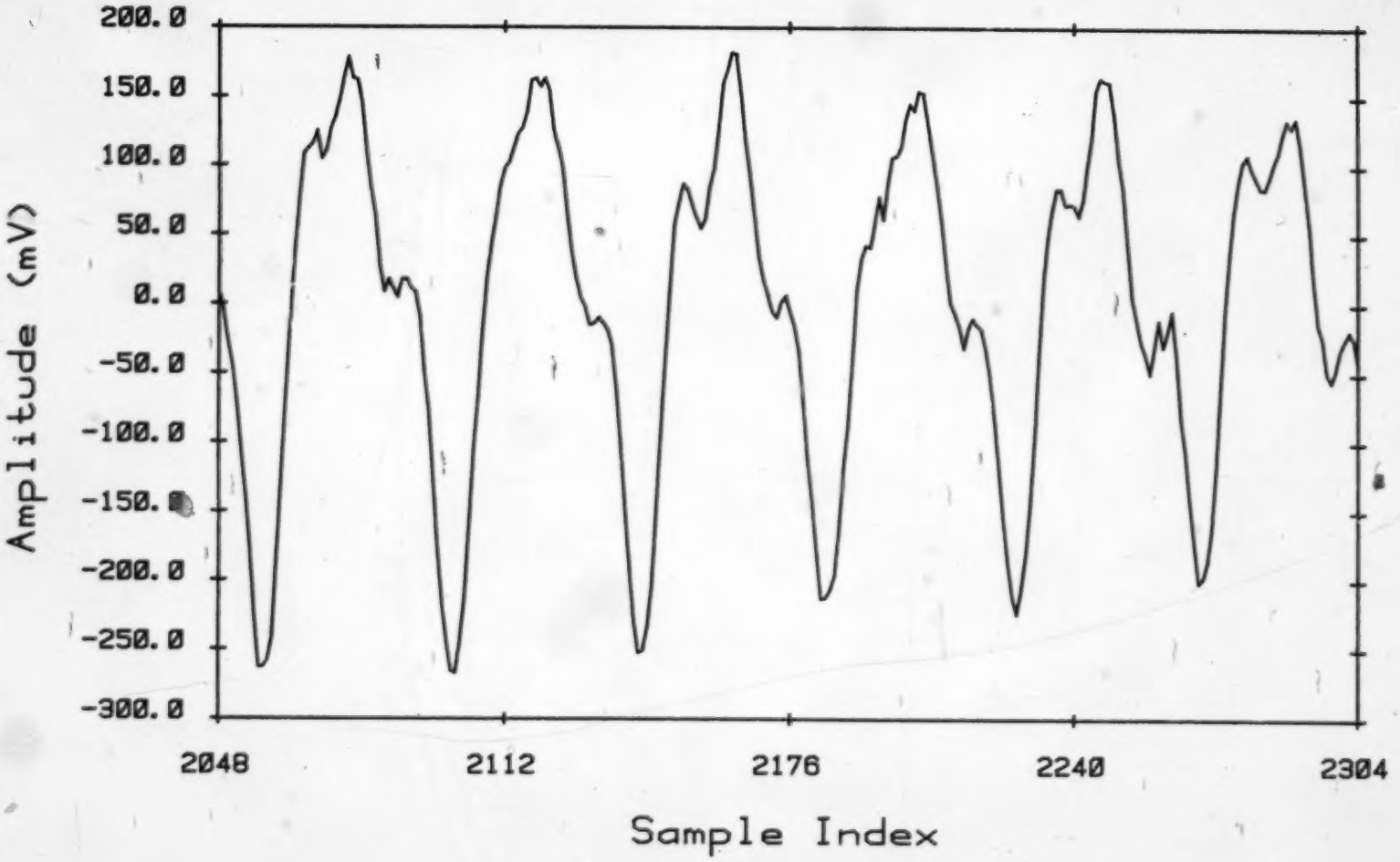


Fig. 5-14: The Output Signal After Convergence

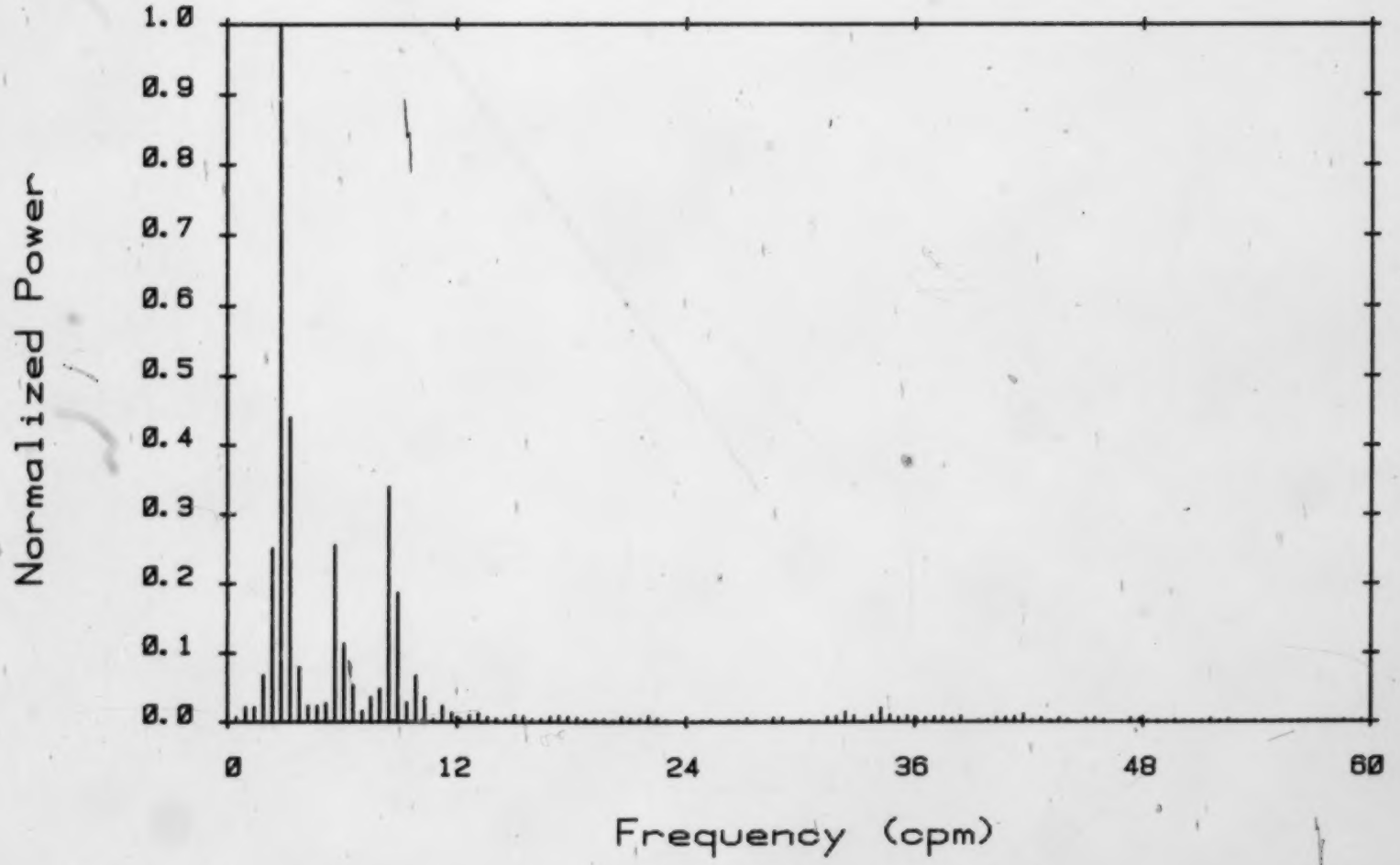


Fig. 5-15: Magnitude Spectrum of Fig. 5-14

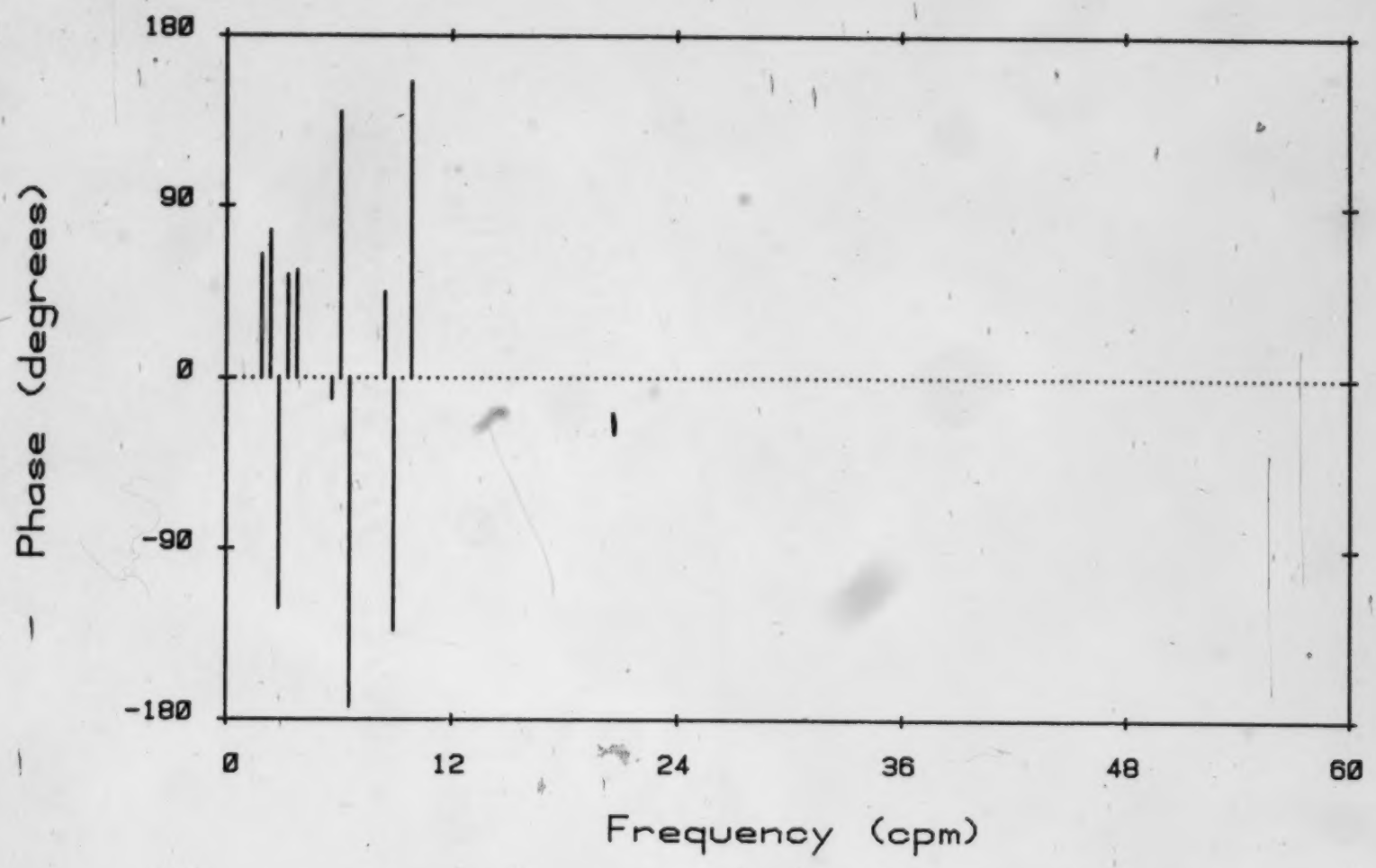


Fig. 5-16: Phase Spectrum of Fig. 5-14

leading edge of the waveform is only slightly steeper than the slope of the trailing edge. The conclusion is that the stomach contractions are travelling aborally in this patient.

### 5.3. Patient Record #3

As a final example of applying adaptive filtering to the transcutaneous EGG, consider Fig. 5-17, which shows the average magnitude spectrum of a third patient record. This, the noisiest of the three records discussed in this chapter (cf. Figs. 5-1 and 5-9), contains a significant amount of noise at all frequencies. There is a large signal present at about 20 cpm which may be due to the patient's respiration. Also, significant power is present at higher frequencies (even after the low-pass filtering performed during the acquisition process). Most notable is the band of frequencies between about 50 cpm and 60 cpm, which might be caused by the patient's ECG. The fundamental component of the EGG again appears in the vicinity of bin six. However, the two harmonics of interest are not clearly visible above the background noise.

Fig. 5-18 shows a window taken from the record. This graph shows that the signal is badly distorted by the noise. Visual examination of the signal reveals nothing about the ratio of the slopes. Since there is so much noise in the record, we can not expect that the plus/minus

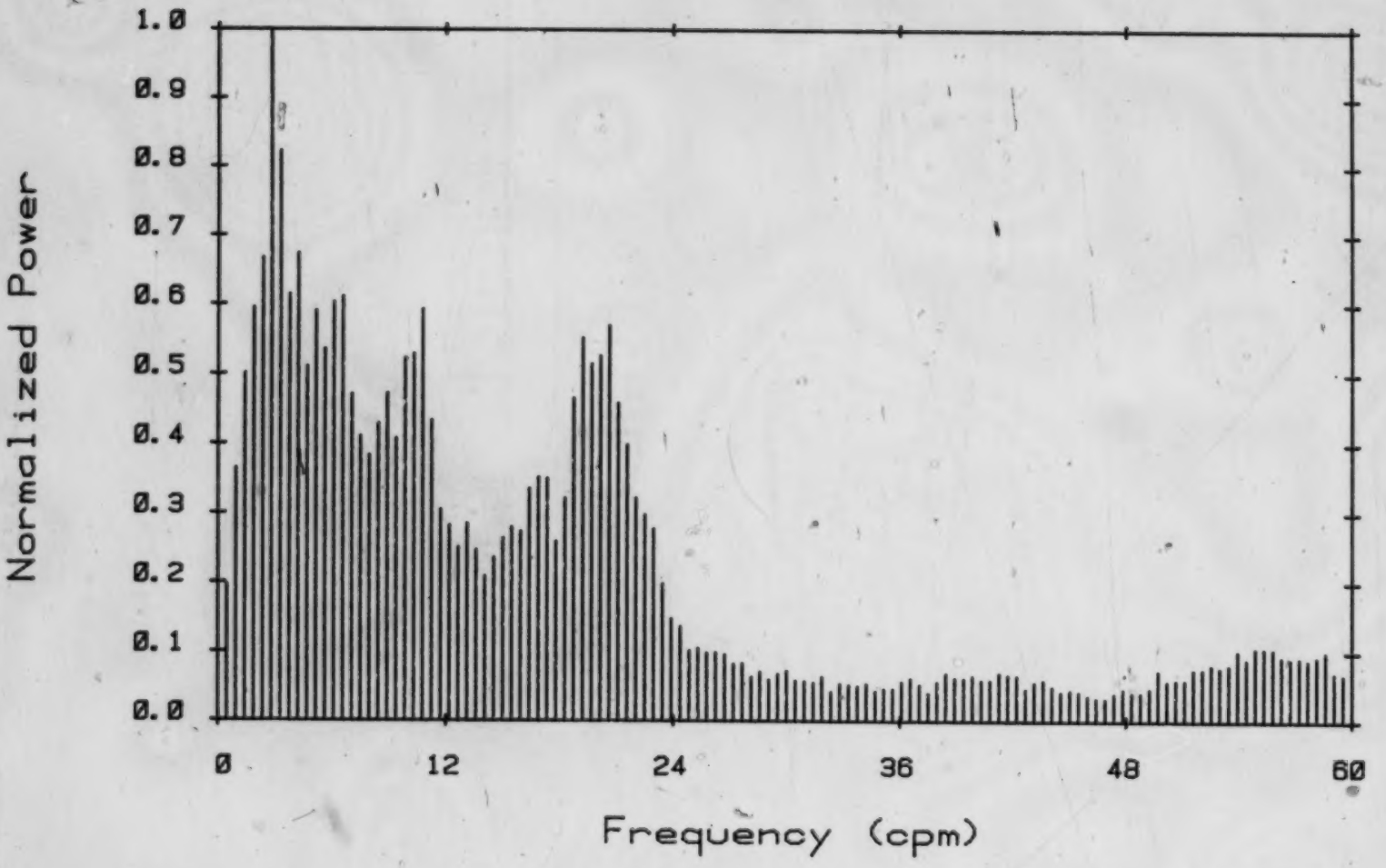


Fig. 5-17: Average Spectrum of Patient Record #3

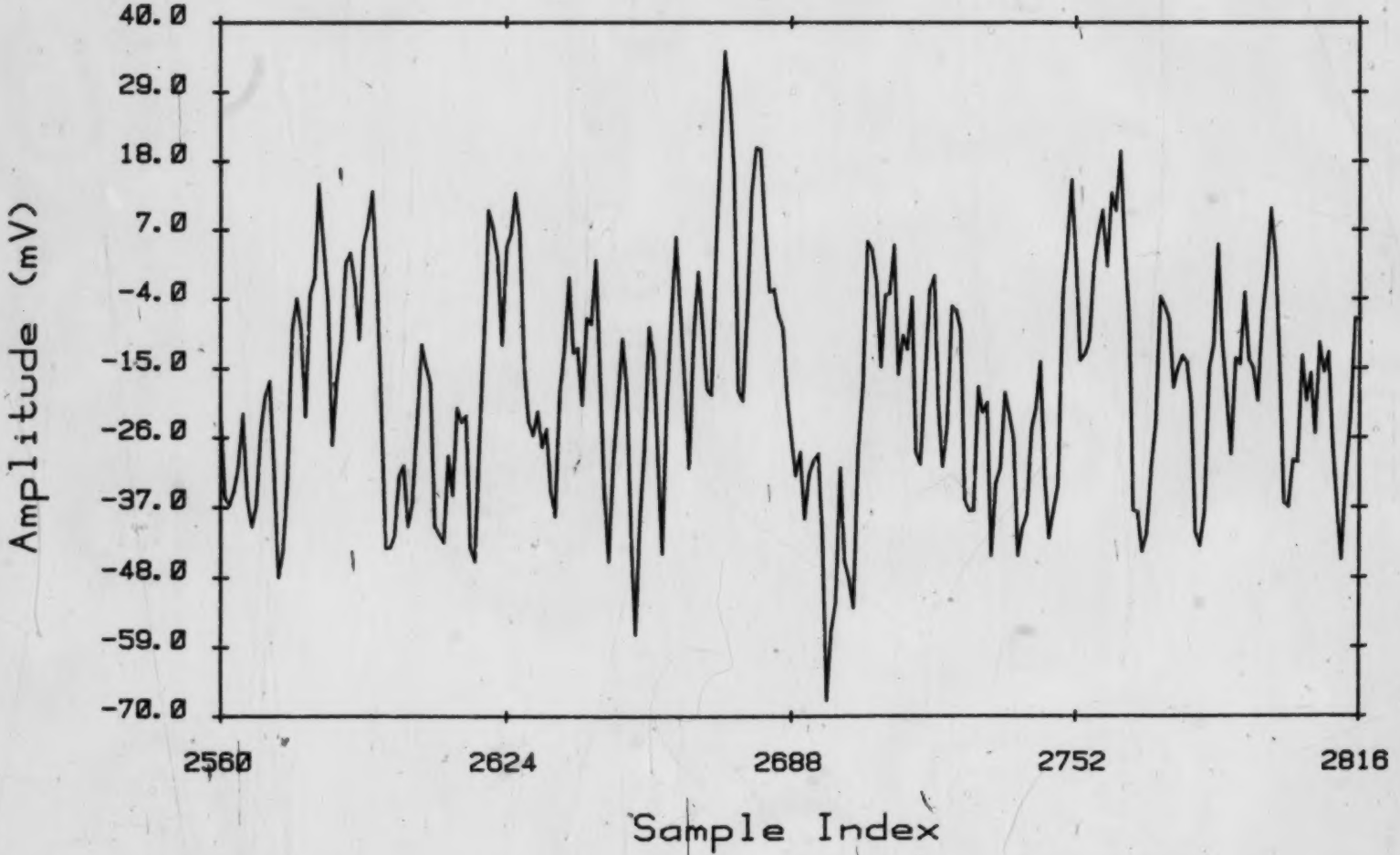


Fig. 5-18: A Window From Patient Record #3

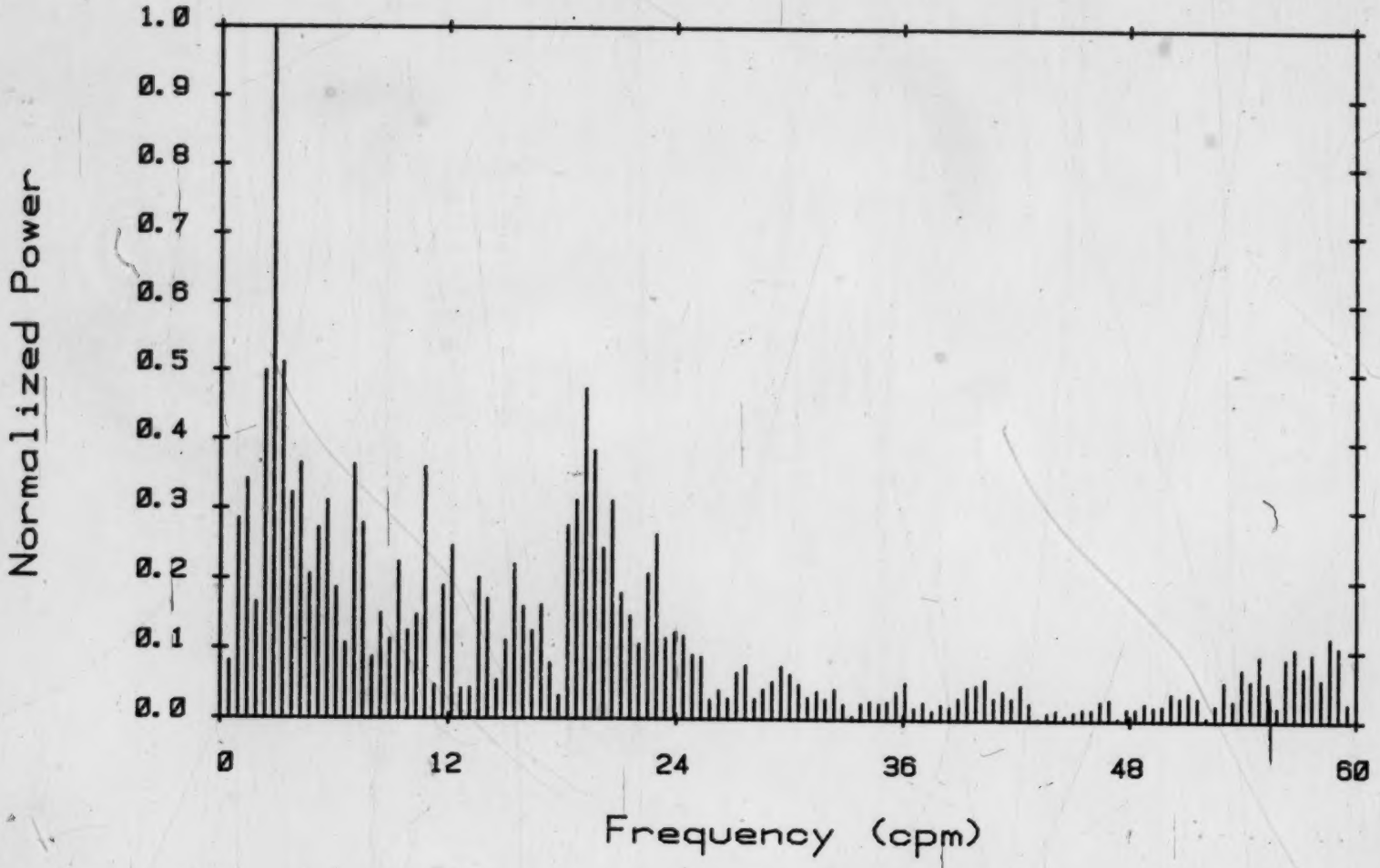


Fig. 5-19: Magnitude Spectrum of Fig. 5-18

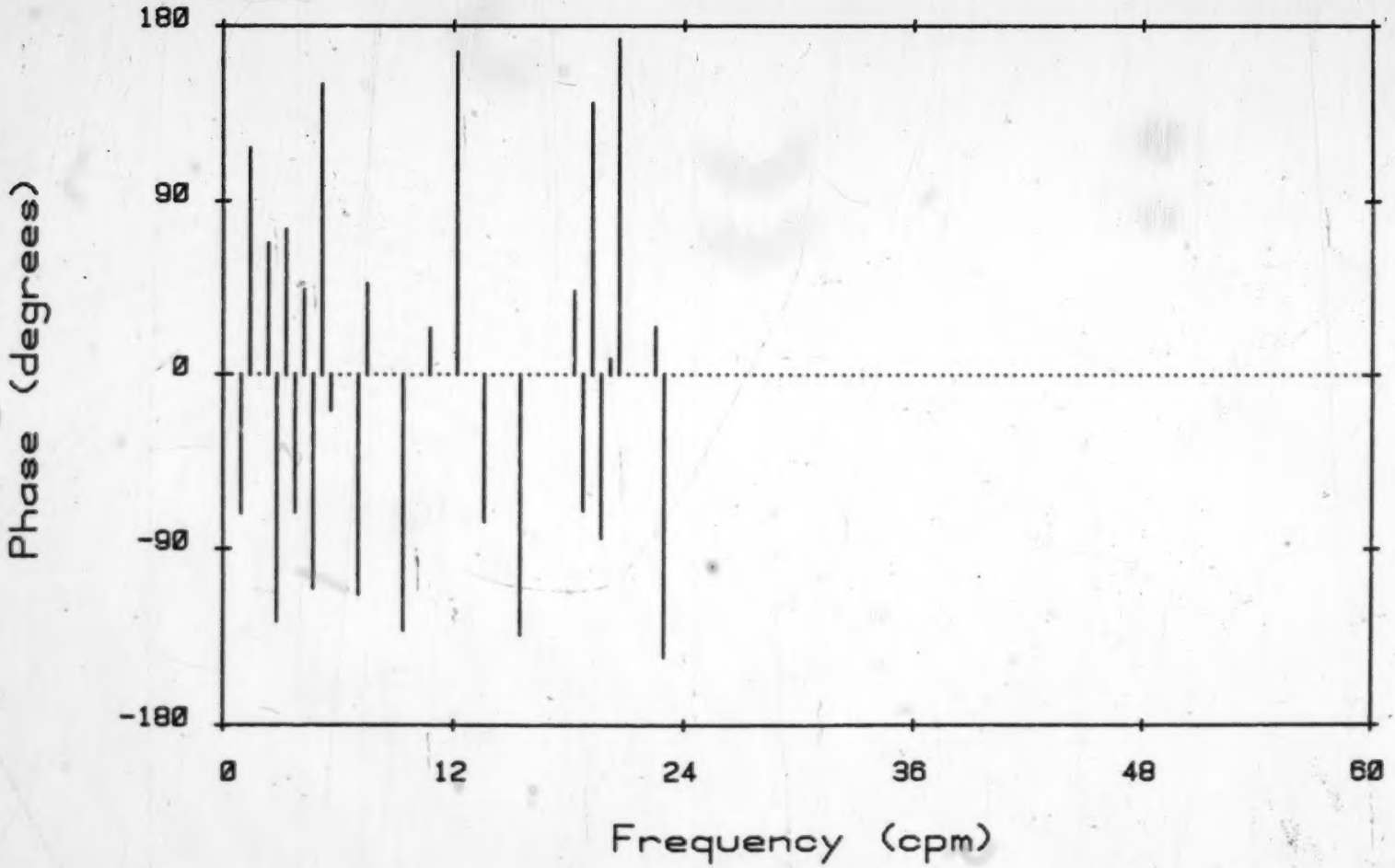


Fig. 5-20: Phase Spectrum of Fig. 5-18

analysis will produce accurate results. For the record, the plus/minus percentage is 5.1%, which suggests that the slope of the trailing edge is steeper than the slope of the leading edge. This is in direct contrast to the results obtained from the first two examples, and suggests that the contractions in this patient's stomach are travelling in the oral direction. However, the severe distortion in this record renders this result questionable, so adaptive filtering must be performed in hopes of recovering the actual EGG waveform.

The adaptive filter is again the same configuration as was used in the previous two examples. However, in this case the values of $\mu$ are set to $8.6 \times 10^{-6}$ and $8.6 \times 10^{-7}$ for the two filter passes, respectively. The average magnitude spectrum of the signal at the output of the adaptive filter is plotted in Fig. 5-21. Comparing this graph with Fig. 5-17, we see that the adaptive filter has increased the SNR dramatically. The graphs show significant suppression of noise at all frequencies, including those between the signal components.

Fig. 5-22 shows a window taken from the output record at a time corresponding to the window plotted in Fig. 5-18. This waveform, although still noisy compared to the output obtained in the first example in this chapter (cf. Fig. 5-6), appears to exhibit a steeper rising slope on the leading edge and a shallower falling slope on the trailing edge. This is confirmed by the plus/minus

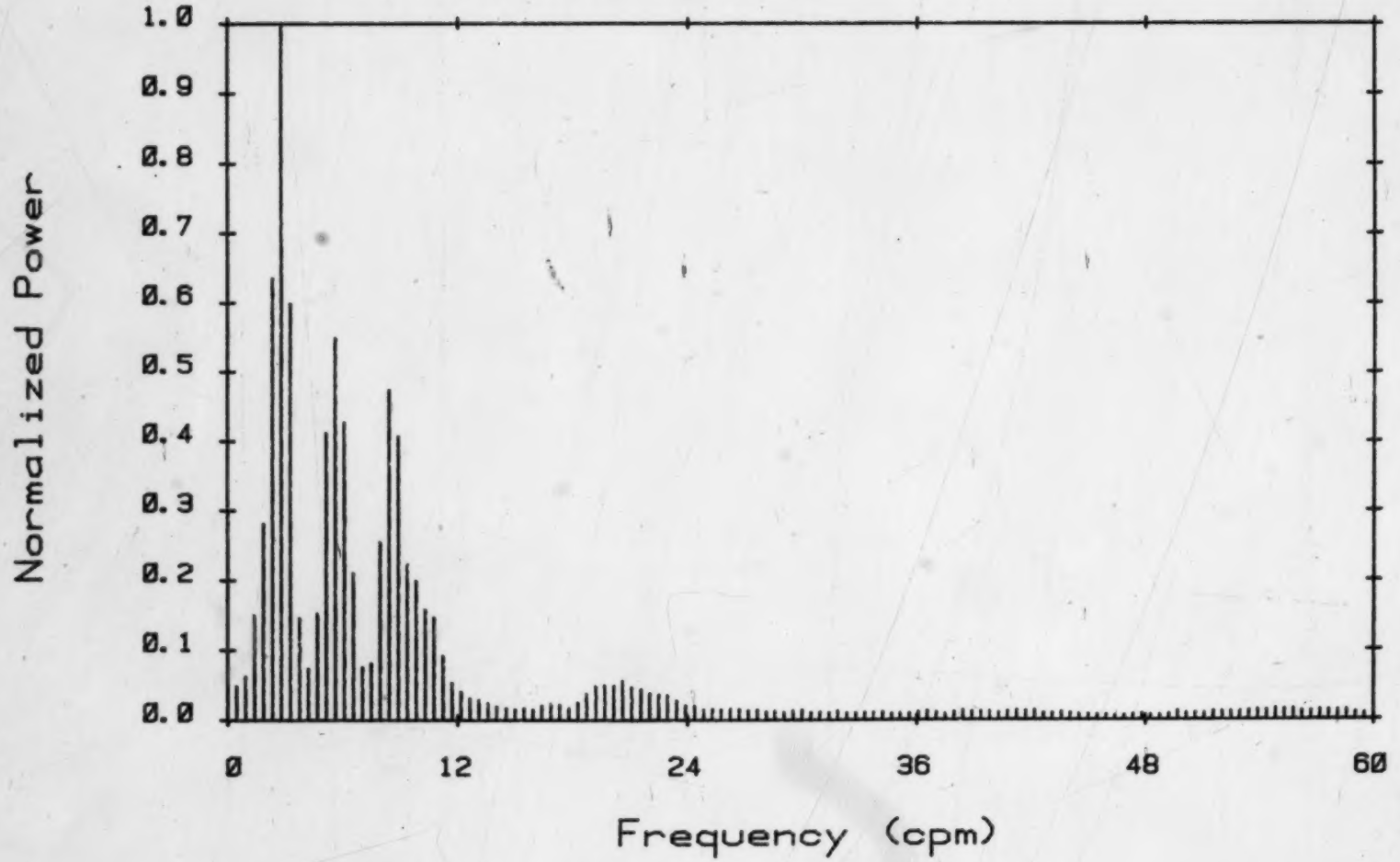


Fig. 5-21: Average Spectrum of Filtered Record #3

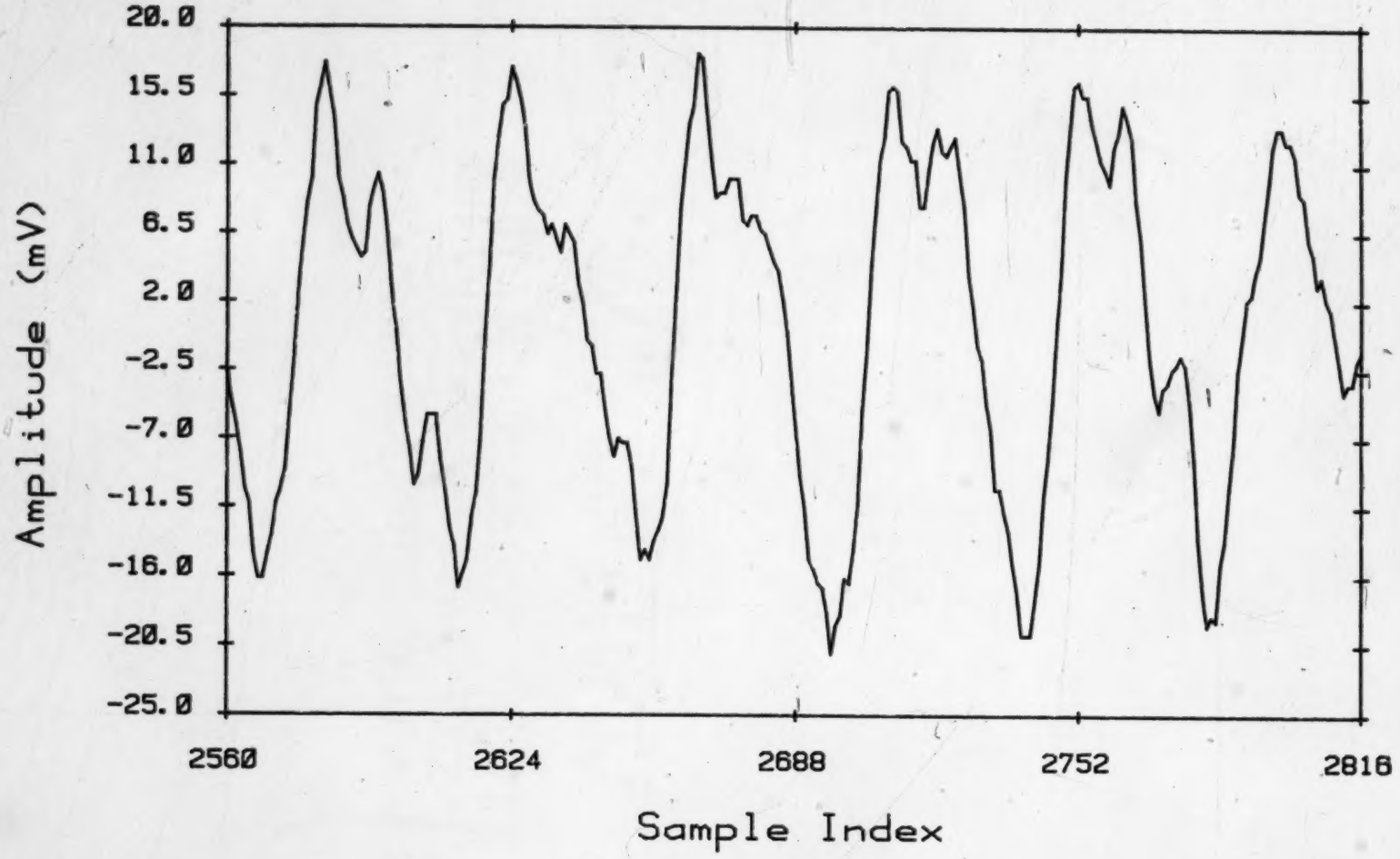


Fig. 5-22: The Output Signal After Convergence

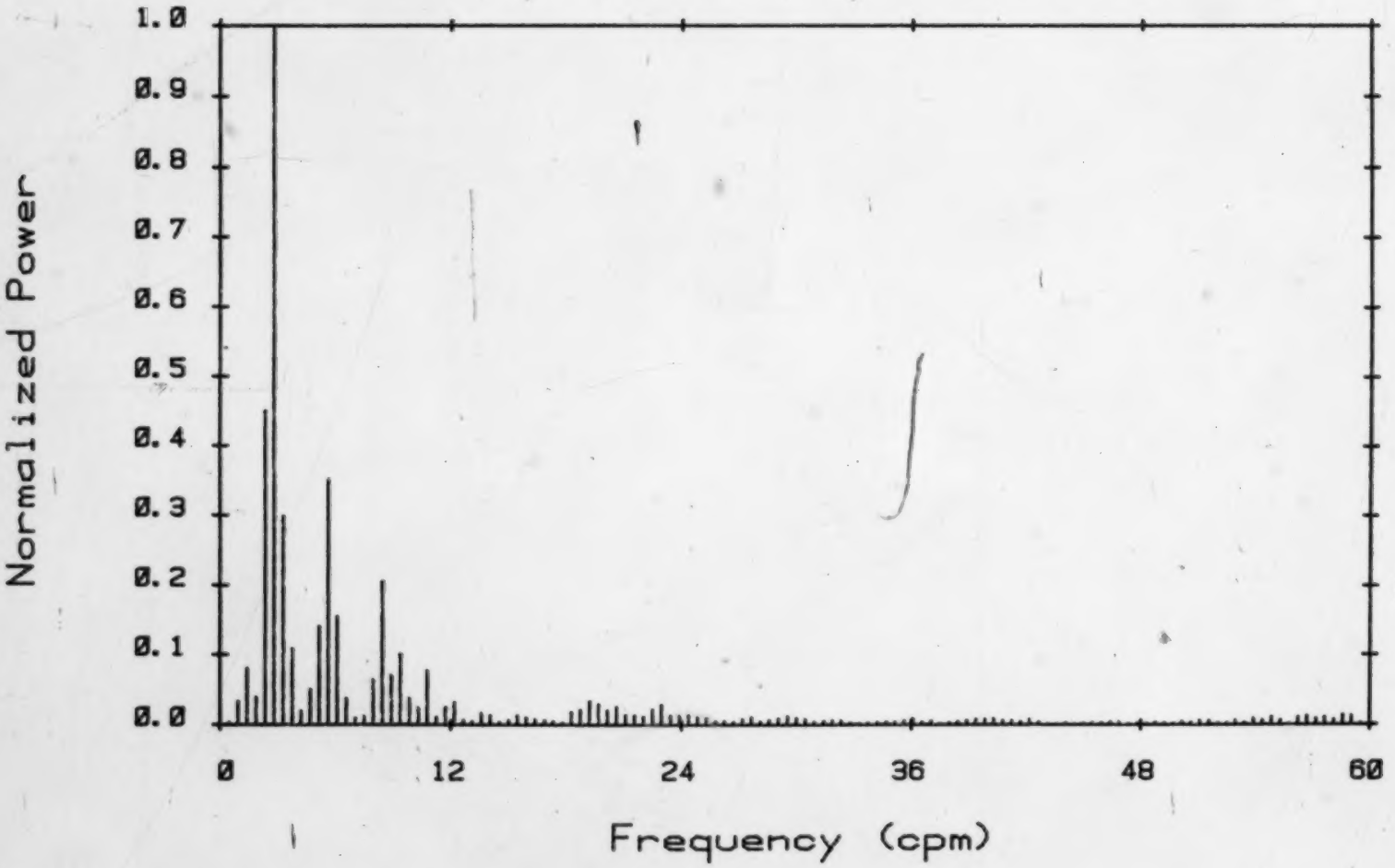


Fig. 5-23: Magnitude Spectrum of Fig. 5-22

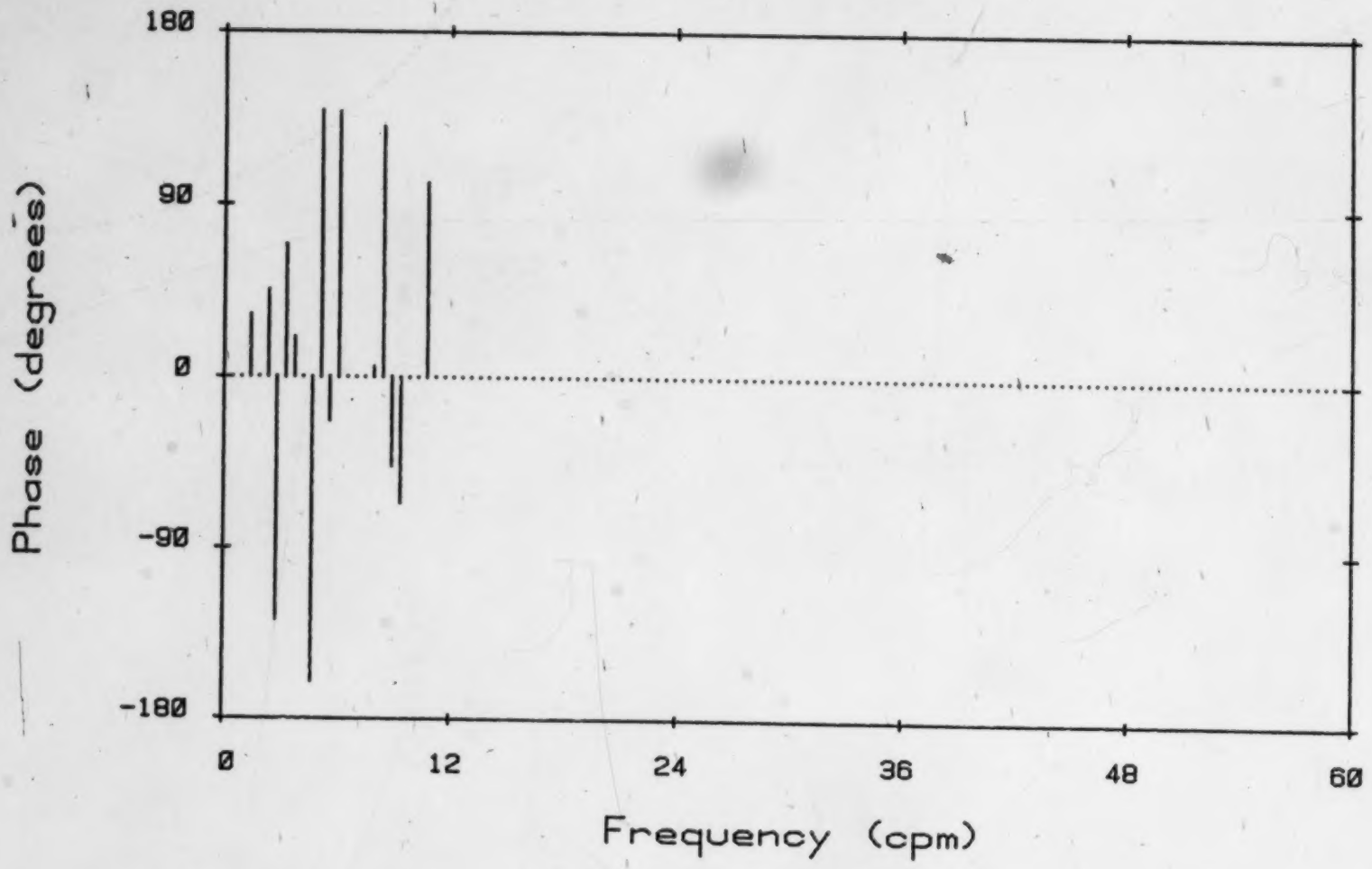


Fig. 5-24: Phase Spectrum of Fig. 5-22

percentage, which is -6.1%. Notice that this is of similar magnitude but opposite sign compared with the plus/minus percentage of the original record. This discrepancy indicates that the conclusions made using the original record are in error, and that the stomach contractions are really travelling in the aboral direction. The magnitude spectrum of Fig. 5-22 is plotted in Fig. 5-23, and the corresponding phase spectrum is shown in Fig. 5-24.

## 6. Conclusions

The LMS adaptive filter is the best choice for recovering the human electrogastrogram from the signal obtained using transcutaneous electrodes. The adaptive filter is capable of learning the characteristics of the EGG and the various noise components that appear with it at the surface of the abdomen. It uses this information to remove additive noise from the waveform, and produces a signal that is a least mean-squared error "best fit" to the actual EGG waveform.

The relative slopes of the rising and falling edges of the EGG can then be examined to extract the medical information therein contained. This can be accomplished by either inspection of graphs or application of the "plus/minus percentage" technique. Since the adaptive filter acts to suppress the noise components in the signal, analysis of the waveform after filtering provides more conclusive information than does the unfiltered signal.

Neither the plus/minus percentage nor visual examination will provide conclusive results in all cases. However, most signals can be accurately evaluated if both methods are used. This will reduce the chance of drawing an incorrect conclusion from a noisy record.

Spectral analysis using the FFT is useful in determining the characteristics of a signal, but does not

provide useful information when used for waveshape analysis. The picket-fence effect, apparent-phase shift, and phase distortion due to random noise all have a detrimental effect on the phase spectra. These phenomena must be carefully considered when interpreting the spectra obtained by computing the FFT of any signal.

## References


[1] Familoni, B. O., "Noninvasive Assessment of Gastric Motor Function in Human," Ph. D. dissertation, University of Alberta, Edmonton, Alberta, April 1986.

[2] Smallwood, R. H., "Analysis of Gastric Electrical Signals From Surface Electrodes Using Phaselock Techniques : Part 1 - System Design," Med. & Biol. Eng. & Comput., pp. 507-512, Sept. 1978.

[3] Smallwood, R. H., "Analysis of Gastric Electrical Signals From Surface Electrodes Using Phaselock Techniques : Part 2 - System Performance with Gastric Signals," Med. & Biol. Eng. & Comput., pp. 513-518, Sept. 1978.

[4] Gray, P. R. and Meyer, R. G., "Analysis and Design of Analog Integrated Circuits, Second Edition," John Wiley & Sons, Inc., pp. 605-632, 1984.

[5] Kentie, M. A. et al, "Adaptive Filtering of Canine Electrogastrographic Signals. Part 1: System Design," Med. and Biol. Eng. and Comput., pp. 759-764, Nov. 1981.

[6] Kentie, M. A. et al, "Adaptive Filtering of Canine Electrogastrographic Signals. Part 2: Filter Performance," Med. and Biol. Eng. and Comput., pp. 765-769, Nov. 1981.

[7] Widrow, B., "Adaptive Sampled-Data Systems," Proc. First International Congress of the International Federation of Automatic Control, pp. 423-428, Moscow, 1960.

[8] Widrow, B., "Adaptive Filters I : Fundamentals," Stanford University Report SU-SEL-66-126, 1966.

[9] Widrow, B. et al, "The Complex LMS Algorithm," Proc. IEEE, vol. 63, no. 4, pp. 719-720, 1975.

[10] Widrow, B. et al, "Adaptive Noise Cancelling : Principles and Applications," Proc. IEEE, vol. 63, no. 12, pp. 1692-1716, 1975.

[11] Widrow, B. et al, "Stationary and Nonstationary Learning Characteristics of the LMS Adaptive Filter", Proc. IEEE, vol. 64, no. 8, pp. 1151-1162, 1976.

[12] Widrow, B. et al, "Adaptive Filtering in the Frequency Domain," Proc. IEEE, vol. 66, no. 12, pp. 1658-1659, 1978.

[13] Widrow, B. and Stearns, S. D., "Adaptive Signal Processing," Prentice-Hall, Inc., Englewood Cliffs, N.J., 1985.

[14] Stanley, W. D., Dougherty, G. R., and Dougherty, R., "Digital Signal Processing, second edition," Reston Publishing Company, Inc., Reston, Virginia, 1984.

[15] Ramirez, Robert W., "The FFT - Fundamentals and Concepts," Prentice-Hall, Inc., Englewood Cliffs, N.J., 1985.